

MINISTRY OF EDUCATION AND SCIENCE OF UKRAINE

Odessa I. I. Mechnikov National
University**SENSOR
ELECTRONICS
AND MICROSYSTEM
TECHNOLOGIES****№ 3 • 2009***Scientific and Technical Journal*It is based 13.11.2003.
The Journal issue four times a year

UDC 681.586

Founded by Odessa I. I. Mechnikov
National University

At support of the Ukrainian Physical Society

Certificate of State Registration KB No 8131

The Journal is a part of list of the issues
recommended by SAC of Ukraine on physical and
mathematical, engineering and biological sciencesThe Journal is reviewed by RJ “Dжерело”
and RJ ICSTI (Russia)Publishes on the resolution of Odessa
I. I. Mechnikov National University
*Scientific Council. Transaction № 1,
September, 29, 2009*

Editorial address:

2, Dvoryanskaya Str., ISEPTC (RL-3),
Odessa I. I. Mechnikov National University,
Odessa, 65082, Ukraine
Ph. /Fax: +38(048)723-34-61,
Ph.: +38(048)726-63-56

МІНІСТЕРСТВО ОСВІТИ І НАУКИ УКРАЇНИ

Одеський національний університет
імені І. І. Мечникова**СЕНСОРНА
ЕЛЕКТРОНІКА
І МІКРОСИСТЕМНІ
ТЕХНОЛОГІЇ****№ 3 • 2009***Науково-технічний журнал*Заснований 13.11.2003 року.
Виходить 4 рази на рік

УДК 681.586

Засновник Одеський національний
університет імені І. І. Мечникова

За підтримки Українського фізичного товариства

Свідоцтво про державну реєстрацію KB № 8131

Журнал входить до переліку фахових видань
ВАК України з фізико-математичних,
технічних та біологічних наукЖурнал реферується РЖ “Джерело”
і ВІНІТІ (Росія)Видається за рішенням Вченої ради Одеського
національного університету
імені І. І. Мечникова
Протокол № 1 від 29 вересня 2009 р.

Адреса редакції:

вул. Дворянська, 2, МННФТЦ (НДЛ-3),
Одеський національний університет
імені І. І. Мечникова, Одеса, 65082, Україна.
Тел. /Факс: +38(048)723-34-61,
Тел.: +38(048)726-63-56

Editorial Board:

Editor-in-Chief **Smyntyna V. A.**

Vice Editor-in-Chief **Lepikh Ya. I.**

Balaban A. P. — (Odessa, Ukraine) responsible editor

Blonskii I. V. — (Kiev, Ukraine)

Verbitsky V. G. — (Kiev, Ukraine)

Gulyaev Yu. V. — (Moscow, Russia)

D'Amiko A. — (Rome, Italy)

Jaffrezic-Renault N. — (Lyon, France)

Dzyadevych S. V. — (Kiev, Ukraine)

Elskaya A. V. — (Kiev, Ukraine)

Kalashnikov O. M. — (Nottingham, United Kingdom)

Kozhemyako V. P. — (Vinnitsa, Ukraine)

Krushkin E. D. — (Ilyichevsk, Ukraine)

Kurmashov S. D. — (Odessa, Ukraine)

Lantto Vilho — (Oulu, Finland)

Litovchenko V. G. — (Kiev, Ukraine)

Machulin V. F. — (Kiev, Ukraine)

Mokrickiy V. A. — (Odessa, Ukraine)

Nazarenko A. F. — (Odessa, Ukraine)

Neizvestny I. G. — (Novosibirsk, Russia)

Ptashchenko A. A. — (Odessa, Ukraine)

Rarenko I. M. — (Chernovtsy, Ukraine)

Rozhitskii N. N. — (Kharkov, Ukraine)

Ryabotyagov D. D. — (Odessa, Ukraine)

Ryabchenko S. M. — (Kiev, Ukraine)

Soldatkin A. P. — (Kiev, Ukraine)

Starodub N. F. — (Kiev, Ukraine)

Stakhira J. M. — (Lviv, Ukraine)

Strikha M. V. — (Kiev, Ukraine)

Tretyak A. V. — (Kiev, Ukraine)

Редакційна колегія:

Головний редактор **Сминтина В. А.**

Заступник головного редактора **Лепіх Я. І.**

Балабан А. П. — (Одеса, Україна)
відповідальний секретар

Блонський І. В. — (Київ, Україна)

Вербицький В. Г. — (Київ, Україна)

Гуляєв Ю. В. — (Москва, Росія)

Д'Аміко А. — (Рим, Італія)

Джаффрезік-Рено Н. — (Ліон, Франція)

Дзядевич С. В. — (Київ, Україна)

Єльська Г. В. — (Київ, Україна)

Калашников О. М. — (Ноттінгем, Велика Британія)

Кожемяко В. П. — (Вінниця, Україна)

Крушкін Є. Д. — (Іллічівськ, Україна)

Курмашов Ш. Д. — (Одеса, Україна)

Лантто Вілхо — (Оулу, Фінляндія)

Литовченко В. Г. — (Київ, Україна)

Мачулін В. Ф. — (Київ, Україна)

Мокрицький В. А. — (Одеса, Україна)

Назаренко А. Ф. — (Одеса, Україна)

Неізнестний І. Г. — (Новосибірськ, Росія)

Птащенко О. О. — (Одеса, Україна)

Раренко І. М. — (Чернівці, Україна)

Рожицький М. М. — (Харків, Україна)

Ряботягов Д. Д. — (Одеса, Україна)

Рябченко С. М. — (Київ, Україна)

Солдаткін О. П. — (Київ, Україна)

Стародуб М. Ф. — (Київ, Україна)

Стахіра Й. М. — (Львів, Україна)

Стріха М. В. — (Київ, Україна)

Третяк О. В. — (Київ, Україна)

ЗМІСТ**CONTENTS**

Some words to the readers 4

V. A. Smyntyna, Ya. I. Lepikh, V. F. Machulin
**INVESTIGATIONS AND ACHIEVEMENTS
 IN SENSORICS AREA IN 2008**.....5

**Фізичні, хімічні та інші явища, на основі яких
 можуть бути створені сенсори**
**Physical, chemical and other phenomena, as the
 bases of sensors**

T. A. Florko, A. V. Loboda, A. A. Svinarenko
**SENSING FORBIDDEN TRANSITIONS
 IN SPECTRA OF SOME HEAVY ATOMS AND
 MULTICHARGED IONS: NEW THEORETICAL
 SCHEME** 10

O. Yu. Khetselius, D. E. Sukharev, Yu. V. Dubrovskaya
**SENSING STRONG INTERACTION EFFECTS
 IN SPECTROSCOPY OF HADRONIC ATOMS**..... 16

Оптичні, оптоелектронні і радіаційні сенсори
Optical, optoelectronic and radiation sensors

*M. V. Kirichenko, V. R. Kopach, R. V. Zaitsev,
 S. A. Bondarenko*
**SENSITIVITY OF SILICON PHOTOVOLTAIC
 CONVERTERS TO THE LIGHT INCIDENCE
 ANGLE ON THEIR RECEIVING SURFACE** 22

*Y. P. Sharkan, N. B. Jytov, I. I. Sakalosh, J. J. Ramsden,
 M. Y. Sichka, I. I. Popovich, S. O. Korposh*
**FIBER-OPTIC SENSOR FOR THE EXPRESS
 CONTROL OF THE CHEMICAL COMPOSITION** ... 27

*M. Yu. Trofimenko, Yu. A. Nitsuk, T. F. Smaglenko,
 L. I. Riabchuk*
**DETERMINATION OF SPECTRAL DEPENDENCE
 OF SOLID BLENDED FUEL TORCH SYSTEM
 RADIATING ABILITY** 35

Акустoeлектронні сенсори
Acoustoelectronic sensors

L. V. Mikhaylovskaya, A. S. Mykhaylovska
**CHARACTERISTIC PROPERTIES OF OPTO-
 ACOUSTIC INTERACTION IN THE “THICK”
 ACOUSTIC GRATING**..... 40

Біосенсори
Biosensors

*S. V. Dzyadevych, A. P. Soldatkin, A. A. Soldatkin,
 V. N. Peshkova, A. D. Vasilenko, V. G. Melnik,
 A. A. Mikhal, L. N. Semenycheva, M. P. Rubanchuk*
**FOUR-CHANNEL BIOSENSOR’S ANALYZER
 OF SACCHARIDES**..... 47

Матеріали для сенсорів
Sensor materials

*A. L. Kukla, A. A. Vakhula, I. V. Kruglenko,
 V. Yu. Khorouzhenko, I. A. Samoylova*
**THIN FILMS OF TRET-BUTYL CALIXARENE
 AS SENSITIVE MATERIALS FOR ORGANIC
 COMPOUND DETECTORS** 54

*V. M. Tsmots, P. G. Litovchenko, Yu. V. Pavlovskyy,
 O. P. Litovchenko, I. S. Pankiv, M. M. Luchkevych*
**IMPACT OF PRE-IRRADIATION ON THE
 MAGNETIC SUSCEPTIBILITY OF CZ-SI
 THERMALLY TREATED AT 700-1000 °C**..... 66

Сенсори та інформаційні системи
Sensors and information systems

S. Y. Yurish
**SENSOR SYSTEM FOR AUTOMATIC PAPER
 THICKNESS DETECTION BASED ON UNIVERSAL
 SENSORS AND TRANSDUCERS INTERFACE**..... 70

I. Voitovych, I. Yavorsky
**CORRELATIVE PROCESSING OF INFORMATION
 IN BIOSENSORS BY SURFACE PLASMON
 RESONANCE** 79

ВИМОГИ ДО ОФОРМЛЕННЯ СТАТЕЙ..... 86

**INFORMATION FOR CONTRIBUTORS. THE
 REQUIREMENTS ON PAPERS PREPARATION**..... 88

SOME WORDS TO THE READERS

DEAR COLLEAGUES, HONORED READERS!

The issue of the present number is dedicated to and certifies that our Journal has reached the first 5-year jubilee. We have decided not to prepare the special issue decorated with requested and prepaid reviews, as we are in concordance with the view of the majority of you who consider our Journal as such which has the recognized scientific-technological level and that it has a significant reserve of the further development.

The Journal "Sensor Electronics and Microsystem Technologies" (SEMST) is the unique publication in Ukraine which corresponds in full to the chosen field and is directed to the discussion of different parts of the sensorics and microsystem technologies as well as to the systematic information of the scientific audience on the newest results in the research and engineering development in the field and international conferences and describes the activities of international research bodies in the scientific and applied problems' of sensorics and microsystem technologies solution.

In such a way, the "SEMST" Journal assists the development of this perspective and significant scientific-technological direction being created at the border of different sciences and technological approaches.

The materials, published in the "SEMST" Journal pass the independent check-up by the professionals of the Journal editorial board as well as by the external, including foreign highly qualified experts, what allows the Journal editorial board to present to the readers' audience only the new original research material of the highest scientific-technological level.

The "SEMST" Journal, being the inter-disciplinary scientific publication, is being placed in the fields of physics, chemistry, biology, microelectronics and devices' design, proposing to the authors' community the possibility to address the widest possible readers' audience the results of the modern research in all mentioned branches of science and technology.

The "SEMST" Journal is included into the list of scientific publications recommended by the Highest

Attestation Council of Ukraine for the presentation of the results of candidate and doctoral dissertations on physics, technical and biological sciences.

Our Journal is being cited by the Ukrainian referative journal "Dzherelo" (Source) as well as by the Referative Journal VINITI (Russian Academy of Sciences, Russia).

Just now, the "SEMST" Journal is considered by the International corporation SCOPUS as the possible candidate for the inclusion into the international Internet-base of the scientific-technological journals.

It should be mentioned, with the sense of satisfaction, that the "SEMST" Journal has become the well-known one quite quickly and received the high enough rating in the circle of the natural sciences scientific journals of the European scientific community.

This statement could be supported by the widest geography of the authors who have published their papers in the "SEMST" Journal being as follows: Belorussia, Bulgaria, Czech Republic, France, Finland, Germany, Great Britain, Italy, Mexico, People Republic of China, Poland, Russian Federation, Slovak Republic, Ukraine, the U.S.A., etc.

We all hope that we could maintain the tendency of the permanent appraisal of the "SEMST" Journal's scientific-technical level and quality of the published papers through the common efforts of our authors, editorial board members, referees and readers.

I congratulate the editorial board members, the authors and readers with the 5-year jubilee of the "Sensor Electronics and Microsystem Technologies" Journal and wish everybody of you the further and greater creative success.

With sincere thanks for cooperation
and best regards
Senior Editor of the Journal
D.Sc. in Physics, Professor,
Honored Creator in Science and Technology
of Ukraine, Winner of the State Prize of Ukraine

Valentin A. Smyntyna



INVESTIGATIONS AND ACHIEVEMENTS IN SENSORICS AREA IN 2008

¹V. A. Smyntyna, ¹Ya. I. Lepikh, ²V. F. Machulin

¹ I. I. Mechnikov Odesa National University, ndl_lepikh@onu.edu.ua

² V. E. Lashkarev Semiconductor Physics Institute, NAS Ukraine

(The scientific review on Sensorics Section of NAS Ukraine Scientific Council on “Physics of Semiconductors and Semiconductor Devices “)

Abstract. The review of the basic results of investigations in sensorics area is presented which were coordinated by Sensorics Section of NAS Ukraine Scientific Council on “Physics of semiconductors and semiconductor devices” for year 2008.

The review contains the results of investigations, which were carried out by scientific schools, sub-units of NAS Ukraine, Ministry of Education and Science of Ukraine, the named below research organizations:

- V.E. Lashkarev Semiconductors Physics Institute;
- Institute of Physics of NAS Ukraine;
- O.V. Palladin Institute of Biochemistry of NAS Ukraine;
- Institute of Molecular Biology and Genetics of NAS Ukraine;
- Taras Shevchenko Kyiv National University;
- National Technical University “Kyiv Polytechnical Institute”;
- Lviv Ivan Franko National University;
- National University “Lviv Polytechnica”;
- Kharkiv National University of Radioelectronics;
- Odesa National Polytechnical University;
- Odesa I. I. Mechnikov National University;
- Odesa State Academy of Communication
- Odesa National Maritime Academy;
- Dnepropetrovsk National University;
- Yu. Fed’kovich Chernivtsy National University.

Investigations were carried out in the following basic scientific and applied science directions:

- physical, chemical and other phenomena on the basis of which sensors could be developed;
- sensor design and mathematical modeling;
- physical sensors;
- chemical sensors;

- biosensors;
- radiation, optical and optoelectronic sensors;
- acousto-electronic sensors;
- nanosensors (physics, materials, technology);
- sensors and information systems;
- materials for sensors;
- technological problems of sensor controls;
- microsystem technologies (MST);
- sensor’s degradation, metrology and certification.

We propose to attribute the following to the basic scientific results and achievements on section interest directions:

Taras Shevchenko Kyiv National University

Electrophysical and adsorption properties of surface barrier structures created at silicon surface through modification by particle irradiation with the purpose of gas-sensitive structures creation that was carried out together with Institute of Nuclear Research of NAS Ukraine were studied in the papers [1, 2].

It is shown, that the sensitivity of structures based on gold — radiation-modified silicon junction to ammonia is higher than for structures gold — non-irradiated silicon. The saturation current of gold — radiation-modified silicon hetero-junction changes nonlinearly with temperature. The account of the resonance-tunnel current allows explaining the dependences observed qualitatively for samples irradiated by doses 10^{15} and 10^{17} protons/cm². This effect is connected with the increase of the effective adsorption area owing to irradiation [3-6]. The new

type sensitive optoelectronic gas sensor is proposed on the basis of the silicon photo-converter (diffusive p-n junction with a thin layer of porous silicon on the back side) with photo-electric transducer. The parameter being sensitive to the adsorption of molecules is the photocurrent which arises at illumination silicon back surface by light from region of silicon heavy absorption and depends on the surface non-equilibrium carriers recombination change which, in turn, depends on the type and concentration of adsorbed molecules. The multi-sensor structure with the optical addressing and 2D cartography of the given photocurrent which is at use of the main components method allows to analyze liquids or gases mixes is created and investigated [7,8].

National University "Lviv Polytechnica"

With the purpose of creation of radiation-resistant physical sensors for cryogenic temperatures, the investigations of irradiation with high-energy electrons influence on jumping conductivity of thread-like Si crystals and p-type $\text{Si}_{1-x}\text{Ge}_x$ solid solutions with impurity concentration near junction metal — dielectric are carried out.

Strong (up to 14 Tl) magnetic field influence on the conductivity of alloy Si micro-crystals, solid $\text{Si}_{1-x}\text{Ge}_x$ solutions and poly-silicon layers on insulator (SOI-structures) is investigated at cryogenic temperatures [9, 10].

The opportunity Si nano-wires with diameters 10-100 nm, creation by the gas-core epitaxy method for sensors development on their basis is shown. The technology of sub-micron sizes auto-emitting silicon cathodes creation with the use of the micron sizes photo-masks on SMIS technologies for device structures creation is developed [11].

With the purpose of sensor operational temperature increase in magnetic field at radiation conditions diagnostics, the technology is created of growing from a gas phase solid solutions $\text{InAs}_{1-x}\text{Sb}_x$ micro-crystals with a different ratio of the fifth group components (As and Sb), where $x = (0,02-0,16)$ [12, 13].

The lattice parameters and structure of brought up $\text{InAs}_{1-x}\text{Sb}_x$ micro-crystals are defined. Brought up micro-crystals electrophysical parameters' research is carried out and the received solid solutions' forbidden zone width is determined.

Multi-functional magneto-sensing probe for simultaneous measurement of three component of a

magnetic field and/or its spatial gradient is developed [14].

The analysis of conditions of spatial magnetic heterogeneity visualization by magneto-optic methods is carried out. The way of reception of quantitative characteristics of spatial distribution of magnetic fields by display film method is offered [15].

Silicon and the modification of porous silicon for photo-electric converters — solar elements (SE) creation are investigated. Effective and profitable technological processes in manufacture SE structure elements, first of all a frontal surface — structure with low integral reflection factor are proposed [16].

The technology and new hetero-structures is developed on the basis of organic and inorganic semiconductors (nickel phthalocyanine alloyed with oxygen) for sensor engineering [16].

V.E. Lashkarev Semiconductor Physics Institute, NAS Ukraine

The γ — and β — radiations detecting blocks are developed and produced on the basis of CdTe:Cl and CdZnTe semiconductor materials with use of laser evaporation methods and contact metal fusion [17].

The device for radiating monitoring of environment which consists of γ -radiation semiconductor detector and the monitoring block which contains the programmed processor as well as the information preservation blocks on γ -radiation doze power and the signaling about the γ -radiation doze power amount excess above the programmed maximum permission is developed [18].

X-rays dispersion by multilayered structures peculiarities are investigated, and also mechanisms quantum points and threads ordering in multilayered structures with use of high resolution diffraction methods are investigated [19].

It is established, that for multi-layered systems of InGaAs/GaAs (100) spatial ensemble ordering of quantum points (QP) on flat GaAs substrate is vertically correlated with insignificant inclined transformation and is laterally built in a primitive oblique-angled lattice which forms a three-dimensional file as the disfigured tetragonal cell.

The nature of interrelation of anisotropy of initial and residual deformations in multi-layered (In, Ga)As/GaAs structures with the quantum threads, subjected fast thermal annealing is established and analyzed. The role of micro- and macro-defects during the self-organized nano-islands growth is established [20].

It is established, that at fast thermal annealing in a temperature interval of 500-800 °C for structures with quantum threads, the significant changes of three-dimensional order of quantum points in the multilayered structure occur, caused by it macro-elbow and intensive diffusion processes. It is shown, that the crystallographic orientation of substrate significantly influences the form, the size and density of quantum points at weak influence on character planar ordering [21].

The opportunity of management in parameters nano-dimensional Ta_2O_5 , Cd_2O_3 , TiO_2 , Er_2O_3 films; Ta_2O_5 -Si, $Cd_2O_3(TiO_2, Er_2O_3)$ -SiC structures and Al(W, TiN)- Ta_2O_5 -Si MDS structures at the influence on them of dosing microwave radiation is shown.

The software for computer modeling and reception of authentic quantitative parameters of probe — surface contact capacity and semiconductor nanostructures local areas doping level (some tens of nanometers) on results of mapping of a surface by a method of scanning capacitor microscopy is advanced. It is shown, that the basic fluctuations break-down layers characteristics are caused by films thickness variations (0.2-0.5 nm) and electrically active defects density distribution heterogeneity [22-24].

Yu. Fed'kovich Chernivtsy National University

Research is carried out and some model developments for quantitative spectrum characteristics of simultaneously several types of defects in crystals high-resolution multi-crystal diffractometry are realized [25].

Some model developments for oblique asymmetrical topography in geometries Laue, Bragg and sliding beams diffraction for diagnostics defects selective on depth in the excited surface layers of mono-crystals and multilayered epitaxial structures (level-by-level diffracto-topography) are realized [26].

Combined investigations by methods X-ray diagnostics of multilayered A^3B^5 structures and structural changes in surface layers materials subjected ionic and high-power electronic irradiation are continued [27].

I. I. Mechnikov Odesa National University

The model of relaxation phenomena in non-ideal hetero-junction is developed, and recommendations for memory elements on the basis of non-ide-

al hetero-junctions manufacturing techniques are offered. The model, which allows the theoretical sensito-metrical characteristics' calculation of the investigated elements is created, the calculations of such characteristics as well as its comparison with experimental one are carried out. The numerical calculation of a characteristic curve with use of generation and recombination model in non-ideal hetero-junction is carried out [26, 29].

The photoluminescence of the nano-dimensional tin dioxides films at room temperature was registered and the dependence of a photoluminescence on gels composition for their reception, which considerably expands the opportunities of these films use in optoelectronics and sensor electronics is established [30].

The structural and electro-physical characteristics of adsorptive sensitive complex compounds are investigated and systematized [31, 32]

It is shown that the mechanism of analyzed compound's interaction with layered structures of complex compounds are determined by the supra-molecular complex compound with macromolecular branched structure, and also the functional material nano-dimensional hollows and the developed surface, and nano-hollows atoms group form physical bond between the analyzed molecule and sensitive layer material [33].

The basic laws of adsorption-desorption phenomena concerning the distribution of acoustic waves in polymeric compound — piezoelectric material layered structures are established [33].

The technique microelectronic sensors creation is developed on the basis of layered structures and acousto-electronic element, which can be introduced at the enterprises of the instrument-making industry [34-36].

The significant part of the received results of investigations is published in the list of the literature given below.

References

1. V. V. Il'chenko, S. O. Gordienko, V. I. Khivrych, P. V. Kuchynski, V. M. Telega The current-voltage characteristics of the structures radiation modified Si — nanostructured SnO_2 at the gas adsorption. // IV International conference "Electronics and applied physics", October, 23-25, 2008, Kyiv, Ukraine, pp. 43-44.
2. V. V. Il'chenko, S. O. Gordienko, V. I. Khivrich, Y. M. Kravchyk, V. M. Telega Research of mechanisms of charge transport in heterostructures on the basis of

- radiation — modified Si at gas adsorption. //Eight international young scientists' conference on applied physics. June 11-13, 2008, Kyiv, Ukraine, pp. 77-78.
3. O. V. Kostiukevich, V. V. Il'chenko The influence of square and perimeter of contacts on the current-voltage characteristics of the heterostructures of the nanoscaled film ($90\% \text{In}_2\text{O}_3 + 10\% \text{SnO}_2$) — p-Si. //Eight international young scientists' conference on applied physics. June 11-13, 2008, Kyiv, Ukraine, pp. 67-68.
 4. N. L. Dmutruk, O. S. Kondratenko, V. V. Il'chenko, S. A. Gordienko, P. V. Kuchinskiy, L. A. Vlasukova, V. I. Khivrich, M. B. Pinkovskaya //The first international scientific conference HAHO — 2008.
 5. N. L. Dmutruk, S. A. Gordienko, O. S. Kondratenko, V. V. Il'chenko, P. V. Kuchinskiy, L. A. Vlasukova, V. I. Khivrich, M. B. Pinkovskaya Nanostructuring Si and Si/SiO₂ surfaces by the accelerated charged particles // the First international conference “ Nanostructured materials “, Minsk April, 22-25, 2008, C. 82.
 6. S. A. Gordienko, V. V. Il'chenko, V. I. Khivrich The possibility of Si surface modification by protons for creation gas-sensitive surface barrier structures //3-rd International Scientific and Technical Conference “Sensors Electronics and Microsystems Technology (SEMST-3), Ukraine, Odessa, 2-6 June, 2008.
 7. Skryshevskiy V. A. Sensor structures with nanosilikon: up-to-date state //Book of abstracts of the 3-rd International Scientific and Technical Conference “Sensors Electronics and Microsystems Technology (SEMST-3), Ukraine, Odessa, 2-6 June, 2008. — “Astroprint”. — P. 6-7.
 8. Litvinenko S. V., Alekseev S. O., Kuznetsov G. V., Skryshevskiy V. A. Porous silicon state control as a hydrogen source with a help of optoelectronic sensor// Book of abstracts of the 3-rd International Scientific and Technical Conference “Sensors Electronics and Microsystems Technology (SEMST-3), Ukraine, Odessa, 2-6 June, 2008. — “Astroprint”. — P. 254.
 9. A. Druzhinin, V. Holota, I. Kogut, S. Sapon, Y. Khoverko The Device-Technological Simulation of The Field-Emission Micro-Cathods Based on Three-Demensional SOI-Structures // ECS Transactions (The Electrochemical Society). — 2008. — Vol. 14, № 1. — P. 569-580.
 10. A. Druzhinin, I. I. Mariamova, I. T. Kogut, Y. M. Khoverko. Physical sensors on the base of “silicon on insulator” structure with recrystallized polysilicon film // Sensors Electronics and Microsystems Technology. — 2008. — №4. — P. 17-26.
 11. A. Druzhinin, I. I. Mariamova, A. P. Kuytakov, I. V. Pavlovskiy Resistive strain sensor on the base of thread-like silicon crystals for low temperatures// Technology and design in electron apparatus — 2008. — № 4(76). — P. 26-30.
 12. Inessa Bolshakova, Yaroslav Kost, Elena Makido, Fedor Shurygin. Mathematical simulation, synthesis, characterization and application of indium arsenide whiskers. // Journal of Crystal Growth — 2008. — Vol. 310, Issues 7-9. — P. 2254-2259.
 13. Murari A., Edlington T., Angelone M., Bertalot L., Bolshakova I., Bonheure G., Brzozowski J., Coccorese V., Holyaka R., Kiptily V., Lengar I., Morgan P., Pillon M., Popovichev S., Prior P., Prokopowicz R., Quercia A., Rubel M., Santala M., Shevelev A., Syme B., Vagliasindi G., Villari R., Zoita V. L., JET- EFDA Contributors. Measuring the radiation field and radiation hard detectors at JET: Recent developments // Nuclear Instruments and Methods in Physics Research A. — 2008. — Vol. 593. — P. 492-504.
 14. S. B. Ubizskii, L. P. Pavlyk, The Pendulum-like Fluxgate Magnetic Field Sensor // Sensors and Actuators, A—Physical. — 2008. — Vol. 141/2. — PP. 440-446.
 15. S. B. Ubizskii, L. P. Pavlyk, The fluxgate wide-band response detection using correlation processing / in: Modern Problems of Radio Engineering, Telecommunications and Computer Science. Proceedings of the International Conference TCSET 2008. — Lviv — 2008, P. 33-34.
 16. Stakhira P. I., Cherpak V. V., Gotra Z. Yu. Investigation of electrical and photodiode characteristics of organic structure on the base of nickel phthalocyanine film doped with oxygen and constructed on flexible electroconductive substrate // Optoelectronic information-power technologies. — 2008. — №1(15). — P. 134-138.
 17. E. Atanassova, R. V. Konakova, V. F. Mitin, D. Spasov, O. S. Lytvyn, V. V. Shynkarenko. Microwave Irradiation Effect on Ti-Doped Ta₂O₅ Stacked Capacitors. //Recent Patents on Electrical Engineering 2008. N1. P. 47-58.
 18. E. Atanassova, V. F. Mitin, R. V. Konakova, D. Spasov, V. V. Shynkarenko. Microwave irradiation impact on Ta₂O₅ stack capacitors with different gates. // Semicond. Sci. Technol. 2008. v. 23. 035004 (10 pp).
 19. E. Yu. Kolyadina, R. V. Konakova, L. A. Matveeva, V. F. Mitin, V. V. Shynkarenko, E. Atanassova. Microwave induced structural-impurity ordering transition region in Ta₂O₅ stacks on Si. //SPQEO. 2008. v. 11. N4. P. 311-318.
 20. Yu. Yu. Bacherikov, R. V. Konakova, V. V. Milenin, O. B. Okhrimenko, A. M. Svetlichnyy, V. V. Poliakov Gadolinium, titanium and erbium oxide films on n-6H-SiC surface characteristics changes under influence of superhigh-frequency processing. //PhSS 2008. v.42. No 7. PP. 888-892.
 21. Yu. Yu. Bacherikov, N. L. Dmitruk, R. V. Konakova, O. S. Kondratenko, V. V. Milenin, O. B. Okhrimenko, L. M. Kapitanchuk, A. M. Svetlichnyy, N. N. Moskovchenko. Formation of titan oxide films on porous silicon carbide surface. // JTP. 2008. v. 78. No 9. PP. 130-133.
 22. Efanov O. M., Klad'ko V. P., Vachulin V. F., Molodkin V. B Dynamic diffraction of X-rays on multy-layer

- ered structures. (Monograph)-2008, Kiev: "Scientific thought"-223 p.
23. V. P. Klad'ko V. P., Slobod'an, V. F. Machulin Multi-layered structures curvature radius influence on X-rays diffraction specters//UPhJ,-2008. =V. 53. — No 2. — P. 167-171..
 24. Klad'ko V., Slobodian M., Machulin V. F. Macrodeformation influence on the three-dimensional quantum dots ordering in multilayer structures. // Phys. Stat. Sol. (A). — 2008, — V. 205, Issue 9, — P. 2167-2171.
 25. V. V. Dovganyuk, N. V. Litvinchuk V. V. Slobodjan, I. M. Fodchuk. Defect structure changes in the single Si-crystals after irradiation by high-energy electrons and long natural aging by high-resolution three-crystal X-ray diffractometry// Proc. of SPIE. — 2008. — V. 7008, 7008 (1B1-1B7).
 26. I. M. Fodchuk, M. D. Borcha, I. I. Kritsun, Ya. D. Garabazhiv, O. V. Kroitor, O. S. Kshevetsky, O. A. Tkach Multiwave coplanar diffraction of X-rays in crystals structural investigations// Metallophysics and the newest technologies. 2008. — 30, No 10. — P. 1280-1295.
 27. Fedortsov D., Fodchuk I. M., Novikov S., A. Struk X-ray images of dislocation loops and barriers in silicon crystals in the case of transmission geometry// Proc. of SPIE. — 2008. — V. 7008, 7008(A1-A5).
 28. V. A. Smyntyna, V. A. Borschak, M. I. Kutalova, N. P. Zatovskaya, A. P. Balaban. Application of notions of sensitometry to the solid-state image sensor based on nonideal heterojunction. // Proc. of EU-ROSENSORS XXII Conf- Dresden. — 7-10 Sep. — 2008. — P. 58.
 29. V. A. Borshchak. A. P. Balaban. The comparative analysis of characteristics and typical photographic materials parameters and a solid-state memory element. //Sensor Electronics and Microsystems Technologies. — 2008. — No 1. — PP. 44-48.
 30. Smyntyna V. A., Filevskaya L. N., Grinevich V. S. Influence precursor content on tin dioxide nanostructured films optical properties//Book of abstracts of the 3-rd International Scientific and Technical Conference "Sensors Electronics and Microsystems Technology (SEMST-3), Ukraine, Odessa, 2-6 June, 2008. — "Astroprint". — P. 308.
 31. Belyaev O. E., Lepikh Ya. I., Kazantseva Z. I., Koshets I., Olikh Ya. M., Snigur P. O., Kal'chenko V. I. Calixarene compound films for detecting acetone and ammonia//Book of abstracts of the 3-rd International Scientific and Technical Conference "Sensors Electronics and Microsystems Technology (SEMST-3), Ukraine, Odessa, 2-6 June, 2008. — "Astroprint". — P. 212..
 32. Lepikh Ya. I., Smyntyna V. A., Snigur P. O., Olikh Ya. M. Germanium coordination compounds — structure, properties and possible applications//Journal of physics: Conference Series 76 (2007) 012050. doi:10.1088/1742-6596/76/1/012050.
 33. Lepikh Ya. I., Belyaev O. E., Kazantseva Z. I., Koshets I., Olikh Ya. M., Snigur P. O., Kal'chenko V. I. Calixarene compound structural and adsorption properties// "Sensors Electronics and Microsystems Technology" 2008. — No 4. — PP. 33-35.
 34. Lepikh Ya. I., Smyntyna V. A. Development and investigation semiconductor materials and complex compounds perspective for photonics// Book of abstracts of International scientific seminar "Electronics Modern problems", 31. 01. — 1. 02. 2008. — Publisher center of Lvov I. Franko Nation. Un., Lvov. — 2008. — PP. 55-56.
 35. Lepikh Ya. I. Sensors electronics — the key direction in informational systems and technologies development//"Sensors Electronics and Microsystems Technology". — 2008. — No 3. — PP. 7-10.
 36. Lepikh Ya., Litovchenko V., Machulin V., Smyntyna V. Sensor electronics — the state and the development perspective// Vesnik NASU. — 2008. — No 8. — PP. 54-56,

ФІЗИЧНІ, ХІМІЧНІ ТА ІНШІ ЯВИЩА, НА ОСНОВІ ЯКИХ МОЖУТЬ БУТИ СТВОРЕНІ СЕНСОРИ

PHYSICAL, CHEMICAL AND OTHER PHENOMENA, AS THE BASES OF SENSORS

PACS 32.15RM;
UDC 539.184

SENSING FORBIDDEN TRANSITIONS IN SPECTRA OF SOME HEAVY ATOMS AND MULTICHARGED IONS: NEW THEORETICAL SCHEME

T. A. Florko¹, A. V. Loboda², A. A. Svinarenko¹

¹Odessa State Environmental University, Odessa

²I. I. Mechnikov Odessa National University, Odessa

SENSING FORBIDDEN TRANSITIONS IN SPECTRA OF SOME HEAVY ATOMS AND MULTICHARGED IONS: NEW THEORETICAL SCHEME

T. A. Florko, A. V. Loboda, A. A. Svinarenko

Abstract. It has been carried out sensing and calculating the energies and oscillator strengths of some forbidden atomic transitions in spectra of heavy atoms and multicharged ions on the basis of new relativistic scheme within gauge-invariant quantum electrodynamics (QED) perturbation theory (PT).

Keywords: sensing forbidden atomic transitions, heavy atoms and multicharged ions, new relativistic approach

ВИЗНАЧЕННЯ ЗАБОРОНЕНИХ ПЕРЕХОДІВ У СПЕКТРАХ ДЕЯКИХ ВАЖКИХ АТОМІВ ТА БАГАТОЗАРЯДНИХ ІОНІВ: НОВА ТЕОРЕТИЧНА СХЕМА

Т. О. Флорко, А. В. Лобода, А. А. Свинаренко

Анотація. Виконано розрахунок енергій, імовірностей та сил осциляторів заборонених атомних переходів у спектрах декотрих важких атомів та багатозарядних іонів на основі нової релятивістської схеми в межах калібровочно-інваріантної КЕД теорії збурень.

Ключові слова: детектування заборонених атомних переходів, важкі атоми та багатозарядні іони, нова релятивістська схема

ОПРЕДЕЛЕНИЕ ВЕРОЯТНОСТЕЙ ЗАПРЕЩЕННЫХ ПЕРЕХОДОВ В СПЕКТРАХ НЕКОТОРЫХ ТЯЖЕЛЫХ АТОМОВ И МНОГОЗАРЯДНЫХ ИОНОВ: НОВАЯ ТЕОРЕТИЧЕСКАЯ СХЕМА

T. A. Флорко, А. В. Лобода, А. А. Сви́наренко

Аннотация. Выполнен расчет вероятностей и сил осцилляторов запрещенных атомных переходов в спектрах некоторых сложных тяжелых атомов и многозарядных ионов на основе новой релятивистской схемы в рамках калибровочно-инвариантной КЭД теории возмущений.

Ключевые слова: детектирование запрещенных атомных переходов, тяжелые атомы и многозарядные ионы, новая релятивистская схема

1. Introduction

The experimental and theoretical studying of the radiation transition characteristics of a whole number of atomic systems, which are interesting and perspective from the point of view of the quantum electronics and photoelectronics, is in last years of a great importance (c.f.[1-27]). It is also very important for search the optimal candidates and conditions for realization of the X-ray lasing. Besides, the forbidden atomic transitions are attracting from the point of view of sensing new physics behind the well known standard model.

The well known multi-configuration Dirac-Fock (MCDF) approach is widely used in calculations of the atoms and ions. It provides the most reliable version of calculation for atomic systems. Nevertheless, as a rule, detailed description of the method for studying role of the relativistic, gauge-invariant contributions, nuclear effects is lacking. Serious problems are connected with correct definition of the high-order correlation corrections, QED effects etc. The further improvement of this method is connected with using the gauge invariant procedures of generating relativistic orbitals basis's and more correct treating the nuclear and QED effects [1-7]. In references [1-7] it has been developed a new ab initio approach to calculating spectra of atomic systems with account of relativistic, correlation, nuclear, QED effects, based on the gauge-invariant QED PT [4] and new effective procedures for accounting the nuclear and radiative corrections [5-7]. Here we use propose a new relativistic scheme for determination and sensing the forbidden atomic transitions basing on the gauge-invariant QED perturbation theory formalism [5]. As object of studying the heavy atoms and Ne-, Zn-like multicharged ions are considered. one of the its versions [18] for calculating the Earlier it has been carried theoretic-

cal studying energy spectra, theoretical determination of the energies and oscillator strengths of some electric dipole transitions in spectrum of the rare-earth atom of Eu [27].

2. New relativistic approach to sensing and determination of the forbidden atomic transition probabilities

Let us describe in brief the important moment of our theoretical approach. As usually, the wave functions zeroth basis is found from the Dirac equation solution with potential, which includes the core ab initio potential, electric, polarization potentials of nucleus (the gaussian form for charge distribution in the nucleus is used). All correlation corrections of the PT second and high orders (electrons screening, particle-hole interaction etc.) are accounted for. The wavefunction for a particular atomic state

$$\Psi(\Gamma P J M) = \sum_r^{NCF} c_r \Phi(\gamma_r P J M) \quad (1)$$

is obtained as the above described self-consistent solutions of the Dirac-Fock type equations. Configuration mixing coefficients c_r are obtained through diagonalization of the Dirac Coulomb Hamiltonian

$$H_{DC} = \sum_i c \alpha_i p_i + (\beta_i - 1) c^2 - V_c(r|n l j) + V_{ex} - V_{nucl}(r|R) + \sum_{i>j} \exp(i\omega r_{ij}) (1 - \alpha_1 \alpha_2) / r_{ij} \quad (2)$$

In this equation the potential:

$$V(r) = V_c(r|n l j) + V_{ex} + V_{nucl}(r|R) \quad (3)$$

This potential includes the electrical and polarization potentials of the nucleus. The part V_{ex} accounts for exchange inter-electron interaction. The main exchange effect are taken into account in

the equation. The rest of the exchange-correlation effects are accounted for in first two PT orders by the total inter-electron interaction [4]. The effective electron core density (potential V_c) is defined by iteration algorithm within gauge invariant QED procedure [4].

Consider the one-quasiparticle system. A quasiparticle is a valent electron above the core of closed electron shells or a vacancy in the core. In the lowest second order of the EDPT a non-zero contribution to the imaginary part of electron energy $\text{Im } \Delta E$ (the radiation decay width) is provided by relativistic exchange Fock diagram. In the fourth order of the QED PT there are diagrams, whose contribution into the $\text{Im} \Delta E$ accounts for the core polarization effects. It is on the electromagnetic potentials gauge (the gauge non-invariant contribution). Let us examine the multielectron atom with one quasi-particle in the first excited state, connected with the ground state by the radiation transition. In the zeroth QED PT approximation we, as usually (c.f.[2-4]), use the one electron bare potential

$$V_N(r) + V_C(r), \quad (4)$$

with $V_N(r)$ describing the electric potential of the nucleus, $V_C(r)$, imitating the interaction of the quasi-particle with the core. The core potential $V_C(r)$ is related to the core electron density $\rho_C(r)$ in a standard way. The latter fully defines the one electron representation. Moreover, all the results of the approximate calculations are the functionals of the density $\rho_C(r)$. In ref.[4] the lowest order multielectron effects, in particular, the gauge dependent radiative contribution for the certain class of the photon propagator calibration is treated. This value is considered to be the typical representative of the electron correlation effects, whose minimization is a reasonable criterion in the searching for the optimal one-electron basis of the PT. The minimization of the density functional $\text{Im } \Delta E_{\text{iniv}}$ leads to the integral differential equation for the ρ_C , that can be solved using one of the standard numerical codes. In ref. [4] authors treated the function ρ_C in the simple analytic form with the only variable parameter b and substituted it to (6). More accurate calculation requires the solution of the integral differential equation for the ρ_C [21,26,27].

The probability is directly connected with imaginary part of electron energy of the system, which is defined in the lowest order of perturbation theory as follows:

$$\text{Im} \Delta E(B) = -\frac{e^2}{4\pi} \sum_{\substack{\alpha > n > f \\ [\alpha < n \leq f]}} V_{\alpha n \alpha n}^{|\omega_{\alpha n}|}, \quad (5)$$

where \sum – for electron and \sum – for vacancy. The potential V is as follows:

$$V_{ijkl}^{|\omega|} = \iint dr_1 dr_2 \Psi_i^*(r_1) \Psi_j^*(r_2) \frac{\sin|\omega|r_{12}}{r_{12}} \times \\ \times (1 - \alpha_1 \alpha_2) \Psi_k^*(r_2) \Psi_l^*(r_1). \quad (6)$$

The separated terms of the sum in (5) represent the contributions of different channels and a probability of the dipole transition is:

$$\Gamma_{\delta_n} = \frac{1}{4p} \cdot V_{\delta_n \alpha_n}^{|\omega_{\delta_n}|}. \quad (7)$$

The corresponding oscillator strength : $gf = \lambda_g^2 \cdot \Gamma_{\alpha_n} / 6.67 \cdot 10^{15}$, where g is the degeneracy degree, λ is a wavelength in angstroms (Å). Under calculating the matrix elements (5) one could use the angle symmetry of the task and write the expansion for potential $\sin|\omega|r_{12}/r_{12}$ on spherical functions as follows:

$$\frac{\sin|\omega|r_{12}}{r_{12}} = \frac{\pi}{2\sqrt{r_1 r_2}} \times \\ \times \sum_{\lambda=0}^{\infty} (\lambda) J_{\lambda+1/2}(|\omega|r_1) J_{\lambda+1/2}(|\omega|r_2) P_{\lambda}(\cos \mathbf{r}_1 \mathbf{r}_2), \quad (8)$$

where J – is the Bessell function of first kind and $(\lambda) = 2\lambda + 1$. This expansion is corresponding to usual multipole one for probability of radiative decay. Substitution of the expansion (7) to matrix element of interaction gives as follows:

$$V_{1234}^{\omega} = [(j_1)(j_2)(j_3)(j_4)] \times \\ \times \sum_{\lambda \mu}^{1/2} (-1)^{\mu} \begin{pmatrix} j_1 j_3 & \lambda \\ m_1 - m_3 & \mu \end{pmatrix} \times \text{Im } Q_{\lambda}(1234); \\ Q_{\lambda} = Q_{\lambda}^{\text{Quil}} + Q_{\lambda}^{\text{Br}}. \quad (9)$$

where j_i are the entire single electron momentums, m_i – their projections; $Q_{\lambda}^{\text{Quil}}$ is the Coulomb part of interaction, Q_{λ}^{Br} – the Breit part. The Coulomb part $Q_{\lambda}^{\text{Quil}}$ is expressed in terms of radial integrals R_{λ} , angular coefficients S_{λ} [2,5]:

$$\text{Re } Q_{\lambda}^{\text{Quil}} = \frac{1}{Z} \text{Re} \{ R_{\lambda}(1243) S_{\lambda}(1243) + \\ + R_{\lambda}(\tilde{1}24\tilde{3}) S_{\lambda}(\tilde{1}24\tilde{3}) + R_{\lambda}(1\tilde{2}\tilde{4}3) S_{\lambda}(1\tilde{2}\tilde{4}3) + \\ + R_{\lambda}(\tilde{1}\tilde{2}\tilde{4}\tilde{3}) S_{\lambda}(\tilde{1}\tilde{2}\tilde{4}\tilde{3}) \}. \quad (10)$$

As a result, the Auger decay probability is ex-

pressed in terms of $\text{Re}Q_\lambda(1243)$ matrix elements [9]:

$$\text{Re} R_\lambda(1243) = \iint dr_1 r_1^2 r_2^2 f_1(r_1) f_3(r_1) \times \\ \times f_2(r_2) f_4(r_2) Z_\lambda^{(1)}(r_2) Z_\lambda^{(1)}(r_2). \quad (11)$$

where f is the large component of radial part of single electron state Dirac function and function Z is [5]:

$$Z_\lambda^{(1)} = \left[\frac{2}{|\omega_{13}| \alpha Z} \right]^{\lambda+1/2} \frac{J_{\lambda+1/2}(\alpha |\omega_{13}| r)}{r^\lambda \Gamma(\lambda + 3/2)}. \quad (12)$$

The angular coefficient is defined by standard way [7]. The other items in (3) include small components of the Dirac functions; the sign “ \sim ” means that in (3) the large radial component f_i is to be changed by the small g_i one and the moment l_i is to be changed by $\tilde{l}_i = l_i - 1$ for Dirac number $\kappa_i > 0$ and $l_i + 1$ for $\kappa_i < 0$. The Breat interaction is known to change considerably the Auger decay dynamics in some cases (c.f. [5]). The Breat part of Q is defined as the sum:

$$Q_\lambda^{\text{Br}} = Q_{\lambda,\lambda-1}^{\text{Br}} + Q_{\lambda,\lambda}^{\text{Br}} + Q_{\lambda,\lambda+1}^{\text{Br}}, \quad (13)$$

where the contribution of our interest is determined as:

$$Q_\lambda^{\text{Br}} = \frac{1}{Z} \text{Re} \left\{ R_\lambda(12\tilde{4}3) S_\lambda'(12\tilde{4}3) + \right. \\ \left. + R_\lambda(\tilde{1}243) S_\lambda'(1243) + R_\lambda(\tilde{1}2\tilde{4}3) S_\lambda'(\tilde{1}2\tilde{4}3) + \right. \\ \left. + R_\lambda(\tilde{1}24\tilde{3}) S_\lambda'(\tilde{1}24\tilde{3}) \right\}. \quad (14)$$

Radial parts F and G of two components of the Dirac function for electron, which moves in the potential $V(r, R) + U(r, R)$, are defined by solution of the Dirac equations (PT zeroth order). All calculations are carried out using the effective Dirac-Superatom-ISAN code developed by Ivanov-Ivanova-Glushkov [1-6].

3. Results and conclusions

We have carried out sensing and calculating probabilities of the magnetic dipole (M1) and electric quadrupole (E2) forbidden transitions for Ne-, Zn-like multicharged ions ($Z=32-92$) and single ionized atom of Hg. In all calculations we used the Ivanov-Ivanova model potential [1] with defining its parameter within above described an initio QED procedure [2]. In fact this potential imitated the self-consistent Dirac-Fock potential. All details can

be found in refs. [1-6, 21]. In table 1,2 we present the energies and E2 probabilities of the $5d^9 6s^2(D_{5/2}, D_{3/2}) - 5d^{10} 6s(S_{1/2})$ transition in Hg^+ . For comparison we listed in this table the theoretical Hartree-Fock (HF), Dirac-Fock (DF) and DF (with fitting to experimental transition energies) values by Ostrovsky-Sheynerman and experimental data by Moore (NBS, Washington) [23-25]. In table 3 we present the oscillator strengths of the $4s^2(^1S_0) - 4s4p(^1P_1)$ transition in the Zn-like multicharged ions. The same calculation was carried out for Ne-like ions ($Z=22-92$). For comparison we listed in this table the theoretical Hartree-Fock (HF), Dirac-Fock (DF), DF (with fitting to experimental transition energies) and model potential (MP) data.

Table 1
The energies of the $5d^9 6s^2(D_{5/2}, D_{3/2}) - 5d^{10} 6s(S_{1/2})$ transition in Hg^+ (in Ry)

Method	E_{6s}	$D_{3/2} - S_{1/2}$	$D_{5/2} - S_{1/2}$
HF	-1.07	0.863	0.863
DF	-1.277	0.608	0.460
This work	-1.377	0.462	0.325
Experiment	-1.378	0.461	0.324

Table 2
The E2 probabilities of the $5d^9 6s^2(D_{5/2}, D_{3/2}) - 5d^{10} 6s(S_{1/2})$ transition in Hg^+ (in s^{-1})

Method	$D_{3/2} - S_{1/2}$	$D_{5/2} - S_{1/2}$
HF	1360	1360
DF	257.0	77.4
DF (exp. E)	63.9	13.3
This work	54.53	11.84
Experiment	53.5 ± 2.0	11.6 ± 0.4

In table 4 we present the M1 and E2 transitions probabilities in some Zn-like ions [23-25,28]. The detailed tables of the transitions energies and probabilities, oscillator strengths for Zn-like ($Z=32-92$) and Ne-like ($Z=22-92$) are presented in ref. [29].

Analysis of the obtained data allows to make the following conclusions. Firstly, one can see that our approach provides physically reasonable agreement with experiment and significantly more advantageous in comparison with standard Dirac-Fock method and the Hartree-Fock approximation approach. Secondly, we have checked that the results for oscillator strengths, obtained within our approach in different photon propagator gauges (Coulomb, Babushkon, Landau gauges) are practically equal, that is provided by using an effective QED energy procedure [4]. Thirdly, calculation has confirmed the great role of the interelectron correlation effects of the second and higher QED PT orders, namely,

effects of the interelectron polarization interaction and mutual screening.

Table 3
The oscillator strengths of $4s^2(^1S_0) - 4s4p(^1P_1^0)$ transition in the Zn-like ions

Ion	Method	f_L	f_V
Ga^+	DF	1.89	1.98
	HF	2.30	2.01
	DF2	1.97	1.95
	MP	1.68	1.73
	Our	1.862	1.861
	Exp.	1.85 ± 0.15	1.85 ± 0.15
As^{3+}	DF	1.87	1.86
	Our	1.575	1.574
	Exp.	1.56 ± 0.23	1.56 ± 0.23
Kr^{6+}	DF	1.75	1.71
Gd^{34+}	DF	1.12	1.10
Yb^{40+}	DF	1.12	1.10
Au^{40+}	DF	1.18	1.15
Pb^{52+}	DF	1.21	1.18
U^{62+}	DF	1.37	1.31
	HF	1.41	1.47
	Our	1.333	1.332
	Exp.	1.31 ± 0.05	1.31 ± 0.05

Table 4
The M1 and E2 transitions probabilities in some Zn-like ions: (a) $4s4p(^3P_2^0) \rightarrow 4s4p(^3P_1^0)$; (b) $4s4p(^1P_1^0) \rightarrow 4s4p(^3P_2^0)$ (our data)

Trans.	M1 (a)	E2 (a)	M1 (b)	E2 (b)
Kr^{6+}	0.072(1)	0.034(-2)	0.033(2)	0.041(1)
Cd^{18+}	0.048(4)	0.132(1)	0.055(4)	0.034(3)
Xe^{24+}	0.042(5)	0.025(3)	0.034(5)	0.232(3)
Gd^{34+}	0.081(6)	0.118(4)	0.047(6)	0.047(5)
Yb^{40+}	0.039(7)	0.399(5)	0.145(6)	0.026(6)
Zn	0.028(8)	0.104(6)	0.119(7)	0.029(7)
Pb^{52+}	0.047(8)	0.067(7)	0.215(7)	0.058(7)
U^{62+}	0.036(9)	0.059(8)	0.128(8)	0.101(8)

References

- Ivanova E. P., Ivanov L. N. Modern Trends in Spectroscopy of Multicharged Ions// Physics Rep. — 1991. — Vol. 166,N6. — P. 315-390.
- Glushkov A. V., Ivanova E. P. Theoretical Study of Multicharged Ions Spectra of F- and Ne- Isoelectronic Sequence// J. Quant. Spectr. Rad. Transfer. — 1986. — Vol. 36, N2. — P. 127-145.
- Ivanova E. P., Ivanov L. N., Glushkov A. V., Kramida

- A. E. High order corrections in the Relativistic Perturbation Theory with the model Zeroth Approximation, Mg-like and Ne-like ions //Phys. Scripta — 1985. — Vol. 32,N4. — P. 512-524.
- Glushkov A. V., Ivanov L. N. Radiation Decay of Atomic States: atomic residue and gauge non-invariant contributions // Phys. Lett. A. — 1992. — Vol. 170,N1. — P. 33-37
- Glushkov A. V., Relativistic quantum theory. Quantum mechanics of atomic systems. — Odessa: Astroprint, 2008. — 900P.
- Glushkov A. V., Lovett L., Florko T. A., et al, Gauge-invariant QED perturbation theory approach to studying the nuclear electric quadrupole moments, hyperfine structure constants for heavy atoms and ions// Frontiers in Quantum Systems in Chemistry and Physics (Springer). — 2008. — Vol. 18. — P. 505-522.
- Sobel'man I. I. Introduction to theory of atomic spectra. — Moscow: Nauka, 1977.
- Bunyakova Yu. Ya., Florko T. A., Glushkov A. V., Prepelitsa G. P., Laser photoemission analysis of the fractal parameters for aerosol environment: New data processing system// Photoelectronics. — 2006. — N15. — P. 48-50.
- Bieron J., Froese-Fischer C., Fritzsche S., Pachucki K., Lifetime and hyperfine structure of the 3D_2 state of radium//J. Phys. B:At. Mol. Opt. Phys. — 2004. — Vol. 37. — P. L305–311
- Khetselius O. Y., Hyperfine structure of radium// Photoelectronics. — 2005. — Vol. 14. — P. 83-85.
- Gurnitskaya E. P., Heavy ion storage ring experimental and theoretical determination of the lifetimes for the iron ion levels// Photoelectronics. — 2005. — Vol. 14. — P. 50-54.
- Glushkov A. V., Ambrosov S. V., Loboda A. V., Gurnitskaya E. P., Khetselius O. Yu., QED calculation of heavy multicharged ions with account for correlation, radiative and nuclear effects// Recent Advances in Theor. Phys. & Chem. Systems. — 2006. — Vol. 15. — P. 285-300.
- Ostrovsky V. N., Sheynerman S. A. Radiation transitions in the external shells of ion Hg^+ // Opt. Spectr. — 1989. — Vol. 67. — P. 16-22.
- Dorofeev D. L., Zon B. A., Kretinin I. Y., Chernov V. E., Method of the Quantum Defect Green's Function for Calculation of Dynamic Atomic Polarizabilities// Opt. Spectr. — 2005. — Vol. 99. — P. 540-548.
- Sahoo B. K., Gopakumar G., Chaudhuri R. K., Das B. P., Merlitz H., Mahapatra U. S., Makherjee D., Magnetic dipole hyperfine interactions in $^{137}Ba^+$ and the accuracies of neutral weak interaction matrix elements//Phys. Rev. A-2003. — Vol. 68. — P. 040501.
- Derevianko A., Porsev S. G., Dressing lines and vertices in calculations of matrix elements with the coupled-cluster method and determination of

- Cs atomic properties// Phys. Rev. A. — 2005. — Vol. 71. — P. 032509.
17. Safronova U. I., Safronova M. S., Third-order relativistic many-body calculations of energies, transition rates, hyperfine constants, and blackbody radiation shift in $^{171}\text{Yb}^+$ //Phys. Rev. A. — 2009. — Vol. 79. — P. 022512.
 18. Glushkov A. V., Relativistic calculation and extrapolation of oscillator strengths in Fr-like ions by model potential method// Opt. Spectr. — 1991. — Vol. 70. — P. 952-955.
 19. Glushkov A. V., New method of accounting for polarization effects in determination of probabilities of the atomic transitions// Opt. Spectr. — 1991. — Vol. 71. — P. 395-397.
 20. Glushkov A. V., Relativistic calculation of oscillator strengths in multicharged ions with single electron above closed shells core// Opt. Spectr. — 1992. — Vol. 72. — P. 542-547..
 21. Glushkov A. V., Florko T. A., Gauge-invariant QED perturbation theory in determination of the oscillator strengths for dipole transitions in spectra of the rare-earth elements// Preprint of I. I. Mechnikov Odessa National University. Institute of Physics: Ph-L-3. — Odessa: 2006. — 25p.
 22. Kotochigova S. A., Identification of VUV absorption spectrum of EuI 1. Calculation of $4f^75d(^9D)np$ -states//Opt. Spectr. — 1983. — Vol. 55. — P. 422-428.
 23. Anderson E. K., Anderson E. M., Calculation of some E1,E2,E3,M1,M2 transitions in the isoelectronic sequence of Zn//Opt. Spectr. — 1983. — Vol. 54. — P. 955-960.
 24. Kunisz M. D., Coulomb approximation oscillator strengths for some transitions in rare earths// Acta Phys. Polon. — 1982. — Vol. a62. — P. 285-296.
 25. Ostrovsky V. N., Sheynerman S. A., Radiation transitions in the external shells of Hg^+ ion //Opt. Spectr. — 1989. — Vol. 67. — P. 16-22.
 26. Glushkov A. V., Malinovskaya S. V., Ambrosov S. V. Spectroscopy of Neutral and Highly-ionized Atoms: Calculation of the Oscillator Strengths for Na- and Fr-like Ions// Atomic Spectra and Oscillator Strengths for Astrophysical and Laboratory Plasmas (Proc. 5th International Colloquium on ASO-SALP). — Meudon: Publications de l'Observatoire de Paris. — 1996. — P. 96-97.
 27. Florko T. A., Theoretical determination of oscillator strengths of some transitions in the rare-earth atom of Eu//Photoelectronics. — 2007. — N16. — P. 86-90.
 28. Ivanova E. P., Gulov A. V. Theoretical investigation of the neon isoelectronic sequence// Atom. Data. Nucl. Data. Tabl. — 1991. — Vol. 49. — P. 1-64.
 29. Florko T. A., Svinarenko A. A., Tables of the transitions energies and probabilities, oscillator strengths for Zn-like ($Z=32-92$ and Ne-like ($Z=22-92$)) // e-Preprint of I. I. Mechnikov Odessa National University. Institute of Physics: Ph-L-1. — Odessa: 2008. — 52p.

PACS: 12.20.-M; 31.15.AR; 31.25,-V; 31.30.JV; 32.10.FN
UDC 539.184

SENSING STRONG INTERACTION EFFECTS IN SPECTROSCOPY OF HADRONIC ATOMS

D. E. Sukharev², O. Yu. Khetselius¹, Yu. V. Dubrovskaya²

¹I. I. Mechnikov Odessa National University, Odessa

²Odessa State Environmental University, Odessa

SENSING STRONG INTERACTION EFFECTS IN SPECTROSCOPY OF HADRONIC ATOMS

O. Yu. Khetselius, D. E. Sukharev, Yu. V. Dubrovskaya

Abstract. The theoretical studying the strong interaction shifts and widths from X-ray spectroscopy of kaonic atoms is fulfilled. Sensing the strong interaction effects and theoretical estimating spectra of kaonic atomic systems can be considered as a new tool for studying nuclear structure and strong K-nucleus interaction.

Keywords: strong interaction effects, spectroscopy, kaonic atoms

ДЕТЕКТУВАННЯ ЕФЕКТІВ СИЛЬНОЇ ВЗАЄМОДІЇ У СПЕКТРОСКОПІЇ АДРОННИХ АТОМІВ

О. Ю. Хецелиус, Д. Є. Сухарев, Ю. В. Дубровська

Анотація. Виконано теоретичну оцінку зсувів і ширин рівнів, які обумовлені ефектами сильної взаємодії, в межах рентгенівської спектроскопії каонних атомів. Детектування ефектів сильної взаємодії і теоретична оцінка спектрів каонних атомів є одним з нових підходів до визначення ядерної структури і параметрів сильної каон- ядерної взаємодії.

Ключові слова: ефекти сильної взаємодії, спектроскопія, каонні атоми

ДЕТЕКТИРОВАНИЕ ЭФФЕКТОВ СИЛЬНОГО ВЗАИМОДЕЙСТВИЯ В СПЕКТРОСКОПИИ АДРОННЫХ АТОМОВ

О. Ю. Хецелиус, Д. Е. Сухарев, Ю. В. Дубровская

Аннотация. Выполнена теоретическая оценка сдвигов и ширин уровней, обусловленных эффектами сильного взаимодействия, в рамках рентгеновской спектроскопии каонных атомов. Детектирование эффектов сильного взаимодействия и оценка спектров каонных атомов являются одним из новых подходов к определению ядерной структуры и параметров сильного каон-ядерного взаимодействия.

Ключевые слова: эффекты сильного взаимодействия, спектроскопия, каонные атомы

1. Introduction

In last years studying the exotic hadronic atomic systems such as kaonic and pionic atoms are of a great interest for further development of atomic and nuclear theories as well as new tools for sensing the nuclear structure and fundamental kaon, pion-nucleus strong interactions. Besides, studying these

systems is very important for further check of the Standard model [1-16]. In the last few years transition energies in pionic [1] and kaonic atoms [2] have been measured with an unprecedented precision. The spectroscopy of kaonic hydrogen allows to study the strong interaction at low energies by measuring the energy and natural width of the

ground level with a precision of few meV [1-5]. Besides, light kaonic atoms can additionally be used to define new low-energy X-ray standards [1] and to evaluate the kaon (pion) mass using high accuracy X-ray spectroscopy. The collaborators of the E570 experiment [6,7] measured X-ray energy of a kaonic helium atom, which is an atom consisting of a kaon (a negatively charged heavy particle) and a helium nucleus. Batty et al [4] had performed theoretical and experimental studying the strong- interaction effects in spectra of high Z kaonic atoms. These authors had applied the naive phenomenological optical model estimates. Now new exciting experiments are being prepared in order to make sensing the strong interaction effects in other hadronic atomic systems. The studies of the low-energy kaon-nuclear strong interaction with strangeness have been performed by measurements of the kaonic atom X-rays with atomic numbers $Z=1-92$ [1]. It is known that the shifts and widths due to the strong interaction can be systematically understood using phenomenological optical potential models. Nevertheless, one could mention a large discrepancy between the theories and experiments on the kaonic helium 2p state. A large repulsive shift (about -40 eV) has been measured by three experimental groups in the 1970's and 80's, while a very small shift (< 1 eV) was obtained by the optical models calculated from the kaonic atom X-ray data with $Z>2$ [1-6]. This significant disagreement (a difference of over 5 standard deviations) between the experimental results and the theoretical calculations is known as the "kaonic helium puzzle". A possible large shift has been predicted using the model assuming the existence of the deeply bound kaonic nuclear states. However, even using this model, the large shift of 40 eV measured in the experiments cannot be explained. A re-measurement of the shift of the kaonic helium X-rays is one of the top priorities in the experimental research activities. In the theory of the kaonic and pionic atoms there is an important task, connected with a direct calculation of the X-ray transition energies within consistent relativistic quantum mechanical atomic and nuclear theory methods. The standard way is based on solution of the Klein-Gordon equation, but there are many important problems connected with accurate accounting for as kaon-nuclear strong interaction effects as QED radiative corrections (firstly, the vacuum polarization effect etc.) [1-5]. This topic has been a subject of intensive theoretical and experimental interest (see [12-22]). In the present paper an effective ab

initio approach to quantum Klein-Gordon equation calculation of X-ray spectra for multi-electron kaonic atoms with an account of the nuclear, radiative effects is proposed and the theoretical studying the strong interaction shifts and widths from X-ray spectroscopy of kaonic atoms is fulfilled. The level energies and energy shifts for these systems are estimated and in whole an analysis of the received data can be considered as a new tool for sensing the nuclear structure and strong kaon-nucleus interaction. The generalized optical potential model with correct defining the proton and neutron densities in a nucleus is used in direct definition of the strong interaction shifts and widths. It is carried out a detailed analysis of theoretical and experimental data on the strong interaction widths and shifts.

2. New quantum Klein-Gordon equation approach in the kaonic atoms theory

Let us describe the key moments of our new approach to quantum calculation of the spectra for multi-electron kaonic (pionic) atoms with an account of nuclear and radiative effects (more details applying to the multi-electron heavy atoms can be found in refs. [16-23]). It is well known that the relativistic dynamic of a spinless particle can be described by the Klein-Gordon equation. The electromagnetic interaction between a negatively charged spin-0 particle with a charge equal to $q=-e$ and the nucleus can be taken into account introducing the nuclear potential A_v in the KG equation via the minimal coupling $p_v \rightarrow p_v - qA_v$. The wave functions of the zeroth approximation for kaonic atoms are found from the Klein-Gordon equation [5]:

$$m^2 c^2 \Psi(x) = \left\{ \frac{1}{c^2} [i\hbar \partial_t + eV_0(r)]^2 + \hbar^2 \nabla^2 \right\} \Psi(x), \quad (1)$$

where \hbar is the Planck constant, c the velocity of the light and the scalar wavefunction $\Psi_0(x)$ depends on the space-time coordinate $x = (ct, r)$. Here it is considered a case of a central Coulomb potential $(V_0(r), 0)$. Usually, we consider here the stationary solution of Eq. (1). In this case, we can write:

$$\Psi(x) = \exp(-iEt / \hbar) \phi(x) \quad (2)$$

and Eq. (1) becomes:

$$\left\{ \frac{1}{c^2} [E + eV_0(r)]^2 + \hbar^2 \nabla^2 - m^2 c^2 \right\} \phi(x) = 0 \quad (3)$$

where E is the total energy of the system (sum of the mass energy mc^2 and binding energy ϵ_0). In prin-

ciple, the central potential V_o should include the central Coulomb potential, the vacuum-polarization potential as well as the kaon-nucleus strong interaction potential (optical model potential). Earlier we have calculated some characteristics of hydrogen-like and other multi-electron ions with using the nuclear charge distribution in the form of a uniformly charged sphere and Gaussian form (c.f. [19-21]). The advantage of the Gaussian form nuclear charge distribution is provided by using the smooth function instead of the discontinuous one as in the model of a uniformly charged sphere [22]. It is obvious that it simplifies the calculation procedure and permits to perform a flexible simulation of the real distribution of the charge in a nucleus. In last years to define the nuclear potential it is usually used the Fermi model for the charge distribution in the nucleus $\rho(r)$ (c.f.[21]):

$$c(r) = c_0 / \{1 + \exp[(r - c) / a]\} \quad (4)$$

where the parameter $a=0.523$ fm, the parameter c is chosen by such a way that it is true the following condition for average-squared radius: $\langle r^2 \rangle^{1/2} = (0.836 \cdot A^{1/3} + 0.5700)$ fm. Further let us present the formulas for the finite size nuclear potential and its derivatives on the nuclear radius. If the point-like nucleus has the central potential $W(R)$, then a transition to the finite size nuclear potential is realized by exchanging $W(r)$ by the potential [19]:

$$W(r|R) = W(r) \int_0^r dr' r'^2 \rho(r'|R) + \int_r^\infty dr' r'^2 W(r') \rho(r'|R). \quad (5)$$

We assume it as some zeroth approximation. Further the derivatives of various characteristics on R are calculated. They describe the interaction of the nucleus with outer electron; this permits recalculation of results, when R varies within reasonable limits. The Coulomb potential for the spherically symmetric density $\rho(r|R)$ is:

$$V_{nucl}(r|R) = -\left(\frac{1}{r}\right) \int_0^r dr' r'^2 \rho(r'|R) + \int_r^\infty dr' r' \rho(r'|R) \quad (6)$$

It is determined by the following system of differential equations [19]:

$$V'_{nucl}(r,R) = \left(\frac{1}{r^2}\right) \int_0^r dr' r'^2 \rho(r',R) \equiv \left(\frac{1}{r^2}\right) y(r,R)$$

$$y'(r,R) = r^2 \rho(r,R) \quad (7)$$

$$c'(r) = (c_0 / a) \exp[(r - c) / a] \{1 + \exp[(r - c) / a]\}^2$$

with the boundary conditions:

$$V_{nucl}(0,R) = -4/(\pi r) \\ y(0,R) = 0, \quad (8)$$

$$c(0) = c_0 / \{1 + \exp[-c / a]\}$$

The new important topic is connected with a correct accounting the radiation QED corrections and, first of all, the vacuum polarization correction. Procedure for an account of the radiative QED corrections in a theory of the multi-electron atoms is given in detail in refs. [17-22]. Regarding the vacuum polarization effect let us note that this effect is usually taken into account in the first PT order by means of the Uehling potential:

$$U(r) = -\frac{2\alpha}{3\pi r} \int_1^\infty dt \exp(-2rt/\alpha Z) \times \\ \times \left(1 + \frac{1}{2t^2}\right) \frac{\sqrt{t^2 - 1}}{t^2} \equiv -\frac{2\alpha}{3\pi r} C(g), \quad (9)$$

where $g = \frac{r}{\alpha Z}$. In our calculation we usually use more exact approach. The Uehling potential, determined as a quadrature (9), may be approximated with high precision by a simple analytical function. The use of new approximation of the Uehling potential [21] permits one to decrease the calculation errors for this term down to 0.5 – 1%. Besides, using such a simple analytical function form for approximating the Uehling potential allows its easy inclusion into the general system of differential equations.

As it is well known, the nuclear absorption is defined by the strength of the strong interaction and overlapping the kaonic atomic wave function with the nuclear ones. The widespread approach to treating the strong interaction between the nucleus and orbiting kaon is in using the phenomenological optical potential of the following form [1,5,10]:

$$V_N = -\frac{2\pi}{\mu} \left[1 + \frac{M_K}{M_N}\right] [A_{Kp} \rho_p(r) + A_{Kn} \rho_n(r)], \quad (10)$$

where μ is the kaon-nucleus reduced mass, M_K and M_N are the kaon and nucleon masses, $\rho_p(r), \rho_n(r)$ are the proton and neutron densities in the nucleus and A_{Kp}, A_{Kn} are the corresponding complex effective Kp and Kn scattering lengths. It is well known the Batty simplifying assumption of the following kind [4]:

$$V_N = -\frac{2\pi}{\mu} \left[1 + \frac{M_K}{M_N} \right] [a\rho(r)],$$

where a is the effective averaged K-nucleon scattering length. Batty et al had analyzed the previous kaon data and found the acceptable value for the a length is as follows [4]:

$$a = [(0.34 \pm 0.03) + i(0.84 \pm 0.03)] \text{ (fm)}.$$

The presented value of the length a has been indeed chosen to describe the low and middle Z nuclei [4]. The disadvantage of the usually used approach is connected with approximate definition of the proton and neutron densities and using the effective averaged K-nucleon scattering length. More correct approach is in the relativistic mean-field (RMF) model for the ground-state calculation of the nucleus. Though we have no guaranty that these wave-functions yield a close approximation to nature, the success of the RMF approach supports our choice [24]. These wave functions do not suffer from known deficiencies of other approaches, e.g., the wrong asymptotics of wave functions obtained in a harmonic oscillator potential. The RMF model has been designed as a renormalizable meson-field theory for nuclear matter and finite nuclei [24]. The realization of nonlinear self-interactions of the scalar meson led to a quantitative description of nuclear ground states. As a self-consistent mean-field model (for a comprehensive review see ref. [22-24]), its ansatz is a Lagrangian or Hamiltonian that incorporates the effective, in-medium nucleon-nucleon interaction. Recently [22] the self-consistent models have undergone a reinterpretation, which explains their quantitative success in view of the facts that nucleons are composite objects and that the mesons employed in RMF have only a loose correspondence to the physical meson spectrum. They are seen as covariant Kohn-Sham schemes and as approximations to the true functional of the nuclear ground state. As a Kohn-Sham scheme, the RMF model

can incorporate certain ground-state correlations and yields a ground-state description beyond the literal mean-field picture. RMF models are effective field theories for nuclei below an energy scale of 1 GeV, separating the long- and intermediate-range nuclear physics from short-distance physics, involving, i.e., short-range correlations, nucleon form factors, vacuum polarization etc, which is absorbed into the various terms and coupling constants. As it is indicated in refs.[24] the strong attractive scalar (S : -400 MeV) and repulsive vector (V : +350 MeV) fields provide both the binding mechanism ($S + V$: -50 MeV) and the strong spin-orbit force ($S - V$: -750 MeV) of both right sign and magnitude. In our calculation we have used so called NL3-NLC (see details in refs. [24]), which is among the most successful parameterizations available.

3. Results and conclusions

In ref. [5] we have presented some calculations for a selection of kaonic atom transitions. Such calculations are obtained solving numerically the Klein-Gordon equation using the effective Dirac Superatom code developed by Ivanov et al [16-21] that has been modified to include spin-0 particles case, even in the presence of electrons [1]. The kaon mass was assumed to be 493.677 ± 0.013 MeV [11]. In table 1 we present the calculated electromagnetic (EM) X-ray energies of kaonic atoms for transitions between circular levels. The transitions are identified by the initial (n_i) and final (n_f) quantum numbers. The calculated values of transition energies are compared with available measured (E_m) and other calculated (E_c) values [1-7]. In a case of the close agreement between theoretical and experimental data, the corresponding levels are less sensitive to strong nuclear interaction. In the opposite case one could point to a strong-interaction effect in the exception cited above.

Table 1

Calculated (E_c) and measured (E_m) kaonic atoms X-ray energies (in keV)

Nucl.	Transition	E_c , our theor	E_c , [4]	E_c [6]	E_c [7]	E_m
W	8-7	346.572	346.54	-	-	346.624(25)
W	7-6	535.136	535.24	-	-	534.886(92)
Pb	8-7	426.174	426.15	-	-	426.221(57)
U	8-7	538.528	538.72	538.013	537.44	538.315(100)

In table 2 we present the calculated (C) and measured (M) strong interaction shifts ΔE and widths G (in keV) for the kaonic atoms X-ray transitions. The

subscripts M and C stands for measured and calculated values correspondingly. The width G is the strong width of the lower level which was obtained by

subtracting the electromagnetic widths of the upper and lower level from the measured value. The shift ΔE is defined as difference between the measured E_M and calculated E_{EM} (electromagnetic) values of transition energies; the calculated value is obtained by direct solving the equation (1) with kaon-nuclear

potential. Besides, the measured values by Miller et al and Cheng et al (from refs. [1,4] are listed in table 2 too. It should be noted that Cheng et al did not make any energy calibration above the 511 e⁺ annihilation and Batty et al [4] indicated that the corresponding difference between the energy values is not serious.

Table 2

Calculated (C) and measured (M) strong interaction shifts ΔE and widths G for the kaonic atoms X-ray transitions: a- the shift was estimated with Miller et al measured energy (see [1]); b — the shift was estimated with Cheng et al measured energy (see [1]); c — the shift by Batty et al [4]; d — this work;

Nucl	ΔE_C (d)	G_C (d)	ΔE_C (c)	G_C (c)	ΔE_M	G_M
W, 8-7	0.038	0.072	-0.003	0.065	0.079 ^c 0.052 ^d	0.070 (15)
W, 7-6	-0.294	3.85	-0.967	4.187	-0.353 ^c -0.250 ^d	3.72 (35)
Pb, 8-7	0.035	0.281	-0.023	0.271	0.072 ^c 0.047 ^d	0.284 (14) 0.370 (150) ^a
U, 8-7	-0.205	2.620	-0.189	2.531	0.120 ^a 0.032 ^b -0.40 ^c -0.213 ^d	2.67(10) 1.50 (75) ^a

From the other side, more correct definition of proton and neutron densities is of a great importance for physically reasonable agreement between the measured and calculated (this work) shifts and widths. In whole we can conclude that the measured strong interaction parameters are reasonably well reproduced by present theory. To understand further information on the low-energy kaon-nuclear interaction, new experiments to determine the shift and width of kaonic atoms are now in preparation in J-Parc and in LNF, respectively (look, for example, refs. [1,8]).

References

1. Deloff A., Fundamentals in Hadronic Atom Theory, Singapore: World Scientific, 2003. — 352P.
2. Hayano R. S., Hori M., Horvath D., Widman E., Antiprotonic helium and CPT invariance//Rep. Prog. Phys. — 2007. — Vol. 70. — P. 1995-2065.
3. Deslattes R., Kessler E., Indelicato P., de Billy L., Lindroth E., Anton J., Exotic atoms//Rev. Mod. Phys. — 2003. — Vol. 75. — P. 35-70.
4. Batty C. J., Eckhause M., Gall K. P., et al. Strong interaction effects in high Z- K⁻ atoms//Phys. Rev. C. — 1989. — Vol. 40. — P. 2154-2160.
5. Khetselius O. Yu., Turin A. V., Sukharev D. E., Florko T. A., Estimating of X-ray spectra for kaonic atoms as tool for sensing the nuclear structure// Sensor Electr. and Microsyst. Techn. — 2009. — N1. — P. 30-35.
6. Okada S., Beer G., Bhang H., et al, Precision measurement of the 3d→2p x-ray energy in kaonic ⁴He// Phys. Lett. B. — 2007. — Vol. 653, N 5-6. — P. 387-391.
7. Ito T. M., Hayano R. S., Nakamura S. N., Terada T. P., Observation of kaonic hydrogen atom x rays// Phys. Rev. C. — 1998. — Vol. 58. — P. 2366 — 2382
8. Ishiwatari T. on behalf of the SIDDHARTA Collaboration, Silicon drift detectors for the kaonic atom X-ray measurements in the SIDDHARTA experiment// Nucl. Instr. and Methods in Physics. Research Sec. A. Accelerators, Spectrometers, Detectors and Associated Equipment. — 2007. — Vol. 581,N1-2. — P. 326-329.
9. Glushkov A. V., Makarov I. T., Nikiforova E. S., Pravdin M. I., Sleptsov I. Ye., Muon component of EAS with energies above 10¹⁷eV//Astropart. Phys. — 1995. — Vol. 4. — P. 15-22
10. Glushkov A. V., Khetselius O. Yu., Gurnitskaya E. P., Loboda A. V., Sukharev D. E., Relativistic Quantum Chemistry of Heavy Ions and Hadronic Atomic Systems: Spectra and Energy Shifts// Theory and Applications of Computational Chemistry (AIP). — 2009. — Vol. 1. — P. 131-134.
11. Santos J. P., Parente F., Boucard S., Indelicato P., Desclaux j. P., X-ray energies of circular transitions and electron scattering in kaonic atoms//Phys. Rev. A. — 2005. — Vol. 71. — P. 032501.
12. Mohr P. J. Quantum Electrodynamics Calculations in few-Electron Systems// Phys. Scripta. — 1993. — Vol. 46,N1. — P. 44-52.
13. Grant I., Relativistic Quantum Theory of Atoms and Molecules Theory and Computation, Springer Series

- on Atomic, Optical, and Plasma Physics. 2007. — Vol. 40. — P. 587–626.
14. Quiney H. M., Grant I. P. Partial-wave mass renormalization in atomic QED calculation // *Phys. Scripta T*. — 1993. — Vol. 46. — P. 132-138.
 15. Wilson S., *Recent Advances in Theoretical Physics and Chemistry Systems*//*Recent Advances in Theor. Phys. and Chem. Systems* (Springer). — 2006. — Vol. 15. — P. 11-45.
 16. Ivanova E. P., Ivanov L. N., Glushkov A. V., Kramida A. E. High order corrections in the Relativistic Perturbation Theory with the model Zeroth Approximation, Mg-like and Ne-like ions // *Phys. Scripta* — 1985. — Vol. 32,N4. — P. 512-524.
 17. Glushkov A. V., Energy Approach to Resonance states of compound super-heavy nucleus and EPPP in heavy nucleus collisions// *Low Energy Antiproton Phys. (AIP)*. — 2005. — Vol. 796. — P. 206-210.
 18. Glushkov A. V., Rusov V. D., Ambrosov S. V., Loboda A. V., Resonance states of compound super-heavy nucleus and EPPP in heavy nucleus collisions // *New Projects and New Lines of research in Nuclear physics*. Eds. Fazio G. and Hanappe F.: Singapore, World Sci. — 2003. — P. 142-154.
 19. Glushkov A. V., *Relativistic quantum theory. Quantum mechanics of atomic systems*, Odessa: Astroprint, 2008. — 900P.
 20. Glushkov A. V., Ambrosov S. V., Khetselius O. Yu., Loboda A. V., Gurnitskaya E. P., QED calculation of heavy multicharged ions with account for the correlation, radiative and nuclear effects// *Recent Advances in Theory of Phys. and Chem. Systems* (Springer). — 2006. — Vol. 15. — P. 285-300.
 21. Glushkov A. V., Khetselius O. Yu., Lovett L., et al, Gauge-invariant QED perturbation theory approach to calculating nuclear electric quadrupole moments, hyperfine structure constants for heavy atoms and ions// *Frontiers in Quantum Systems in Chemistry and Physics* (Springer). — 2008. — Vol. 18. — P. 505-522.
 22. Glushkov A. V., Lovett L., Khetselius O. Yu., Gurnitskaya E. P., Dubrovskaya Yu. V., Loboda A. V., Generalized multiconfiguration model of decay of multipole giant resonances applied to analysis of reaction (μ -n) on the nucleus ^{40}Ca //*International Journal of Modern Physics A. Particles and Fields*. — 2009. — Vol. 24. — P. 611-615.
 23. Glushkov A. V., Malinovskaya S. V., Dubrovskaya Yu. V., Vitavetskaya L. A., Quantum calculation of cooperative muon-nuclear processes: discharge of metastable nuclei during negative muon capture// *Recent Advances in Theory of Phys. and Chem. Systems* (Springer). — 2006. — Vol. 15. — P. 301-318.
 24. Serot B. D., Walecka J. D., *Advances in Nuclear Physics Vol. 16: The Relativistic Nuclear Many Body Problem*. Plenum Press, New York, 1986.

ОПТИЧНІ, ОПТОЕЛЕКТРОННІ І РАДІАЦІЙНІ СЕНСОРИ

OPTICAL, OPTOELECTRONIC AND RADIATION SENSORS

UDC 539.2:648.75

SENSITIVITY OF SILICON PHOTOVOLTAIC CONVERTERS TO THE LIGHT INCIDENCE ANGLE ON THEIR RECEIVING SURFACE

M. V. Kirichenko, V. R. Kopach, R. V. Zaitsev, S. A. Bondarenko

National Technical University "Kharkiv Polytechnical Institute",
21, Frunze Str., 61002, Kharkiv, Ukraine
e-mail: kirichenko_mv@mail.ru

SENSITIVITY OF SILICON PHOTOVOLTAIC CONVERTERS TO THE LIGHT INCIDENCE ANGLE ON THEIR RECEIVING SURFACE

M. V. Kirichenko, V. R. Kopach, R. V. Zaitsev, S. A. Bondarenko

Abstract. The results of output parameters dependences researches for multijunction silicon photovoltaic converters (PVC) upon solar radiation incidence angle on their receiving surface are presented. It has been shown that for improving of PVC efficiency is necessary to achieve the increased values of minority charge carriers lifetime in their base crystals as well as the optical reflection coefficient for metal/Si boundaries (interfaces) inside multijunction PVC, while for using multijunction PVC in the optical location systems the forced reduction of these values is reasonable.

Keywords: photoconverter, photovolt, light incidence angle, reflection coefficient, parameters

ЧУТЛИВІСТЬ КРЕМНІЄВИХ ФОТОЕЛЕКТРИЧНИХ ПЕРЕТВОРЮВАЧІВ ДО КУТА ПАДІННЯ СВІТЛА НА ЇХ ПРИЙМАЛЬНУ ПОВЕРХНЮ

М. В. Кіріченко, В. Р. Копач, Р. В. Зайцев, С. О. Бондаренко

Анотація. Наведено результати досліджень залежностей вихідних параметрів багатоперехідних кремнієвих фотоелектричних перетворювачів (ФЕП) від кута падіння сонячного випромінювання на їх приймальну поверхню. Показано, що для збільшення ККД ФЕП необхідно забезпечити підвищені значення часу життя неосновних носіїв заряду в базових кристалах та коефіцієнта оптичного відбиття від границь метал/Si всередині багатоперехідних ФЕП, у той час, як при використанні багатоперехідних ФЕП у системах оптичної локації визначення напрямку розповсюдження випромінювання доцільним є примусове зниження цих величин.

Ключові слова: фотоперетворювач, фотовольт, кут падіння світла, коефіцієнт відбиття, параметри

ЧУВСТВИТЕЛЬНОСТЬ КРЕМНИЕВЫХ ФОТОЭЛЕКТРИЧЕСКИХ ПРЕОБРАЗОВАТЕЛЕЙ К УГЛУ ПАДЕНИЯ СВЕТА НА ИХ ПРИЕМНУЮ ПОВЕРХНОСТЬ

М. В. Кириченко, В. Р. Копач, Р. В. Зайцев, С. А. Бондаренко

Аннотация. Приведены результаты исследований зависимостей выходных параметров многопереходных кремниевых фотоэлектрических преобразователей (ФЭП) от угла падения солнечного излучения на их приемную поверхность. Показано, что для увеличения КПД ФЭП необходимо обеспечить повышение значений величин времени жизни неосновных носителей заряда в базовых кристаллах и коэффициента оптического отражения от границ металл/Si внутри многопереходных ФЭП, в то время как при использовании многопереходных ФЭП в системах оптической локации целесообразным является принудительное снижение этих величин.

Ключевые слова: фотопреобразователь, фотовольт, угол падения света, коэффициент отражения, параметры

Introduction

The short circuit current density J_{sc} and open circuit voltage U_{oc} of photovoltaic converters (PVC) are increased with the intensity growth of illumination flux penetrating into the semiconductor base. It causes the expediency of concentrated solar radiation (CSR) using for increasing of such devices efficacy η , since $\eta \sim J_{sc} U_{oc}$ and $U_{oc} \sim \ln(J_{sc} / J_0)$, where J_0 — diode saturation current density [1-4].

One of the most favorable types of multi-junction Si-PVC specially created for the use in CSR conditions [3,4] named “photovolt”, represents a monolithic design from set (more than 10) of single crystal silicon flatly-parallel diode cells with p–n junctions oriented perpendicularly to reception surface and connected in-series by means of metal layers between the adjacent cells.

The essential advantages of considered PVC type at CSR conditions in comparison with single-junction Si-PVC of planar design p–n junction which is oriented parallel to reception surface, are: i) potential capability to much more effective conversion of CSR into electric energy and ii) generating 10–30 times greater output voltage. The last circumstance simplifies the problem of high-voltage photoelectric systems development and provides reduction of electrical energy losses in solar batteries interconnections as well as in electrical energy transmission line from solar batteries to the consumer.

Besides, the manufacturing of “photovolt” type PVC, the necessity of using of sufficiently expensive photolithography process disappears since on the receiving surface (in difference from planar design PVC [2]) crested or grid current-collecting electrode with narrow and thin ($\sim 10 \mu\text{m}$) streaky elements di-

vided by the gaps less than 1 mm is absent. However, it is necessary to take into account that the significant part of CSR goes to PVC receiving surface under the angle $\alpha > 0$ to it normal [5]. Therefore, J_{sc} , U_{oc} and efficacy should depend on α , as far as the irradiance E of PVC receiving surface changes with α according to the law $E = E_0 \cos \alpha$, where $E_0 = E$ at $\alpha = 0$ [6]. Therefore, the angular dependence of multi-junction Si-PVC output parameters minimization is one from the urgent problems with regard to creation of such type PVC with increased efficacy for the use at CSR conditions.

On the other hand in optical location systems the Si-PVC of “photovolt” type could be serious alternative to the well-known semiconductor radiation sensors requiring the external source of electrical energy. Thus in this case the angular dependence of J_{sc} and U_{oc} should be so more tangible as it possible.

In the present work the influence of single crystal Si-PVC “photovolt” design features on J_{sc} and U_{oc} dependence upon α was investigated in connection with practical importance of two above mentioned problems. Concerning to both problems simultaneously the greatest interest represents the $U_{oc}(\alpha)$ dependence owing to simplicity of this parameter measurement.

Experimental details

In connection with above mentioned the serial “photovolt” type Si-PVC with the area of receiving surface about 2 cm^2 manufactured on the basis of p-type conductivity single crystal silicon with resistivity about $10 \text{ Ohm}\cdot\text{cm}$ were investigated. Schematic

image of the samples is presented at Fig 1. Devices had overall dimensions $33 \text{ mm} \times 6 \text{ mm} \times 1 \text{ mm}$ and consisted from 35 elementary diode cells by thickness $150 \mu\text{m}$ everyone with $n^+ \text{-p-p}^+$ -structure which were connected in-series through the metal inter-layers by thickness about $10 \mu\text{m}$.

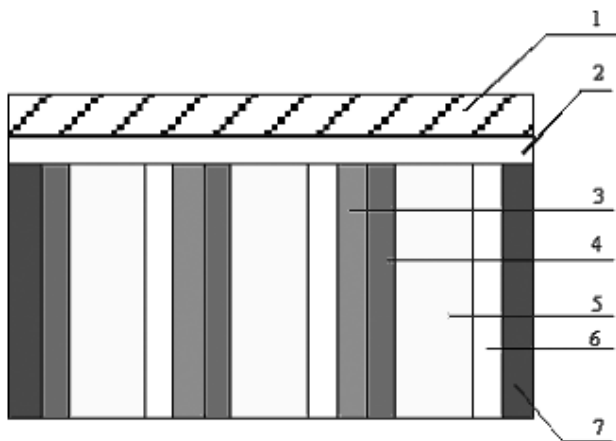


Fig. 1. Schematic image of “photovolt” type multi-junction Si-PVC cross-section: 1 — metal layer by thickness $t_m \approx 10 \mu\text{m}$; 2 — layer of n^+ -type conductivity silicon; 3 — layer of p-type conductivity silicon; 4 — layer of p^+ -type conductivity silicon; 5 — solid metal electrode.

Determination of J_{sc} and U_{oc} values for investigated Si-PVC was carried out by measurement and following analytical processing of loading illuminated current versus voltage characteristics LI CVC. The measurement of LI CVC was carried out similarly to [7] under the Si-PVC receiving surface irradiation power of 5712 W/m^2 , that corresponds to the degree of AM0 irradiation concentration equal to 4.2.

For light incidence angle α change on its surface the investigated Si-PVC was fixed on goniometer device allowing varying the angle α in the range from 0° up to 90° with the accuracy of 0.01° . Measurements of LI CVC were carried out at the following values of α : from 0° up to 20° with a step 2° ; from 20° up to 40° with a step 4° ; from 40° up to 60° with a step 5° ; also LI CVC were measured at angles $70^\circ, 80^\circ, 85^\circ$ and 90° . Temperature of samples 25°C at LI CVC measurements was supported with the help of the thermostat. The analytical processing of LI CVC realized similarly to [8].

Results and discussion

The normalized angular dependences of open circuit voltage $U_{oc}^{norm}(\alpha)$ (curve 1) and short circuit current $J_{sc}^{norm}(\alpha)$ (curve 2), calculated according to the

experimental values of the corresponding magnitudes in the following way: $J_{sc}^{norm}(\alpha) = J_{sc}(\alpha) / J_{sc}(\alpha = 0)$, $U_{oc}^{norm}(\alpha) = U_{oc}(\alpha) / U_{oc}(\alpha = 0)$, are presented

on the Figure 2. Earlier [9] it was shown that in the range of α values from 40° up to the Brewster angle φ_B (74.5° for silicon) trend of $U_{oc}^{norm}(\alpha)$ dependence is well described by the ratio $U_{oc}^{norm}(\alpha) \approx 1 + \frac{\ln[f(R, \alpha) \cos \alpha]}{2.3(\xi_2 - \xi_1)}$, where

$0 \leq f(R, \alpha) \leq 1$ is a correcting function, taking into account the real values of reflection coefficient from the metal/Si boundaries into “photovolt” type Si-PVC. In expanded form this ratio is presented in [9], where $\xi_1 < \xi_2$ are absolute values of indexes in degrees of short circuit current and diode saturation current densities, accordingly. As a result of analysis of such $U_{oc}^{norm}(\alpha)$ dependence it has been established that, varying parameters R and $\Delta\xi = \xi_2 - \xi_1$ it is possible to purposefully effect on its character. So, for example, it is necessary to maximally increase parameters R and $\Delta\xi$ for minimization of $U_{oc}^{norm}(\alpha)$ angular dependence with the purpose of “photovolt” type Si-PVC efficiency rising.

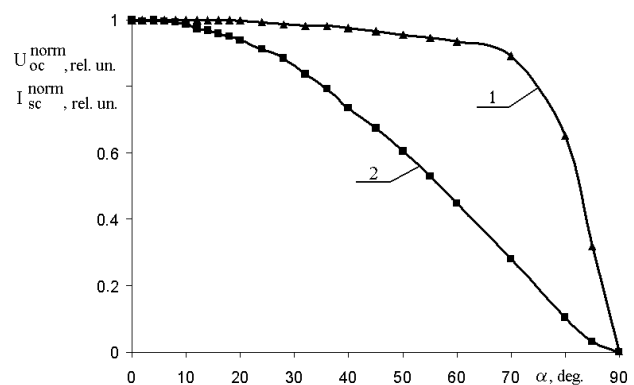


Fig. 2. Normalized values of open circuit voltage (1) and short circuit current density (2) versus light incidence angle on Si-PVC of “photovolt” type receiving surface.

In the present work it is suggested to using “photovolt” type Si-PVC as sensor in the optical location systems. Obviously, that for the successful solving of such problem the device, using in the specified capacity, must provide the possibility of output signal registration, and also to have the strikingly expressed, desirably linear, dependence of the registered parameter from the α angle. As follows from above stated, the characteristic peculiarity of “photovolt” type Si-PVC is high photovoltage that provides simple and reliable registration of this param-

eter. At the same time, from Fig. 2 evidently, that concerned “photovolt” type Si-PVC has the weakly expressed $U_{OC}^{norm}(\alpha)$ dependence in the range of light incidence angles on their receiving surface from 0 up to 74° . However, the results of work [9] let to suppose that varying parameters R and $\Delta\xi$ will allow to provide the strikingly expressed character of $U_{OC}^{norm}(\alpha)$ dependence.

Therefore, we carried out the numerical simulation of $U_{OC}^{norm}(\alpha) \approx 1 + \frac{\ln[f(R, \alpha)\cos\alpha]}{2.3\Delta\xi}$ dependence at $40^\circ \leq \alpha \leq 70^\circ$ for different values of R and $\Delta\xi$. Results of the simulation as a family of $U_{OC}^{norm}(\alpha, \Delta\xi)$ surfaces for different values of parameter R are presented at Fig. 3. From Fig. 3 it is evident, that varying of parameter R practically does not result in the varying $\frac{\partial U_{OC}^{norm}(\alpha)}{\partial \alpha}$ — speed of change U_{OC}^{norm} from α , but provides the change of U_{OC}^{norm} absolute value, i.e. this magnitude growth with R growing.

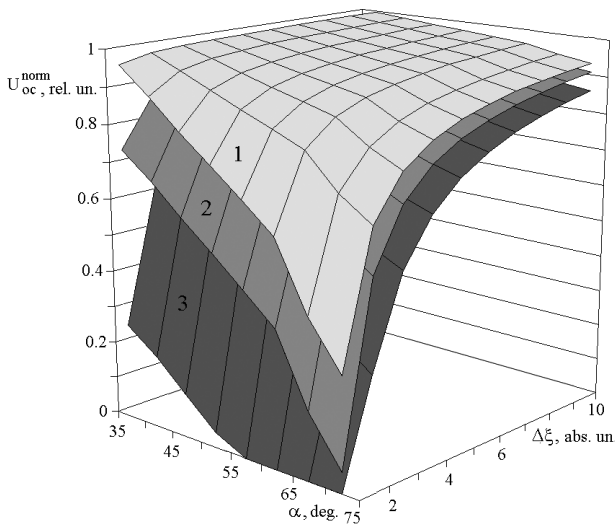


Fig. 3. Theoretical U_{OC}^{norm} values versus α and $\Delta\xi$ for considered Si-PVC of “photovolt” type at the light reflection coefficients from metal/silicon boundaries: 1 — $R = 1.0$; 2 — $R = 0.6$; 3 — $R = 0.2$.

At the same time, as it evidently from Figure 3, the determining influence on the $\frac{\partial U_{OC}^{norm}(\alpha)}{\partial \alpha}$ renders $\Delta\xi$ parameter, being the difference of J_{SC} and J_0 orders values. Really, from stated Figure evidently that by realization of situation, characteristic for concerned “photovolt” type Si-PVC, when $\Delta\xi \approx 7-8$, the value $\frac{\partial U_{OC}^{norm}(\alpha)}{\partial \alpha} \rightarrow 0$ as

well as on Figure 2 at $\alpha < 74^\circ$. However at decrease of difference between J_{SC} and J_0 , that corresponds to $\Delta\xi$ decrease, dependence of $U_{OC}^{norm}(\alpha)$ suffers substantial changes and at $\Delta\xi = 1-2$ obtains practically linear character in the concerned range of α angles with sufficiently large value $\frac{\partial U_{OC}^{norm}(\alpha)}{\partial \alpha} \approx -(7.3-14.6) \cdot 10^{-3}$ relat.un./deg.

Thus, the obtained results argues that in the case of using “photovolt” type Si-PVC as sensors in the optical location systems the U_{OC} sensitivity of such sensors to the light incidence angle on their receiving surface increased with decreasing of difference between J_{SC} and J_0 , characterized by parameter $\Delta\xi$. Value of the registered parameter U_{OC} increased with growth of reflection coefficient from metal/Si boundaries into “photovolt” type Si-PVC. At the same time it is necessary to take into account the technological difficulties of $R \rightarrow 1$ achievement in the conditions of Ukrainian Si-PVC production, and, also, that, as it evidently from Figure 3, the value of U_{OC}^{norm} less than at $R = 1$ only on 5% is provide at $R = 0.6$.

Therefore for using “photovolt” type Si-PVC as sensor in the optical location systems optimum is the next combination of parameters influencing on $U_{OC}^{norm}(\alpha)$ dependence: $\Delta\xi = 1-2$ and $R = 0.6$.

At the same time achievement of such reflection coefficient from the metal/Si boundaries into “photovolt” type Si-PVC offers no special complication in conditions of national Si-PVC production.

It is well known [1] that values of J_{SC} and J_0 , and consequently $\Delta\xi$, substantially depends from minority charge carriers lifetime $\tau_{n,p}$ in PVC base crystals. Therefore, the required value of $\Delta\xi$ at using such PVC as sensors, it is possible to achieve by a purposeful decrease of $\tau_{n,p}$ values in base crystals bulk. Since $\tau_{n,p} \sim N_r^{-1}$, where N_r is bulk concentration of recombination centers, then with above mentioned purpose the base crystals for such sensors in the process of appropriate devices manufacturing can be subject to thermal, mechanical or other types of processing directed at introduction in their bulk as greater as possible amount of recombination centers. It will be result in substantial decrease of $\tau_{n,p}$ value. A similar effect can be achieved and by using of heavily doped silicon single crystal for manufacturing of concerned sensors. Such silicon, intended for electronic industry, has small $\tau_{n,p}$ values due to high doping level.

Conclusions

The results of carried out experimental and theoretical researches of silicon photo-converters sensitivity to the light incidence angle on their receiving surface allow to make the following conclusions:

1. The character of $U_{oc}(\alpha)$ dependence for multi-junction “photovolt” type Si-PVC considerable depends on the minority charge carriers lifetime $\tau_{n,p}$ value in the PVC base crystal, while reflection coefficient R from metal/Si boundaries into PVC effects on absolute value of U_{oc} .

2. It has been shown that purposeful decrease of $\tau_{n,p}$ value and increase of R value will allow to create the PVC with practically linear and easily registered $U_{oc}(\alpha)$ dependence. Such character of $U_{oc}(\alpha)$ dependence will allow to use the multi-junction “photovolt” type Si-PVC as sensors in the optical location systems.

References

1. Blakers A.W., Smeltik J., Proceedings of the 2nd World Conference and Exhibition on Photovoltaic Solar Energy Conversion; July 6–10, 1998, Vienna, Austria, p. 2193.
2. Verlinden P.J. High-efficiency concentrator silicon solar cells, p. 436–455. In: “Practical Handbook of Photovoltaics: Fundamentals and Applications”, edited by T. Markvart and L. Castaner; Elsevier Science Ltd., Kidlington, Oxford, 2003.
3. Sater B.L., Sater N.D. High voltage silicon VMJ solar cells for up to 1000 suns intensities // Proceedings of the 29th IEEE Photovoltaic Specialists Conference, May 20 — May 24, 2002. — New Orleans, USA, 2002. — P. 1019–1022.
4. Guk E.G., Shuman V.B., Shwartz M.Z. Proceedings of the 14th European Photovoltaic Solar Energy Conference, June 30 — July 4, 1997, Barcelona, Spain, p. 154.
5. Andreev V.M., Grilikhes V.A., Rumjantsev V.D. Photovoltaic conversion of solar concentrated irradiation. Nauka, Leningrad, 1989. — 310 p., (in Russian).
6. Landsberg G. S. Optics. Nauka, Moscow, 1976. — 928 p., (in Russian).
7. Keogh W., Cuevas A. Simple flashlamp I–V testing of solar cells // Proceedings of the 26th IEEE Photovoltaic Specialists Conference, Anaheim, CA, September 30 — October 3. — 1997. — P. 199–202.
8. Kerschaver E., Einhaus R., Szlufcik J., Nijs J., Mertens R. Simple and fast extraction technique for the parameters in the double exponential model for I–V characteristic of solar cells // Proceedings of the 14th European Photovoltaic Solar Energy Conference, June 30 — July 4, 1997. — Barcelona, Spain, 1997. — P. 2438–2441.
9. Kopach V.R., Kirichenko M.V., Shramko S.V. et al. New approach to the efficiency increase problem for multijunction silicon photovoltaic converters with vertical diode cells // Functional Materials. — 2008. — Vol. 15. — No. 2. — P. 253–258.

UDC 535.3

PACS: 42.81.PA

FIBER-OPTIC SENSOR FOR THE EXPRESS CONTROL OF THE CHEMICAL COMPOSITION

*Y. P. Sharkan¹, N. B. Jytov², I. I. Sakalosh¹, J. J. Ramsden³, M. Y. Sichka¹,
I. I. Popovich¹, S. O. Korposh¹*

¹Institute of Solid-State Physics & Chemistry, Uzhgorod National University,
Voloshina St 54, 88000 Uzhgorod, Ukraine, e-mail: shark@univ.uzhgorod.ua

²"Technomedica", Moscow, Russia

³Department of Advanced Materials, Cranfield University, MK 43 0AL, UK

FIBER-OPTIC SENSOR FOR THE EXPRESS CONTROL OF THE CHEMICAL COMPOSITION

*Y. P. Sharkan, N. B. Jytov, I. I. Sakalosh, J. J. Ramsden,
M. Y. Sichka, I. I. Popovich, S. O. Korposh*

Abstract. On the example of the aqueous-ethanol solutions we proposed fiber-optic sensor system of the evaluation of the concentration of the liquid solutions with the known qualitative composition. The deposition of the thin film chalcogenide layer with the high refractive index permitted to improve in one order the precision of the refractive index measurements of the aqueous solutions for the quartz Y-shaped splitter. We proposed and tested the method of the definition of the aqueous solutions concentration thanks to the measurement of the time of the total drying of the film of the solution on the fiber end, and thanks to the measurements of the changes of the interference signal which appears on the film in course of the drying process.

Keywords: Fiber-optic sensor, Fabry-Perot interferometer, aqueous solutions concentration, the process of drying of the film of the solution

ВОЛОКОННО-ОПТИЧНИЙ СЕНСОР ЕКСПРЕСНОГО КОНТРОЛЮ ХІМІЧНОГО СКЛАДУ ВОДНИХ РОЗЧИНІВ

*Й. П. Шаркань, М. Б. Житов, І. І. Сакалош, Дж. Дж. Рамсден,
М. Ю. Січка, І. І. Попович, С.О. Корпош*

Анотація. На прикладі водно-спиртових розчинів запропонована волоконно-оптична сенсорна система оцінки концентрації рідких розчинів з відомим якісним складом. Нанесення тонкоплівкового халькогенідного шару з високим показником заломлення дозволило на порядок підвищити точність вимірювання показника заломлення водних розчинів для Y-подібного кварцового розгалужувача. Запропоновано та випробувано метод визначення концентрації водних розчинів шляхом визначення повного часу висихання плівки розчину на торці волокна, а також вимірюванням змін інтерференційного сигналу, що виникає на плівці в процесі висихання.

Ключові слова: Волоконно-оптичний датчик, інтерферометр Фабрі-Перо, концентрація водних розчинів, процес висихання плівки розчину

ВОЛОКОННО-ОПТИЧЕСКИЙ СЕНСОР ЭКСПРЕССНОГО КОНТРОЛЯ ХИМИЧЕСКОГО СОСТАВА ВОДНЫХ РАСТВОРОВ

*И. П. Шаркань, Н. Б. Житов, И. И. Сакалош, Дж. Дж. Рамсден,
М. Ю. Сичка, И. И. Попович, С. А. Корнош*

Аннотация. На примере водно-спиртовых растворов предложена волоконно-оптическая сенсорная система оценки концентрации жидких растворов с известным качественным составом. Нанесение тонкопленочного халькогенидного слоя с высоким показателем преломления позволило на порядок повысить точность измерения показателя преломления водных растворов для Y-образного кварцевого разветвителя. Предложено и испытано метод определения концентрации водных растворов путем определения полного времени высыхания пленки раствора на торце волокна, а также измерением изменений интерференционного сигнала, который возникает на пленке в процессе высыхания.

Ключевые слова: Волоконно-оптический датчик, интерферометр Фабри-Перо, концентрация водных растворов, процесс высыхания пленки раствора

Introduction

Determination of the chemical composition of liquid solutions continues to be a task of current importance, covering a very wide spectrum of applications ranging from the control of physico-chemical technological processes and ecological monitoring to the analysis of medical and biological processes. The development and creation of sensors for rapid analysis is the especially topical. The sensors should also be cheap, small in size, requiring a small amount of the investigated medium and able to work under the conditions of intensive electromagnetic fields and ionizing radiation.

Fiber-optic sensors meet the demands for precise, rapid and reliable monitoring of media of different kinds [1]. The small size of the mono-fiber permits its use for the analysis of a small amount of the investigated medium. This is especially important for medical purposes. Sensors with sensitive elements on the fiber end are suitable for the determination of chemical compositions [2-5]. The sensitive element can either be the fiber end itself or a film or layer from a material sensitive to the influence of investigated medium [6].

The principle of operation of such sensors can be the amplitude measurement [7-9], in which the change of a signal is due to change of absorption or refractive index of the investigated environment, with which the fiber end contacts. More sensitive are interference fiber-optic sensors, in which the film from the investigated material [10, 11] or created at the fiber end beforehand the Fabry-Perot interferometer, the parameters of which vary during the interaction with the investigated medium [3], are used in the role of interferometer [12].

In this work, a fiber-optic sensor for the determination of quantitative changes in chemical composition of solutions is presented. The operating principle of the sensor is a method of determination of the reflection coefficient at the boundary between the fiber end and the investigated medium and the determination of the parameters of the film drying process, which occurs at the fiber end during withdrawal of the fiber from solution.

Direct measurements of the solutions concentration

The most convenient method for the determination of the refractive index of the solutions is the measurement of the amplitude of the inverse light reflection due to reflection coefficient at the boundary between fiber end and investigated medium. In this case, using the single-mode quartz optic fiber the reflection coefficient is defined as follows:

$$R = \left(\frac{n_f - n_m}{n_f + n_m} \right)^2, \quad (1)$$

where n_f — the refraction coefficient of quartz core of the single-mode fiber; n_m — refraction coefficient of the investigated medium.

The sensor (see, please, Fig.1) contains a Y-shaped splitter that divides the power equally between the input and output channels. From the input channel the signal propagates into the common channel, which is placed in contact with the sample. The optical signal is reflected from the fiber-sample interface, returns to the common channel, and then propagates into the output channel. The output sig-

nal is amplified and sent through an ADC to reach a computer for information processing.

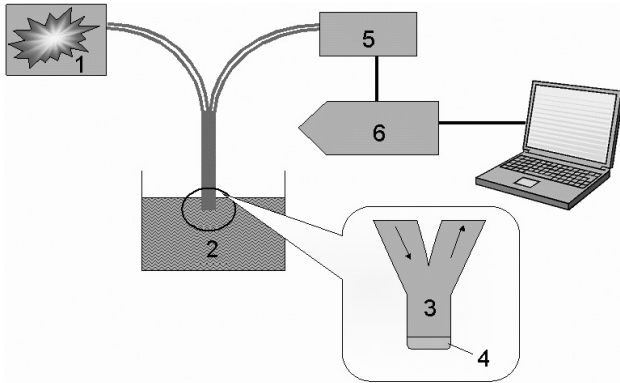


Fig. 1. Scheme of the mono-fiber optical sensor: 1 – light source ($\lambda=0.95 \mu\text{m}$ in the present work); 2 – investigated medium (sample); 3 – fiber optic Y-shaped splitter; 4 – liquid film on the fiber end; 5 – photodiode and amplifier; 6 – ADC.

Fiber-optic Y-shaped splitter contains the quartz fiber with core diameter and covering 8 and 150 μm , correspondingly, as far as exactly the quartz fibers, comparatively with polymer, due to the chemical stability provide the possibility to investigate the parameters of the physiological liquids in the “in vivo” mode.

The light emitting diode was used as a light source with the illumination wavelength 950 nm and possesses the width of the emission band at the level of 0.5 of about 30 nm. Unfortunately use of quartz fibers with the core refractive index of 1.45, leads to a low reflection when measuring the aqueous solutions, in which the refractive index doesn't differ too much from the n_f . The use of the fibers with the high refractive index, for example chalcogenides, will considerably increase the reflection coefficient at the *fiber end–investigated medium* interface.

Fig. 2 shows the calculated dependences of the fiber end reflection value from the investigated medium for quartz and chalcogenides fibers with a refraction index of 2.05 in the range of refractive indexes inherent to the aqueous solutions. As it is evident from figure, not only reflection value but also the slope considerably increases, and that significantly increases the sensitivity of measurement.

However, the complexity of the creation technology, the Y-shaped splitter on the base of chalcogenide fibers force to search the compromise decision for the given task. In order to increase the sensor sensitivity we used the single-mode quartz Y-shaped splitter on the end of the common channel

of which was deposited the thin film chalcogenide layer GeS_2 with the refractive index 2.05.

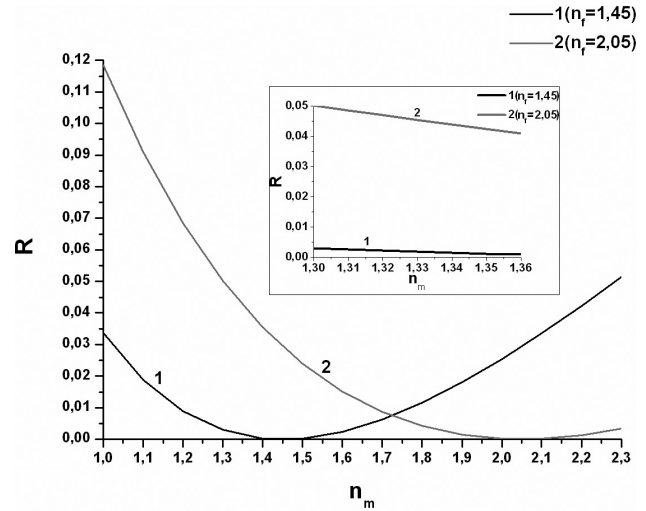


Fig 2. Calculated dependences of fiber end reflection from the investigated medium for a quartz fiber $n_f=1.45$ (curve 1), and for a chalcogenide fiber $n_f=2.05$ (curve 2); the inset expands the plot for refractive indexes typical for aqueous solutions.

Changing the concentration of the investigated medium, with which the common channel end of the chalcogenide monofiber sensor is in contact, the reflection coefficient R also changes; and change of signal amplitude is recorded:

$$U = kR = k \frac{(r_{12} + r_{23})^2 - 4r_{12}r_{23} \sin^2(\delta)}{(1 + r_{12}r_{23})^2 - 4r_{12}r_{23} \sin^2(\delta)}, \quad (2)$$

$$r_{12} = \frac{n_f - n_l}{n_f + n_l}, \quad r_{23} = \frac{n_l - n_m}{n_l + n_m}, \quad \delta = \frac{2\pi n_l d}{\lambda}, \quad (3)$$

where k is a proportionality coefficient; U – the signal amplitude output of the photodiode, r_{12} and r_{23} – reflection coefficients on the boundary *quartz single-mode fiber – thin film chalcogenide layer – the investigating medium* correspondingly, δ – phase shift at the light passing at wavelength λ through the thin film chalcogenide layer with thickness d , n_f – the refractive index of the core of the optic single-mode fiber, n_l – the refractive index of the thin film chalcogenide layer, n_m – the refractive index of the investigated solution. Hence by simply making optical contact of the mono-fiber end of the sensor with the investigated medium it becomes possible to determine the index of refraction of the given medium. Upon a change of the chemical composition of the solution its refractive index varies.

Fig. 3 shows the reflection coefficient of the *fiber end–air* interface and how the reflection coef-

efficient changes during immersion of the fiber end into solutions containing different concentrations of ethanol.

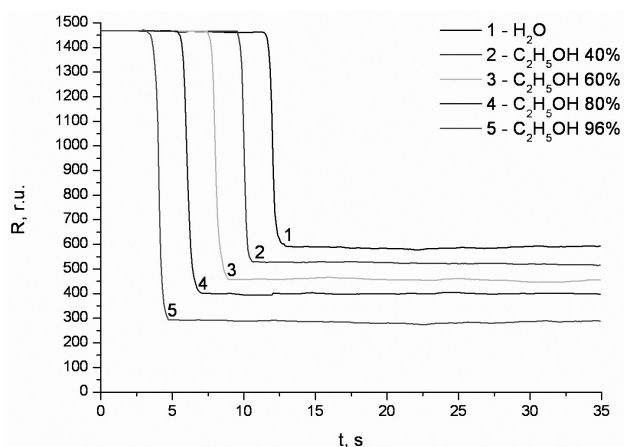


Fig. 3. Experimental determination of the reflectivities of aqueous ethanol solutions and pure water.

From these data the calibration curve of the dependence of the optical signal on the ethanol concentration was plotted (Fig. 4).

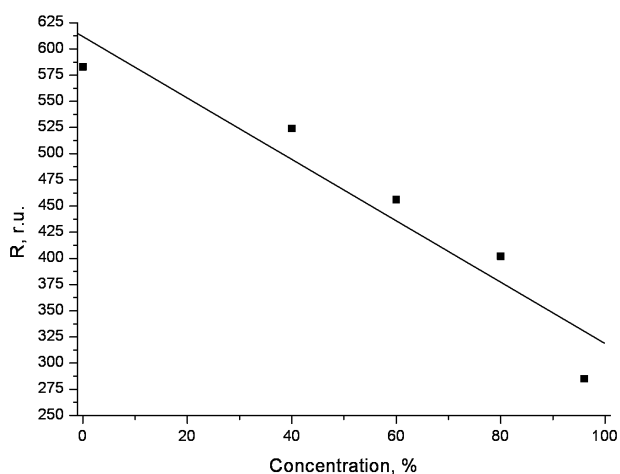


Fig. 4. Calibration curve, linking the optical output signal with ethanol concentration.

The measured value of the refractive indexes of the ethanol solutions are in a good agreement with tabular data [13] within an accuracy 10^{-3} . It is worth noting that the repeatability of these results was very good. Thus the suggested fiber-optic sensor (Fig. 1) of the amplitude type with single-mode quartz Y-shaped splitter permits directly to measure the refractive index of the investigated solution and due to the change of the refractive index to determine the concentration change.

Also, monitoring of the solutions concentration of the known chemical composition may be carried

out using the sensor calibration on the standard samples, in this case there is no necessity to measure directly the refractive index of the investigated solution, that permits to use the multi-mode optic fiber and by this to decrease the losses of the optic signal on the optic connections and to increase the reliability of the sensor as a whole.

The process of solution drying on the fiber end

The second procedure reported here is the study of the dynamics of optical signal changes during the withdrawal of the fiber end from solution and during the drying processes of the film which is formed on the fiber end: during withdrawal of the fiber from a wetting solution, a drop forms on the fiber end, which then remains due to surface tension; its size depends on the composition of the solution from which it is formed (we neglect here any possible changes of the drop composition compared with the bulk composition due to the proximity of the air water interface in the drop).

The drying process was studied with the help of the sensor depicted on figure 1. It was held at the same conditions of 25 °C and 55 % relative humidity. Aqueous ethanol solutions were chosen for the experiment.

In order to explain the processes which occur on the fiber end of the sensor after breaking optical contact of the fiber with the investigated medium, a CCD camera was used.

Dependence of the change of the signal value in the process of measurement is shown at Fig.5.

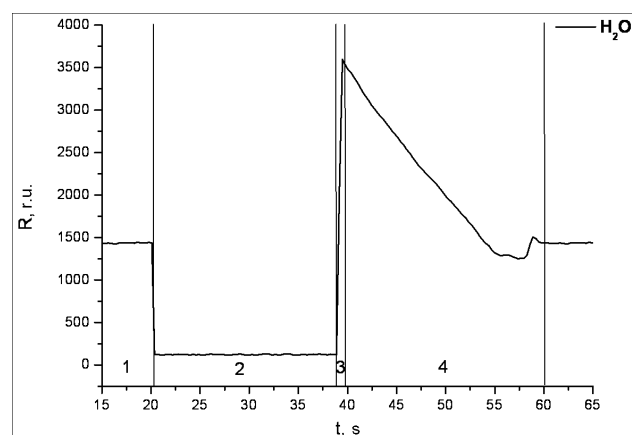


Fig. 5. The change of the signal value in the process of measurement: 1 — the monofiber end-air interface; 2 — fiber end-investigated medium interface; 3 — withdrawal of the fiber end from solution and formation of a drop-shaped film on the monofiber end; 4 — reduction of film thickness as a result of drying.

The 1st region corresponds to the fiber end-air interface; the 2nd region to the fiber end-investigated medium interface; the 3rd region to the formation of the drop-shaped film on the fiber end.

The sharp increase of the signal amplitude initially observed is due to the drop-shaped form of the film; all the light is reflected into the mono-fiber; the subsequent decrease of the signal is due to a change of the drop geometry, and correspondingly the radius of curvature of the spherical mirror, which exists at the investigated medium-air interface is continually changing. Further drying leads to an increase of the radius of curvature, and eventually the solution film on the fiber end becomes plane-parallel and light interference arises, due to the formation of a Fabry-Perot interferometer on the fiber end.

The 4th region shows a changing in the reflected signal as the film thickness on the fiber end decreases due to evaporation of the plane-parallel solution film; when the film thickness reaches the coherence length for the sensor, the interference occurs.

Additional confirmation of such division of the dependence of the amplitude on the film form was received in the course of the investigation of evaporation with the help of the video recording of the process on the CCD camera. On the end of the mono-fiber the drop of the investigated solution is formed. In time the evaporation of the liquid from the end of the mono-fiber occur, the volume decreases and the radius of the drop curvature increases, as a result on the end of the mono-fiber the plane parallel film is formed in which the multiple-beam interference is taking place.

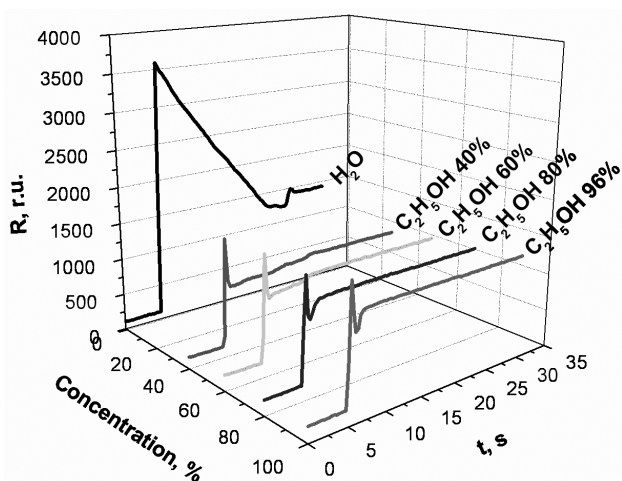


Fig. 6. Drying dynamics for aqueous ethanol solutions of different concentrations.

Fig. 6 shows the optical signal of the drying dynamics for aqueous ethanol solutions of different concentrations. The correlation between the drying time and the solution concentration is evident, i.e. with increasing ethanol concentration film drying is faster. The calibration graph of the drying time dependence on ethanol concentration $C=C(t)$ is plotted at Fig. 7.

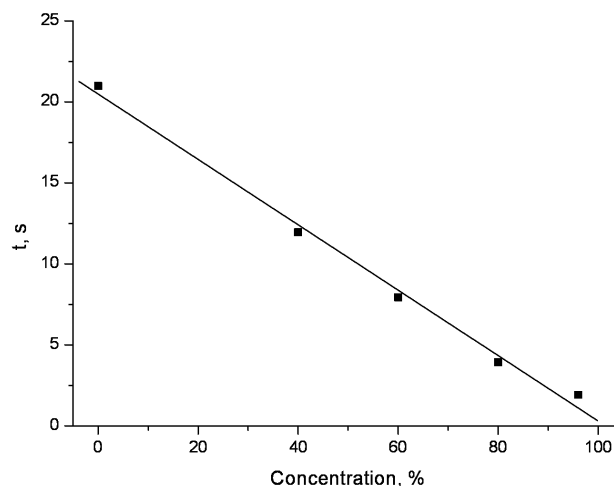


Fig. 7. Dependence of the drying time of the film on the concentration of the aqueous solution of the ethanol.

In such way by the measurement of the time of the process of the total drying of the aqueous solution on the end of the fiber it is possible to determine its concentration.

Interference in the drying solution film

The interference that appears in the drying film on the fiber end enables the development of interference fiber optic sensors for the determination of solution concentrations, which are more sensitive in comparison with amplitude sensors.

For studying the interference of the solution drying on the fiber end a fiber-optic spectrophotometer (Ocean Optics HR2000) and a white light source (Ocean Optics HL-2000 tungsten halogen lamp) were used. Measurements of the reflection spectrum from the end of the fiber-optic Y-shaped splitter with a diameter of 400 μm was carried out; the diameter of the connector of the common channel, which was immersed into the investigated medium, was 3 mm. Aqueous ethanol solutions were also chosen for this experiment.

At Fig. 8, the reflection spectra of the drop formed on the end of the optical connector for different drying time of 50 % aqueous ethanol solution are shown.

Curve 1 corresponds to the reflection spectrum from the investigated solution when the fiber end is in solution, curve 2 to the spectrum of a solution drop formed on the fiber end after withdrawing it from the investigated liquid. During the drying process a change of reflection occurs due to change of the drop form (curve 3). Gradually the radius of curvature of the drop is so increased, that interference in the solution film appear (curve 4), characteristic for a thin-film Fabry-Perot interferometer.

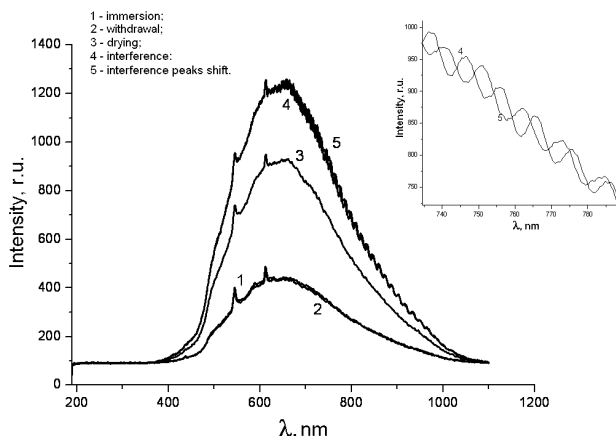


Fig. 8. Reflection spectra of the drop formed on the end of the optical connector for different drying times of a 50% aqueous ethanol solution. The inset shows an enlargement of part of the curves 4 and 5.

Further decreasing of the solution film thickness due to drying leads to a shift of the interference maxima in the reflection spectrum (curve 5).

Using the well-known equation for interference, it is possible to assess only the optical thickness $n_m d$, but it is impossible to define the absolute value of the refractive index and thickness, because both values vary simultaneously in time for the solutions:

$$\frac{\lambda_2 - \lambda_1}{\lambda_2 \lambda_1} = 2n_m d \quad (4)$$

where λ_1 and λ_2 are the wavelengths corresponding to the positions of two neighbor interference peaks; n_m is refractive index of the solution film at the time of measurement; and d is the geometric film thickness at the time of measurement.

The decrease of the geometrical film thickness takes place due to evaporation; and the change of the index of refraction takes place due to the change of the film chemical composition during the drying, which occurs because of the differential rate of evaporation of the various solution components.

The index of refraction will be constant in time only for pure liquids. Thus, measuring the reflection

spectrum, in other words the change of the interference peak positions in time, and calibrating the signals for given solution compositions, application of the given technique for the quantitative determination of solution compositions whose composition is qualitatively known is possible.

However, the processing of the spectral interference curves requires powerful software, because of the presence of large data arrays, and needs also quite expensive and complex hardware, which considerably complicates the application of this method.

Therefore, a system of monitoring the interference in the drying liquid film without spectral determination is offered. For this purpose the scheme depicted in figure 1 was used, single mode quartz fiber was used as the fiber-optic Y-shaped splitter, and a semiconductor laser diode with an illumination wavelength of 1320 nm and width of emission band at the level of 0.5 of about 5 nm, mean emitted power of 1 mW and frequency of direct modulation 10 kHz, was used as the emitter. The connector of a single mode optical fiber with a diameter of 2.5 mm was used as a fiber end of the common channel, which was immersed into the investigated solution and on which the drying drop was formed.

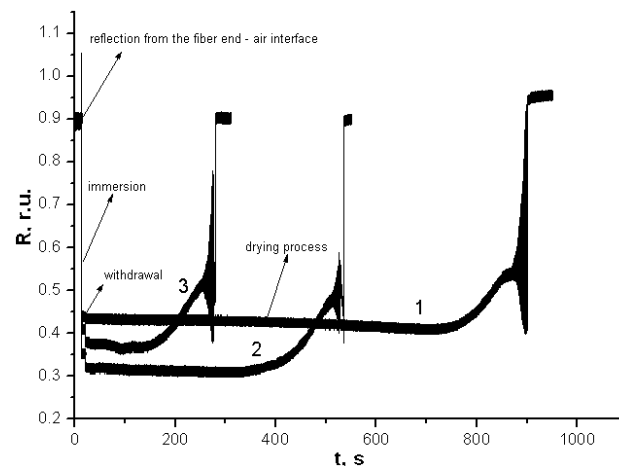


Fig. 9. Reflection changes for the complete process comprising immersion into solution, withdrawal from solution and drying. 1 — pure water; 2 — 50 % ethanol solution; 3 — 80 % ethanol solution.

The drying of aqueous ethanol solution drops of various concentrations formed on the end of the single mode optical fiber was investigated.

Fig. 9 shows the graph of the reflection change for the complete process including immersion into the solution, withdrawal from the solution and drying. Since the diameter of the optical fiber connector end is much bigger than for the technique

described in the first part of this paper, the times of drying are also much bigger.

The course of the complete drying process, as shown in figure 9, correlates with the data presented in the first part of this work, i.e. with increasing ethanol concentration the time for complete drying is decreased.

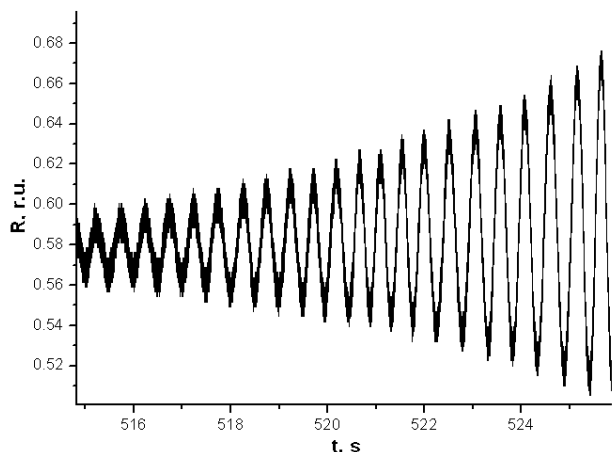


Fig. 10. The interference picture for a 50% aqueous ethanol solution.

At the same time, for the given measurement system, the region of evaporation of the formed planar film appears more clearly. The reason is connected with the different film geometry at the fiber end (the bigger dimensions in comparison with the first part of this work) and coherence length of the emitter.

The study of the interference picture for the investigated solutions has shown that as well as the spectral changes of reflection during film drying, the rate of the change of the film optical thickness ($n_m d$) varies in time for solutions. This is evident from the change of period of the interference maxima (Fig. 10 and Table 1). During the film drying of their pure components individually (ethanol or water), the period remains at a constant value.

Thus, by measuring the speed of the period change of the interference maxima the determination of the concentration of the drying liquid is possible. In other words, it is necessary to solve the task of measurement of the distance between the peaks on the interference picture. One possible hardware implementation of a solution to this task is introduction of a differential chain after the signal amplifier (Fig. 11, a), which will allow the creation of impulse fronts from the incoming signal (Fig. 11, b) with a much higher amplitude than the oscillations of the average signal level (Fig. 11, c). After the differential chain, a comparator (threshold device) is

placed, which will evaluate the moments of intersection of the impulse with the value of the threshold level (Fig. 11, d).

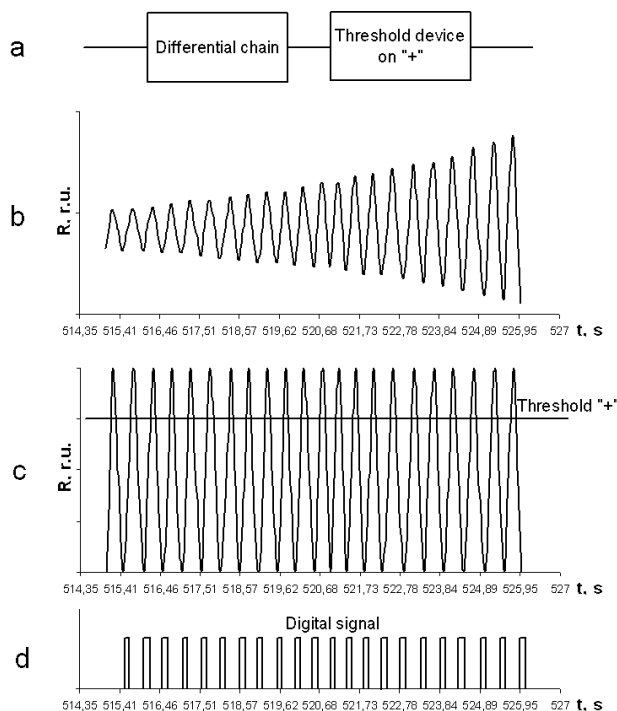


Fig. 11. Schematic illustration of the determination method of the distance between the peaks on the diagram of the interference pattern.

Table 1

Values of the period of the interference maxima for aqueous solutions of ethanol of definite concentrations.

Number of period	T, s			
	H ₂ O	C ₂ H ₅ OH – 50 %	C ₂ H ₅ OH – 80 %	C ₂ H ₅ OH – 96 %
1	1.6809	1.0588	0.6856	0.4874
2	1.6816	1.0630	0.6901	0.4867
3	1.6808	1.0658	0.6930	0.4853
4	1.6813	1.0697	0.6975	0.4873
5	1.6803	1.0731	0.7012	0.4863
6	1.6812	1.0776	0.7035	0.4867
7	1.6813	1.0816	0.7078	0.4853
8	1.6805	1.0847	0.7109	0.4873
9	1.6812	1.0877	0.7157	0.4874
10	1.6808	1.0921	0.7189	0.4863
11	1.6816	1.0961	0.7222	0.4853

Hence, the periods of the interference maxima will be estimated. Further measurement of the temporal distance between impulses can be accomplished by filling the measured interval by time impulses and counting them, which can be easily carried out with the help of a personal computer.

On the base of the received results the plot of the dependence of the middle value of the period of the

interference maxima on the concentration of the aqueous ethanol solution was constructed (Fig. 12), which permits to measure the ethanol concentration in aqueous solutions.

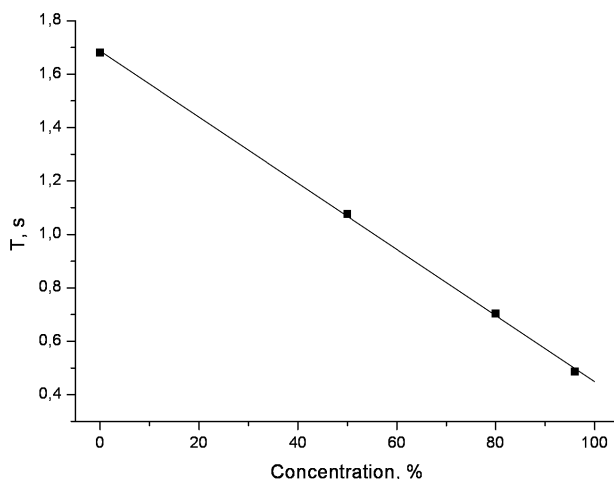


Fig. 12. Dependence of the middle value of the period of the interference maxima on the concentration of the aqueous ethanol solution.

The method of determination of the components concentration for the qualitatively known solution composition was developed that permits to observe the quantitative changes in the composition of the film of the investigated solution and also according to the value of the change of the period of the interference maxima in the process of the measurement, to determine whether the investigated solution is *ideal* or *not ideal* [14].

Conclusions

The work carried out and discussion have shown that:

1. By attaching a chalcogenide glass fiber with a high refractive index to the common channel of a fiber-optic Y-shaped splitter, the sensitivity of the refractometer is increased by almost one order of magnitude compared with conventional silica glass fibers.

2. The measurement of the changes in the reflection coefficient during drying of a solution film on the end of the optical fiber allows the sensitive determination of the concentration of aqueous solutions whose composition is known qualitatively.

References

1. E. Udd "Fiber Optic Sensors: An Introduction for Engineers and Scientists" // Wiley-Interscience, 1st edn., 1991.

2. A. Cusano, A. Cutolo, Michele Giordano, and Luigi Nicolais "Optoelectronic Refractive Index Measurements: Application to Smart Processing" // IEEE Sens. J. 3 (6), 781-787, 2003.
3. M. Giordano, M. Russo, A. Cusano, and G. Mensitieri "An high sensitivity optical sensor for chloroform vapours detection based on nanometric film of Δ -form syndiotactic polystyrene" // Sens. Actuators B, 2004.
4. A. Cusano, G. V. Persiano, M. Russo, and M. Giordano "Novel optoelectronic sensing system for thin polymer films glass transition investigation" // IEEE Sens. J., 1-8, 2004.
5. R. Wolthuis, G. Mitchell, J. Hartl, and E. Saaski "Development of a dual function sensor system for measuring pressure and temperature at the tip of a single optical fiber" // IEEE Trans. Biomed. Eng., 40 (3), 298-302, 1993.
6. M. Giordano, M. Russo, A. Cusano, G. Mensitieri, and G. Guerra "Syndiotactic polystyrene thin film as sensitive layer for an optoelectronic chemical sensing device" // Sens. Actuators B, 2004.
7. A. A. Chtcherbakov, P. L. Swart, S. J. Spammer, P. V. Bulkin "Long dual-cavity fiber optic Fabry-Perot strain sensor with rugate mirrors" // Opt. Eng. 35(4), pp. 1059-1063, 1996.
8. V. Arya, M. J. de Vries, M. Athrya, A. Wang, R. O. Claus "Analysis of the effect of imperfect fiber endfaces on the performance of extrinsic Fabry-Perot interferometric optical fiber sensors" // Opt. Eng. 35(8), pp. 2262-2265, 1996.
9. A. M. Murphy, M. F. Gunther, A. M. Vengsarkar, and O. R. Claus "Quadrature phase-shifted, extrinsic Fabry-Perot optical fiber sensor" // Opt. Lett. 16(4), pp. 273-275, 1991.
10. Шаркань Й. П., Миголинец И. М., Житов Н. Б., Муличка И. И., Бандровская И. К., Конопальцева Л. И., Попович И. И., Гаврик Е. В. Способ определения градиента показателя преломления пленки по толщине // А. с СССР, № 1474524, 1987.
11. R. Todoran, J. P. Sharkany Nondestructive laser system for the in-situ study of the kinetics of the adsorption processes at solid/liquid interface // 1999, SPIE Proceedings Vol. 3687, Paper #: 3687-05, pp. 26-28.
12. M. Giordano, M. Russo, A. Cusano, G. Mensitieri "An high sensitivity optical sensor for chloroform vapours detection based on nanometric film of Δ -form syndiotactic polystyrene" // Sensors and Actuators B: Chemical, Volume 107, Issue 1, 27 May 2005, p. 140-147
13. O. N. Grigorov, A. I. Zaslavskii, Yu. V. Morachevskii // "Chemical Data", 2nd ed., Vol. 3, Moscow: "Khimia" 1965.
14. Зенин Г. С., Пенкина Н. В., Коган В. Е. Физическая химия: ч. 3. Фазовые равновесия и учение о растворах: Учебное пособие. —СПб.: СЗТУ, 2005. — 119 с.

UDC 662.611:535

DETERMINATION OF SPECTRAL DEPENDENCE OF SOLID BLENDED FUEL TORCH SYSTEM RADIATING ABILITY

M. Yu. Trofimenko, Yu. A. Nitsuk, T. F. Smaglenko, L. I. Riabchuk

I. I. Mechnikov Odesa National University,
Dvoryanskaya Str., 2, Odesa, 65082,
E-mail: nitsuk@mail.ru, Tel. 723-62-27

DETERMINATION OF SOLID BLENDED FUEL TORCH SYSTEM RADIATING ABILITY SPECTRAL DEPENDENCE

M. Yu. Trofimenko, Yu. A. Nitsuk, T. F. Smaglenko, L. I. Riabchuk

Abstract. Multichannel optical pyrometer is described. Temperature measurement and emissivity definition methods are presented. Role of dispersed condensed phase of exterior torch layers is discussed.

Keywords: burning, radiating ability, temperature, condensed phase, flame

ВИЗНАЧЕННЯ СПЕКТРАЛЬНОЇ ЗАЛЕЖНОСТІ ВЕЛИЧИН ВИПРОМІНЮВАЛЬНОЇ ЗДАТНОСТІ ФАКЕЛА ТВЕРДОЇ СУМІШНОЇ СИСТЕМИ

М. Ю. Трофіменко, Ю. А. Ніцук, Т. Ф. Смагленко, Л. І. Рябчук

Анотація. Описано багатоканальний оптичний пірометр, який виготовлено авторами, і методи визначення з його допомогою температури та випромінювальної здатності на різних довжинах хвиль полум'я. Звертається увага на роль концентрації дисперсної фази зовнішніх шарів факела при визначенні температури і випромінювальної здатності полум'я.

Ключові слова: горіння, випромінювальна здатність, температура, конденсована фаза, полум'я

ОПРЕДЕЛЕНИЕ СПЕКТРАЛЬНОЙ ЗАВИСИМОСТИ ВЕЛИЧИНЫ ИЗЛУЧАТЕЛЬНОЙ СПОСОБНОСТИ ФАКЕЛА ТВЕРДОЙ СМЕСЕВОЙ СИСТЕМЫ

М. Ю. Трофименко, Ю. А. Ницук, Т. Ф. Смагленко, Л. И. Рябчук

Аннотация. Описан многоканальный оптический пирометр, который изготовлен авторами, и методики определения с его помощью температуры и излучательной способности пламени на разных длинах волн. Показана роль концентрации дисперсной фазы внешних слоев факела при определении температуры и излучательной способности факела.

Ключевые слова: горение, излучательная способность, температура, конденсированная фаза, пламя

Introduction

The original multi-channel optical pyrometer, developed by authors, and the methods of temperature and irradiating ability of a flame determination at different wavelengths have been discussed. It is

necessary to pay attention to the concentration of disperse condensed phase of outer layers of flame during the determination of temperature and irradiation ability of the flame.

The existing experimental data of coefficient of

flame irradiation ability ε were obtained for metal oxides or carbon parts [1-3]. In early papers [4] for solid blended systems (SBS) flames based on per-chlorate ammonia the ε values were detected for local fields of torch experimentally (2·0.3)mm² at pressures of (4-6) MPa in the region of spectra about (1-1.8) micrometers.

The use possibility of the SBS for welding doping and obtaining of light sources with determined parameters was the important reason to detect the ε of full torch (or their extended parts) as well as to determinate the flame brightness at the flame temperatures. The measuring regions of working temperatures for those SBS are in 2000-3000 K. The major part of emitted energy of the torch is placed in the wave region of less than 1 μ m.

The spectra of SBS to be investigated at pressures of 4 MPa and more have a continual character [9] and consist of two components. The first component is the emission of burning particles of initial SBS and condensed products of their burning (K-phase). Second component is the irradiation of gas phase which is the enveloping curve of the molecular strips (in case of small spectral discrimination of the measuring device) of their electron-rotating structure, the intersection and self-reversal of different strips at high density of burning products.

Sometimes the SBS emission spectra at pressure of 0.6 MPa except of continual irradiation of the flame may be presented the lines and strips specific to some elements or compounds placed in torch. This fact can be due to the increasing of probability of entering the one of working wave of the pyrometer to this line, and, hence, the violation of the "gray" condition ($\varepsilon = \text{const}$) for flame emission. Analyzing of registered flame emission at full number of wavelengths as it is possible in experiment, may sufficiently reduce these measurement errors.

Hence, in order to increase the accuracy of measurement according to [4] it is necessary to enlarge the spectral region of ε , and quantity of working wavelength of the pyrometer and it would be necessary to have a possibility to register the emission of torch part.

Besides, the serial pyrometers which satisfied the previously mentioned conditions, multichannel and large scope in noted spectral region are not manufactured.

So, it is necessary to produce the multichannel pyrometer and measuring temperatures and ε of extended parts of optically solid torch. (Optical solid torch contains the "K-phase" in a quantity

that makes it non-transparent for own irradiation of flame reflected by outer mirror).

The temperature region of flames to be investigated are (2÷4)·10³ K. Maxima of energy are placed in (0.8÷1.5) μ m according to Wien displacement law. Moreover, the interesting spectra region of (0.4-0.8) μ m because of methodologic error while measuring the brightness temperature is low that in the region of (0.8-1.5) μ m.

We produced the 7-channel optical pyrometer with scope of $\approx 8^\circ$. Working wavelengths for registration are determined by changeable interference filters of $\lambda_1 = 0.589$ μ m, $\lambda_2 = 0.621$ μ m, $\lambda_3 = 0.766$ μ m, $\lambda_4 = 1.165$ μ m, $\lambda_5 = 1.37$ μ m, $\lambda_6 = 1.55$ μ m, $\lambda_7 = 1.8$ μ m. We have measured the 7 brightness temperatures, color temperature by spectral dots of continual spectra and as well the color temperatures by two spectral dots. During the same experiment, we calculated the emissive ability ε for optical solid flames in seven dots. The value of relative device error of color temperature in this region of spectra not has not exceeded $\Delta T_{\text{гр}}/T_{\text{гр}} \cdot 100\% = 1.75\%$ [10].

The burning of SBS samples based on ammonia perchlorate reaction with elastic polyacrylates binded with doping of spherical aluminum powder ASD — 1, (dispersion of grains is 16 μ m) have been investigated. The burning of samples of 20 mm, height — 20 mm was investigated at pressures of 0.6 MPa in the set of constant pressures (SCP) in nitrogen atmosphere. In order to provide the flat (by layers) burning, the side was sealed by TSIATIM grease.

The outer window of SCP has the round diaphragm diameter of 2.5mm. As far as combustion of standard flame passes through a diaphragm light from more remote of the flat surface of burning samples of flame's area. Building the graph of dependence $\ln b_\lambda \cdot \lambda^5 = f(1/\lambda)$ for five wave-lengths from the area of continual spectrum, find the interesting us temperature of initial area (diameter of 2.5 mm) of flame in the set of torch section.

In composition, the explored standards of SBS metals sodium and potassium are present. The sensitiveness of the applied method is such that the lines of radiation are due to the technological admixtures of sodium and potassium, registered by our device through channels with wave-lengths $\lambda_2 = 0.621$ μ m and $\lambda_3 = 0.766$ μ m, accordingly. Values ε in the proper spectral points, the radiation of the indicated metals occasionally approached the value of 0.85. Temperatures of brightness, found at such values of ε near to the color temperatures of

distribution. Thus, the possibility of comparison of results appears got in the conditions of the experiment ($T_{\text{col}}=2250$ K; $T_b=2205$ K).

In the case, when a metal (for example, B) is entered into the explored composition for the improvement of burning parameters of the radiation of products of combustion of metal, it is possible to draw conclusion about his role in the process of burning (start, intensity and the end of reaction with its participation).

Measurement was conducted using the method described in [5]. The offered method, as specified higher, settles in the same experiment simultaneously to define a temperature and estimate the value of a flame radiating ability. The formula for calculation of ε for wavelength λ is shown below:

$$\varepsilon = \frac{\frac{c_2}{e^{\lambda T_i} - 1}}{\frac{c_2}{e^{\lambda T_b} - 1}},$$

here $c_2 = 1.4388 \cdot 10^4 \mu\text{m} \cdot \text{K}$ — second constant of irradiation at Plank's law, T_b —brightness temperature for wavelength λ , T_i is T_{col} detected for according local-extended parts of the flame.

Measurement of ε was conducted in the spatial areas of torch near to the area, where the maximal values of temperature of flame are achieved and, in our case, maximal values of size of integral radiation. Dependence ε on a wave-length took low-reduced character with multiplying a wave-length (see at Fig.1). The absolute value of a radiating ability for this wavelength (ε_λ) depends on the site of investigated area in a torch [6]. It is stated that dispersion of K-phase and its concentration (in particular in the external cold layer of flame) is different along a torch. Indicated absolute values $\varepsilon (1\div 4) \cdot 10^{-1}$ and motion of dependence ε_λ at a change λ , characteristic as for $P = 0.6$ MPa, so for $P = 0.1$ MPa. Advancing pressure up to $P = 1.4$ MPa type of dependence ε from λ remains as formerly, and the absolute values diminish up to $(2 \div 6) \cdot 10^{-3}$.

With respect to potassium and sodium, it was found by us in the same experiment, the radiate ability is proper to their lines in flame being higher, than in the nearby areas of continuous spectrum. Thus, as far as moving of measured area toward the top of torch there is at first an increase ε (e.g. the intensification increase of the reaction with metals participation) transition of the curve 1 to the curve 2, then fading of reaction (curve 2-5). It is explained, that the admixtures of sodium and potassium are contained in initial composition as connections

and appearance of their lines in the spectrum of radiation talks about decomposition of these connections, freeing of the indicated metals and their readiness to react.

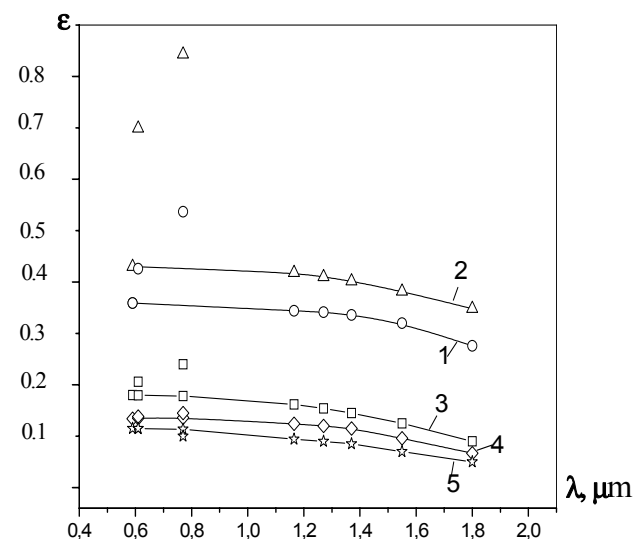


Fig. 1. Spectra dependence of ε for the STS-flame at pressure $P = 0.6$ MPa.

Numbers of curves are growing accordingly to the distance between the object and sample's flat end. 1 — $T = 2220$ K; 2 — $T = 2250$ K; 3 — $T = 2914$ K; 4 — $T = 2742$ K; 5 — $T = 2417$ K.

It is necessary to mark the complicated structure of SBS torch [4,6], consisting of hot radiative central part and more cold external area from the considerable concentration of particles of K-phase. As the influence of the particles is specified in the paper [7], the influence of K — phase particles on the form of distribution ε on wave-lengths can be deciding, and a change dispersion of particles of K-phase change ε in short-wave and long-wave parts of spectrum differently.

That in the conditions when size of particles of d of the condensed phase (appearing particles of not reacted carbon and being in flame, reactive particles of initial SBS) of $d \approx \lambda$, the ε depends on a change λ slightly, the insignificant change of d (advancement is higher on a torch, change of pressure, blowing, reserving, technologically entered additive in the complement of standard) could change both inclination of the got curve and its form (increasing dependence could become decreasing).

At comparison of papers [4, 6] statements, where measurement of ε conducted at pressure of $P = 4$ MPa and 6 MPa and the present work ($P = 0.6$ MPa and 1.4 MPa), it is necessary to mark as the general conformities of ε law conduct and the dif-

ferences. To general conformities to the law behavior detail that with the increase of pressure in both cases, the absolute value of ε diminishes, and the principal reason of it, being as we get the increase of concentration of K-phase and change its dispersion in a torch.

The size of absolute value of a radiate ability depends on a location in the torch of measured area, terms of burning of standard and formation of K-phase.

So in [6] the terms of combustion SBS in SCP at 4 MPa is such, that in the overhead area of torch more homogeneous distributing of temperatures is achieved on the diameter of torch, the concentration of particles of K-phase is less. All of it results in diminishing of radiation dispersion influence of hot kernel in more cold layers of torch.

In the real experiment and, in particular, the measurement ε conducted in area of torch, where the maximal values of size of optical radiation of flame and maximal values of his temperature are achieved. At $P = 0.6$ MPa, this area could be sufficiently extensive, with the large difference of temperatures between central and external parts of torch. After passing the area of maximal temperature (higher on a torch) intensity of radiation of flame not immediately diminishes and it results in active education and accumulation in the torch of K-phase, that causes its large concentration and small sizes of particles. All of the results, in multiplying the influence of radiation dispersion and diminishing of value ε as far as advancement of the explored area upwards at the torch area of maximal temperature. Detailed information about the spatial distributing of temperatures and change of structure of torch SBS presented in paper [9], K-phase flames SBS on the basis of ammonium perchlorate, presented in [8].

To provide the needed values, the complicated calculation was done, if the task decided in general, and the experimental methods of information receipt are so important on the size and frequency dependence ε in every case.

Conclusions:

The experimental results' discussion have shown that:

1. The original optical pyrometer gives the possibility to extend the spectral region of optical descriptions (parameters) of flame measurement.
2. The offered method lets us to determine

the absolute values ε and distribution ε on wave-lengths in different parts of torch at decompressed from the locally extensive ($\varnothing 2.5$ mm) areas of flame with the same precision of the temperature measurement.

3. Presence of large number of working wave-lengths in the original optical pyrometer enables to involve part of them for registration of radiation in lines characteristic for a reaction with certain elements or connections (the potassium and sodium in our case), and to conclude about their role in burning and to specify a place in a torch, where their influence is maximal, specifying the same the mechanism of burning SBS.

4. The experimental results specify the complex structure of torch HUSH and considerable role of K-phase (dispersion and concentration) at optical description of flame determination.

5. Size of absolute value of a radiate ability ε depends on a concentration and dispersion of K-phase and area of maximal change ε observed on wave-lengths near to the sizes dispersive particles of K-phase of external layer of torch.

References

1. Belinskiy N. M., Skogarev V. G., Florko A. V. Radiative Characteristics of Magnesium and Aluminium Oxides at the Temperatures of Burning// Physics of Aerodispersive Systems (in Russian). — 1986. — Odesa: № 30. — P. 97-99.
2. Olson O. H., Morris J. Handbook of Thermophysical Properties of Solid Materials, N. Y., Pergamon Press. — 1961. — V. 3.
3. Bloh A. G., Zhuravlyov Yu. A., Ryzhkov L. N. Thermal Exchange with Radiation. Energoatomizdat. — Moskva. — 1991. — 431p.
4. Trofimenko M. Yu., Chesnokov M. N., Smaglenko T. F. Changes of Radiative Ability of the Solid Mixture Systems Torch in Dependence on the Pressure // Physics of Aerodispersive Systems (in Russian). — 2002. — Odesa: № 39. — P. 95-99.
5. Trofimenko M. Yu. Studies of the Solid Mixture Systems Burning with the Use of the Optical Methods /Proceedings of XXI International Pyrometrical Seminar. Moskva, Russia. — 1995. — P. 884-890.
6. Trofimenko M. Yu., Chesnokov M. N., Smaglenko T. F. Measurement of the Radiative Ability of the Optically Dense Flames of the Solid Mixture Fuel Systems. // Physics of Aerodispersive Systems (in Russian). — № 38, Odesa. — 2001. — P. 106-111.
7. Ilchenko E. P., Florko A. V. The Influence of the Gaseous Mixture Parameters on its Optical and Radiative Abilities (heterogeneous burning). / Reports

- of the XX Scientific Conference of former USSR countries "Dispersive systems". — Odesa. — September 2002. — P. 118-119.
8. Chesnokov M. N. Creation Dynamics and Physical Characteristics of the Condensed Dispersive Phase in Low-Temperature Plasma of the Model Aluminized Fuels. Dissertation of the Doctor of Science Degree in Physics. — Odesa. — 1986.
 9. Trofimenko M. Yu. Peculiarities of the Flame of Solid Mixture Systems Structure Based on the Ammonia Perchlorates. Dissertation of the Candidate of Science Degree in Physics. — Odesa. — 1999.
 10. Trofimenko M. Yu. Evaluation of the Mixture System Flame Temperature on the Local Fluctuations of the Brightness in Torch // Physics of Aerodispersive Systems (in Russian). Odesa. №35. — P. 38-45.

АКУСТОЕЛЕКТРОННІ СЕНСОРИ
ACOUSTOELECTRONIC SENSORS

UDC 535.42

PACS: 42.25.FX, 78.20.HP

CHARACTERISTIC PROPERTIES OF OPTO-ACOUSTIC INTERACTION
IN THE “THICK” ACOUSTIC GRATING

L. V. Mikhaylovskaya, A. S. Mykhaylovskaya***

* I. I. Mechnikov National University, 65082, Odessa, Ukraine

**Ruhr-Universität Bochum, 44780 Bochum, Germany

E-mail: lidam@onu.edu.ua

CHARACTERISTIC PROPERTIES OF OPTO-ACOUSTIC INTERACTION IN THE “THICK”
ACOUSTIC GRATING

L. V. Mikhaylovskaya, A. S. Mykhaylovskaya

Abstract. The theoretical analysis of the diffraction spectrum at the normal incidence of the plane light wave onto a sound wave in the isotropic medium is developed. In the framework of the bound waves pattern the diffraction spectrum behavior is investigated. At the same time the parameters of the sound wave such as a width and intensity of the sound beam was modifying. As a result of this investigation it was showed that the behavior of the diffraction maximums intensity depending on intensity of the sound intensity is essentially modified under increase of the width of the acousto-optic layer even at the orthogonal orientation of interacting fields

Keywords: acousto-optic effect, Raman-Nath diffraction, Bragg diffraction

ОСОБЛИВОСТІ АКУСТООПТИЧНОЇ ВЗАЄМОДІЇ В “ТОВСТІЙ” АКУСТИЧНІЙ ГРАТЦІ

Л. В. Михайловська, А. С. Михайловська

Анотація. Проведено теоретичний аналіз дифракційного спектру у випадку ортогонального падіння плоскої світлової хвилі на звукову хвилю в ізотропному середовищі. При цьому в рамках моделі зв'язаних хвиль досліджується поведінка дифракційного спектру при зміні параметрів звукової хвилі, зокрема, ширини та інтенсивності звукової хвилі. Показано, що при збільшенні товщини прошарку акустооптичної взаємодії поведінка інтенсивності світла в дифракційних максимумах в залежності від інтенсивності звука суттєво змінюється навіть при ортогональній орієнтації взаємодіючих полів.

Ключові слова: акустооптичний ефект, дифракція Рамана-Ната, дифракція Брега

ОСОБЕННОСТИ АКУСТООПТИЧЕСКОГО ВЗАИМОДЕЙСТВИЯ В “ТОЛСТОЙ” АКУСТИЧЕСКОЙ РЕШЕТКЕ

Л. В. Михайловская, А. С. Михайловская

Аннотация. Проведен теоретический анализ дифракционного спектра в случае ортогонального падения плоской световой волны на звуковую волну в изотропной среде. При этом в рамках модели связанных волн исследуется поведение дифракционного спектра при изменении параметров звуковой волны, в частности, ширины и интенсивности звукового пучка. Показано, что при увеличении ширины слоя акустооптического взаимодействия поведение интенсивности света в дифракционных максимумах в зависимости от интенсивности звука существенно меняется даже при ортогональной ориентации взаимодействующих полей.

Ключевые слова: акустооптический эффект, дифракция Рамана-Ната, дифракция Брэгга

Introduction

The interest to investigations of opto-acoustic interaction is determined by extensive practice application of the acousto-optic methods for effective control of the space-temporary parameters of an optic radiation [1-3], for laser diagnostic of acoustic fields in liquids and gases, in the area of the measuring of the moving of liquids and gases [4,5]. In the latter years the works with using of the acousto-optic interaction for investigation optic characteristic of the scattering mediums, in particular, for acousto-optic visualization in turbid mediums, were published [5-7]. The interest to this works is stimulated by modern applications of optic methods for the medical diagnostic [7].

In the many tasks which are connected with light diffraction by sound wave it is necessary to know as those or other sound characteristics have an effect upon characteristics of passed light beam.

It is well known that the light diffraction by sound waves depends on incidence angle of light, on wave length of the incidence light, on length of the sound wave, on intensity and width of the sound beam. However at the theoretical analysis of this problem the most authors are guided themselves by approximations of the limit cases, so in the result the applications of finding results have limit. In the present work the intermediate case of diffraction between the Raman-Nath's regime and Bragg's diffraction is discussed greater detail

Theoretical analysis

In many papers the theory of the acousto-optics interaction is built upon base of general solutions of the wave equations obtained from Maxwell's equations [1,8-11].

Let in an isotropic medium the electromagnetic wave $E = E_0 \exp[j(k_{0y}y + k_{0z}z - \omega_0 t)]$ falls on the plane $z=0$ at the angle θ_0 to axis z . A plane acoustic wave propagates along y axis between the planes $z=0$ and $z=L$. For presenting geometry on account of the symmetry of our task it could consider that all fields are not depend on x coordinate. In the case of using an approximation of plane acoustic and optic waves the wave equation in the region of the interaction of light and sound ($0 \leq z \leq L$) can be write in a form $\frac{\partial^2 E}{\partial y^2} + \frac{\partial^2 E}{\partial z^2} = \frac{1}{c^2} \frac{\partial^2}{\partial t^2} (\epsilon \cdot E)$. Here perturbed by sound the dielectric permeability of the medium has form $\epsilon(y) = n^2 \approx n_0^2 - 2n_0 \Delta n_0 \cos(k_s y - \Omega t)$, where n_0 — the refractive index in the absence of sound, $\Delta n_0 = \sqrt{0.5 \cdot M \cdot I_s}$ — amplitude of modulation of the refractive index by sound wave, M — acousto-optic quality factor, I_s — intensity of sound wave, $k_s = \frac{2\pi}{\Lambda}$, Λ , Ω — wave number, length and frequency of sound wave respectively. It is clear, that the perturbations of the refractive index and dielectric permeability by sound wave considerably depend on the sound intensity.

If angle of incidence light beam $\theta_0 \ll 1$ and $\lambda \ll \Lambda$ (or $k_s \ll k$), then solutions of given wave equation may be search in the form of the expansion in series of the plane waves with slowly verified amplitudes [14]

$$E(y, z, t) = \exp[j(k \sin \theta_0 \cdot y + k \cos \theta_0 \cdot z - \omega_0 t)] \sum_{-\infty}^{\infty} V_m(z) \exp[jm(k_s y - \Omega t)]. \quad (1)$$

In accordance with choice of such series expansion the incident light beam breaks up into series of

plane waves. These waves propagate at small angles θ_m relative to the direction of the incident light beam. The following relations define values of these angles $\sin \theta_m = \sin \theta_0 + m \frac{k_s}{k} = \sin \theta_0 + m \frac{\lambda_0}{n_0 \Lambda}$. Here $m = 0, \pm 1, \pm 2, \dots$ — diffraction orders.

Substitution of the expansion (1) into wave equation makes it possible to derive differential equations for finding of the amplitudes $V_m(z)$. These equations have form of the recurrence relations. Using the approximation of the relatively slow changes of the functions $V_m(z)$ in the range $0 \leq z \leq L$ the following infinite system of the first order differential equations was obtained for determination $V_m(z)$ [1,13,14]

$$\frac{dV_m}{dz} + j\mu_m V_m = j \frac{q}{2} (V_{m+1} + V_{m-1}). \quad (2)$$

$$\begin{aligned} \text{Here } \mu_m &= \frac{mk_s (2k \sin \theta_0 + mk_s)}{2k \cos \theta_0} \\ &= \frac{2\pi m}{\Lambda \cos \theta_0} \left(\sin \theta_0 + m \frac{\lambda_0}{2n_0 \Lambda} \right), \\ q &= \frac{k \Delta n_0}{n_0 \cos \theta_0} = \frac{2\pi \Delta n_0}{\lambda_0 \cos \theta_0}. \end{aligned}$$

This system of equations (2) must be solved with boundary conditions $V_0(0) = E_0$ and $V_m(0) = 0$ for all $m \neq 0$. The relation $I_m = V_m \cdot V_m^*$ determines intensity of light in m diffraction maximum. Number of the excite diffraction maximums depends on both intensity of sound wave and width of sound beam.

In present work the case of orthogonal incidence of plane light wave onto the sound wave in the isotropic medium are considered. At the same time in the framework of the stated above model of the coupled waves the dependence of diffraction spectrum on the parameters of sound wave namely width and intensity of sound wave is investigated.

In the case of perpendicular incidence of light ray onto the sound beam the parameters μ_m, μ_{-m} take the following forms $\mu_m = \mu_{-m} = m^2 \frac{\pi \lambda_0}{n_0 \Lambda^2}$. The energy of the incidence radiation disperses between set of the diffraction orders symmetrically relative to transmitted light, i.e. (that is) $V_m = V_{-m}$. The system of equations (2) becomes simpler and takes on form

$$\begin{aligned} V_0' &= jqV_1, V_m' + j\mu_m V_m = \\ &= 0.5jq(V_{m-1} + V_{m+1}), m = 1, 2, 3, \dots \end{aligned} \quad (2a)$$

The intensity of incident radiation is defined by expression $I_i = E_0^2 = I_0(z) + 2 \sum_1^m I_m(z)$.

Under the condition $Q = \frac{k_s^2}{k} L = \frac{2\pi \lambda_0}{\Lambda^2 n_0} L \ll 2\pi$ the Raman-Nath diffraction mode takes place. For this mode the approximation of the two-dimensional (plane) phase grating is true. For this approximation the diffraction maximum distribution of the light intensity at going out from sound layer is described by Bessell functions $I_{mB} = I_i \cdot J_m^2(qL)$. Here $qL = \frac{2\pi \Delta n_0}{\lambda_0} L$ — dimensionless Raman-Nath parameter. (It should be noted that Raman-Nath approximation follow from (2) if all parameters $\mu_m = 0$). In accordance with these expressions an increase of the modulation amplitude of the refractive index Δn_0 (that is sound intensity) affects on diffraction phenomena as well as an increase of the sound field width L . So for Raman-Nath approximation number of the excited diffraction maximums by same way depends on sound intensity and width of sound beam. This number may be estimated by using relation $J_0^2(qL) + 2 \sum_1^m J_m^2(qL) = 1$. It is easily to make sure by direct calculation that equality $J_0^2(qL) + 2 \sum_1^m J_m^2(qL) = 1$ is satisfied sufficiently exactly if $qL \leq m$. For example, for $qL = 3$ it is easy to calculate sum $J_0^2 + 2 \cdot (J_1^2 + J_2^2 + J_3^2) = 0.9613$. So it may be expect that the number of the observable diffraction maximums in each concrete case do not exceed considerably the magnitude $m = qL$.

In present paper the condition of smallness of the sound beam width that necessary to satisfy condition $Q \ll 2\pi$ does not use. The system of equations (2a) was solved successively for three cases: 1) $m = 0, 1$. 2) $m = 0, 1, 2$. 3) $m = 0, 1, 2, 3$. Thereby we neglect by diffraction in more high orders 1)second, 2)third, 3)fourth respectively. We try to estimate accuracy our used approximations by successively increasing of the number the diffraction maximums that taken into account in numerical calculations. So, if in some of region of system parameters the accounting $m + 1$ diffraction orders do not vary but only define more exactly solutions for m diffraction orders then it can state that for given region it may be confined oneself only by m diffraction orders.

In the beginning we consider first case of diffraction permitting analytic solution. In this case

after sound beam passage by light beam only two symmetrical maximums relative to the transmitted main light beam are observed. This means that it is need to solve next system of two differential equations

$$\begin{cases} V_0' = jqV_1 \\ V_1' + j\mu_1 V_1 = 0.5jqV_0. \end{cases} \quad (3)$$

With accounting of boundary conditions $V_0(0) = E_0$, $V_1(0) = 0$ the following solutions for amplitudes of the diffraction maximums were obtained

$$\begin{aligned} V_0(z) &= \frac{E_0}{r_2 - r_1} (r_2 e^{jr_1 z} - r_1 e^{jr_2 z}), \\ V_1(z) &= \frac{E_0 r_1 r_2}{q(r_2 - r_1)} (e^{jr_1 z} - e^{jr_2 z}), \end{aligned}$$

where $r_{1,2} = \frac{-\mu_1 \pm \sqrt{\mu_1^2 + 2q^2}}{2}$ — roots of the characteristic equation $r^2 + \mu_1 r - 0.5q^2 = 0$. These solutions can be overwritten in form

$$\begin{aligned} V_0(z) &= E_0 \sqrt{\frac{\mu_1^2 + 2q^2 \cos^2(0.5\sqrt{\mu_1^2 + 2q^2} z)}{\mu_1^2 + 2q^2}} \times \\ &\quad \times \exp\left(-j\frac{\mu_1 z}{2} + j\varphi_0(z)\right) \\ V_1(z) &= E_0 \frac{q \sin(0.5\sqrt{\mu_1^2 + 2q^2} z)}{\sqrt{\mu_1^2 + 2q^2}} \exp\left(-j\frac{\mu_1 z}{2} + j\frac{\pi}{2}\right). \end{aligned}$$

For phase $\varphi_0(z)$ following expression is true $tg\varphi_0 = \frac{\mu_1}{\sqrt{\mu_1^2 + 2q^2}} tg(0.5\sqrt{\mu_1^2 + 2q^2} z)$. In this writing the amplitude and phase modulations of the transmitted and diffracted beams are separated. Ultrasonic (ultrasound) wave generates in medium amplitude-phase diffraction grating.

The intensities of the transmitted and diffracted waves going out of (withdrawal from) layer with width L of acousto-optic interaction equal

$$\begin{aligned} I_0(L) &= V_0 V_0^* = E_0^2 \times \\ &\quad \times \left[1 - \frac{2q^2}{\mu_1^2 + 2q^2} \sin^2(0.5\sqrt{\mu_1^2 + 2q^2} \cdot L) \right] \\ I_1(L) &= I_{-1}(L) = V_1 V_1^* = \\ &= \frac{E_0^2 q^2}{\mu_1^2 + 2q^2} \sin^2(0.5\sqrt{\mu_1^2 + 2q^2} \cdot L) \end{aligned} \quad (4)$$

Results of calculations and these discussions

The numerical calculations were made for diffraction of light beam wave length $\lambda_0 = 0.6328 \mu m$ on propagating in water ultrasonic wave with sound wave length $\Lambda = 150 \mu m$. In this case system parameters are refractive index of medium $n_0 = 1.33$, value $\mu_1 = \frac{\pi\lambda_0}{n_0\Lambda^2} = 0.66$, parameter $q = \frac{2\pi\Delta n_0}{\lambda_0} = 1.0 \cdot 10^5 \cdot \Delta n_0$, wave parameter $Q = 2\mu_1 L = 1.32 \cdot L$, the direction of diffraction maximums are defined by following angles $\sin\theta_m = m \cdot 32 \cdot 10^{-4} rad = m \cdot 11'$.

As is seen from obtained expressions (4) the behavior of the intensities owing to changes of range of interaction of light and sound L differ from the behavior of the intensities owing to changes power of sound wave, that described by parameter q . Only phase components of diffraction spectrum intensities explicitly depend on layer width of the acousto-optic interaction. Into these components wave parameter of diffraction $Q = 2\mu_1 L$ enters also. On fig.1 the dimensionless intensities I_m/I_0 are plotted as a function of dimensionless Raman-Nath parameter qL . Here $I_0 = E_0^2$ — intensity of incident radiation, I_m — intensity of diffraction maximums of zero and first orders. Two cases are considered. Firstly when width of sound layer is held fixed ($L = const$) and only sound intensity is changed. Secondly when sounds intensity is kept steadily, i.e. $\Delta n_0 = const, q = const$, but only sound width L is varied. On these figures there are also the dependences light intensity in diffraction rays that was calculated in Raman-Nath approximation. It is seen that for values Raman-Nath parameter $qL \leq 1$ in both cases dependences for transmitted beam and first diffraction maximums coincide with distribution of Raman-Nath accordingly Bessell function. However, with increasing $qL > 1$ the deviation of dependences from Bessell function are observed. At that these deviations are different for this two analyzing cases in the same region of changes of parameter qL .

The increase of the number of diffraction maximums brings to necessity solving system of linear homogeneous differential equations of first order with large number of equations. The results of numerical calculations for orders $m = 0, 1, 2$ for just the same values of width of sound beam and index refractive that on fig.1 are shown on fig.2. It is seen, that in case of more accurate calculation with taking account of $m = 0, 1, 2$ the coincidence with Ra-

man-Nath approximation of first two maximums $m=0$ (transmitted radiation) and $m=1$ (first order) is more exact (better) than in case of calculations with account only $m=0,1$ over the same range of changes values of parameter (product) qL . And that with variation of sound beam width the difference from Bessell distribution is much (rather) more than at change intensity of sound wave when width of layer of acousto-optic interaction is fixed.

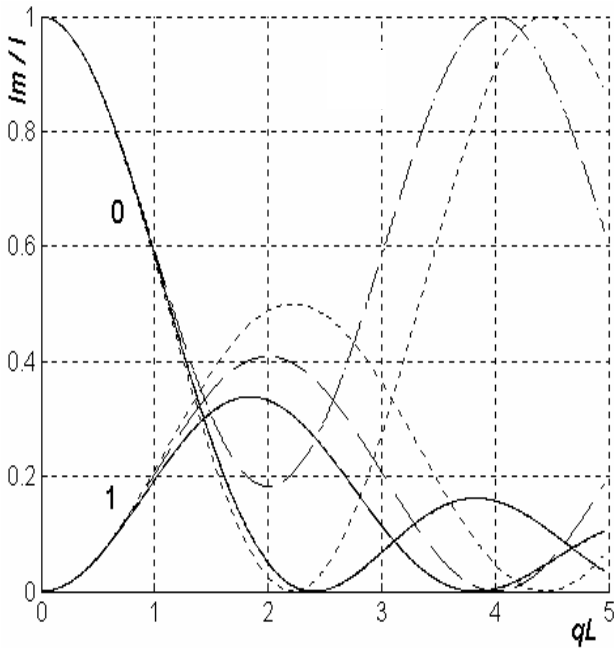


Fig. 1. Dependences of intensities of zero (0) and first (1) diffraction maximums on parameter qL , calculated by formula (4). Dashed lines— $L=0.1$ cm, $\Delta n=(0 - 5 \cdot 10^{-4})$. Dotted lines — $\Delta n=10^{-5}$, $L=(0 - 5)$ cm. Solid lines — Raman-Nath approximation

Numerical calculations was done with account of diffraction maximums $m = 0, 1, 2, 3$ and showed that the values of amplitudes of diffraction maximums which was derived with using of lowest degree of approximations only these are defined more exactly with using of more high degrees of approximations.

The dependencies of the difference $\Delta I_m = (I_m^{(2)} - I_m^{(3)})/I_0$ ($I_m^{(2)}$ — light intensity in m diffraction maximum calculated by approximation $m = 0,1,2$ and $I_m^{(3)}$ — light intensity in m diffraction maximum calculated in next approximation $m = 0,1,2,3$) are presented in fig. 3 and 4. It is seen that in one and the same range of values of dimensionless parameter qL the dependences of intensity of zero, first, second orders on sound layer size do not differ for given approximations. However for dependences on parameter q there is considerable difference especially for thin layers.

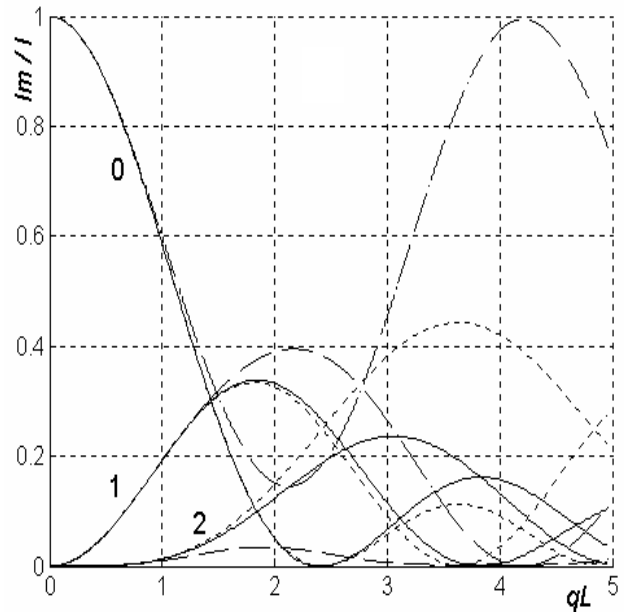


Fig. 2. Dependences of intensities of zero (0), first (1) and second (2) diffraction maximums on parameter qL . Dashed lines— $L=0.1$ cm, $\Delta n=(0 - 5 \cdot 10^{-4})$. Dotted lines — $\Delta n=10^{-5}$, $L=(0 - 5)$ cm. Solid lines — Raman-Nath approximation

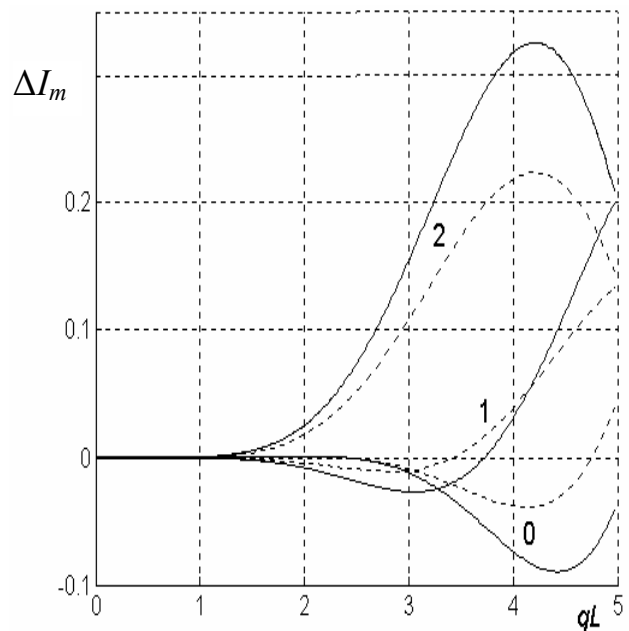


Fig. 3. Dependences of difference between solutions received by different approximations for zero (0), first (1) and second (2) diffraction maximums on value q (intensity of sound wave). Solid lines— $L=0.1$ cm, dashed lines — $L=0.5$ cm.

The dependencies of the difference $\Delta I_m = I_m^{(3)}/I_0 - J_m^2$ on sound intensity with its constant width and on width of sound beam with constant its intensity are shown in fig.5 and 6. It is seen that behavior of diffraction spectra depending on

intensity of sound wave for taken widths of interaction coincides with Raman-Nath approximation. However with increase of width sound beam even for small (not great) sound intensity the behavior of the intensity of diffraction maximums is distinguished from Bessel function.

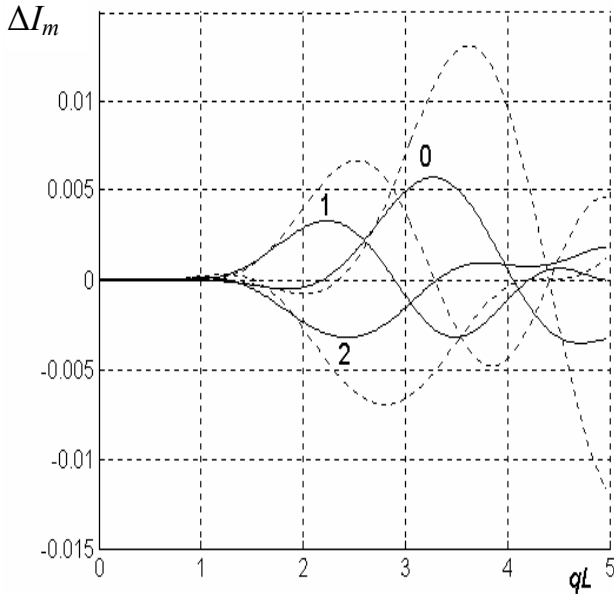


Fig. 4. Dependences of difference between solutions received by different approximations for zero (0), first (1) and second (2) diffraction maximums on width of sound layer L . Solid lines— $\Delta n=10^{-5}$, dashed lines — $\Delta n=1.2 \cdot 10^{-5}$.

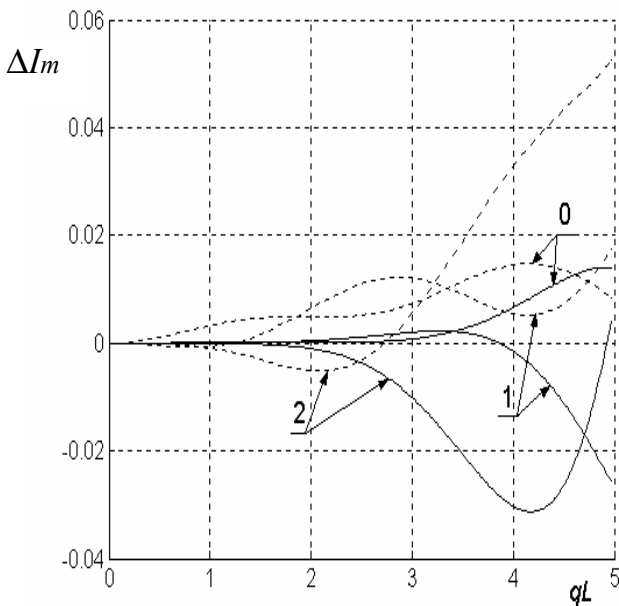


Fig. 5. Dependences of difference between Raman-Nath solution and solution received by approximation $m=0,1,2,3$ for zero (0), first (1) and second (2) diffraction maximums on value q (intensity of sound wave). Solid lines— $L=0.1$ cm, dashed lines — $L=0.5$ cm.

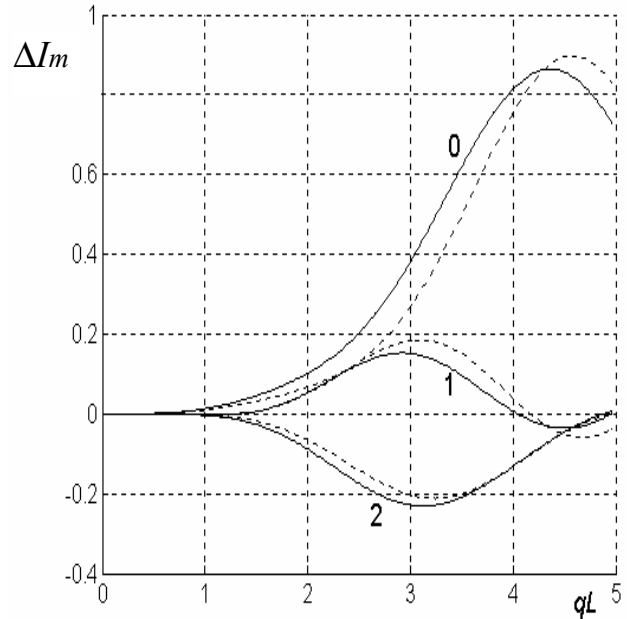


Fig. 6. Dependences of difference between Raman-Nath solution and solution received by approximation $m=0,1,2,3$ for zero (0), first (1) and second (2) diffraction maximums on width of sound layer L . Solid lines— $\Delta n=10^{-5}$, dashed lines — $\Delta n=1.2 \cdot 10^{-5}$.

In present paper modifications of diffraction spectra with change of sound beam width are investigated. The calculating dependences of light intensity in diffraction maximums zero (transmitted without angular deflection), first, second and third orders on amplitude of index refraction (sound intensity) with increase of sound beam width are presented in fig.7,8. It is seen that with moderate width of acousto-optic interaction when wave parameter $Q \approx 1$ the light intensity distribution in diffraction maximums there is far from Bessel function. The increase of width L produces to growth of light intensity oscillations with increase of sound intensity. At that even for examining orthogonal alignment of the interacting fields with increase of width of sound field the decreases of amplitudes of diffraction maximums of second and third orders are observed. The calculating dependences of light intensity in diffraction maximums are presented in fig.8 for width of sound field $L=0.6$ cm, $Q=2.3206$. It is seen that for some values of Δn_0 only transmitted beam $m = 0$ and two symmetrical diffraction maximums first order $m = 1$ и $m = -1$ are remained in diffraction spectrum. At that, light intensities in diffraction maximums of second order and, particularly, third in this range of changes Δn_0 are neglect small. Besides, for some value of amplitude of index refraction the intensity of the transmitted light ray

coincides with intensity of two refractive and equal one third of intensity of incidence light.

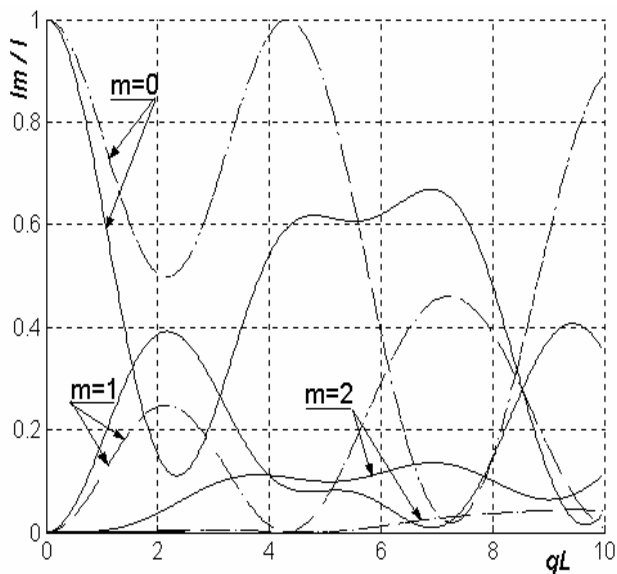


Fig. 7. Computed dependences of light intensity in diffraction maximums on value q (intensity of sound wave). Solid lines – $Q=2.66$, $L=2$ cm, dashed lines – $Q=5.32$, $L=4$ cm.

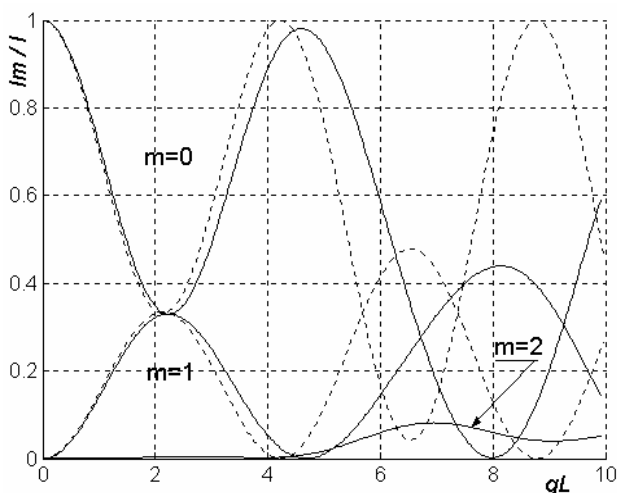


Fig. 8. Calculated dependences of light intensity in diffraction maximums on value q for different approximations. Solid lines – $m=0,1,2,3$; $Q=4.26$, $L=3.21$ cm, dot lines – $m=0,1$; $Q=3.92$, $L=2.95$ cm.

Conclusion

In present paper the theoretical analysis and calculation of the acousto-optic interaction was done for case of orthogonal orientation of interaction plane light and sound fields. At the same time dependences of diffraction spectra on both inten-

sity of sound beam and its width are presented. The comparison of received results by numerical calculations with solutions received by Raman-Nath approximation was made. It was shown the behavior of diffraction spectra with changes of sound wave intensity substantially depend on sound beam width. Particularly, even with perpendicular incidence of light ray onto acoustic grating one can split light ray into three light ray with equal intensity propagated at small (not great) angles. In addition, investigation of behavior of diffraction spectra makes it possible to estimate intensity sound wave and connected with its parameters of medium.

References

1. Balakshiy V. I., Parygin V. N., Chirkov L. E. Physical bases of acousto-optic. – M.: Radio and communication, 1985. – 280 p.
2. Antonov S. N., Rezvov Yu. G. High-efficient multi-beam Bragg acoustooptic diffraction with phase optimization of multifrequency acoustic wave // *JrTech-Phys.* – 2007. – V. 77, №8. – P. 93-100.
3. Kotov V. M., Shkerdin G. N., Shkerdin D. G., Kotov E. V. Filtration of partial coherence optical radiation by means of multiphonon Bragg diffraction// *Opt. and spectr.* – 2005. – V. 98, №1. – P. 109-113.
4. Grechikhin V. A., Raskovskaya I. L., Pinkevichus B. S., Tolkachev A. F. Investigation acoustooptic effect in interference range of laser beams // *Kvant. electr.* – 2003. – V. 33, №8. – P. 742-746.
5. Pelivanov I. M., Belov S. A., Solomatin V. S., Khokhlova T. D., Karabutov A. A. Direct measurement of space distribution of laser radiation intensity in biological environments in vitro optics-acoustic method // *Kvant. electr.* – 2006. – V. 36, №12. – P. 1089-1096.
6. Solovjev A. P., Sinichkin A. P., Zyuryukina O. V. Acousto-optic visualization of scattering mediums // *Opt. and spectr.* – 2002. – V. 92, №2. – P. 245-251.
7. Tuchin V. V. Investigation of biotissues by light scattering methods. // *UFN.* – 1997. – V. 167, №5. – P. 517-537.
8. Born M., Volf E. Basic of optic. – M.: Science, 1973. – 721 p.
9. Kino G. Acoustic waves. – M.: World, 1990. – 656 p.
10. Bergman L. Ultrasonic and its application in science and technique. Transl. from German. M.: Publ. Foreign literature, 1957. – 728 p.
11. Korpel A. Acousto-optics. By Transl. from English. M.: World, 1993. – 240 p.

БІОСЕНСОРИ

BIOSENSORS

UDC 577.15+543.6

FOUR-CHANNEL BIOSENSOR-ANALYZER OF SACCHARIDES

*S. V. Dzyadevych¹, A. P. Soldatkin¹, A. A. Soldatkin¹, V. N. Peshkova¹,
A. D. Vasilenko², V. G. Melnik², A. A. Mikhal²,
L. N. Semenycheva², M. P. Rubanchuk²*

¹ Institute of Molecular Biology and Genetics, 150 Zabolotnogo Str., Kiev 03143
Phone: (044)-200 03 28

² Institute of Electrodynamics, 56 avenue Pobedy, Kiev 03680
Phone: (044)-4542511, E-mail: melnik@elan-ua.net

FOUR-CHANNEL BIOSENSOR'S ANALYZER OF SACCHARIDES

*S. V. Dzyadevych, A. P. Soldatkin, A. A. Soldatkin, V. N. Peshkova, A. D. Vasilenko,
V. G. Melnik, A. A. Mikhal, L. N. Semenycheva, M. P. Rubanchuk*

Abstract. The problems of realization of highly sensitive and precise conductometric biosensor systems are considered. Composition, structural schemes, software functions of multisensor analyzer of saccharides are described, general view is presented. Preliminary experimental research testifies that the system suggested allows separate determination of concentrations of saccharose, glucose, lactose and maltose with commercially necessary sensitivity. It can be a basis for development of modern analytical equipment for efficient concurrent measurement of concentrations of several saccharides in food industry.

Keywords: Biosensor, analyzer, measuring system, saccharides

ЧОТИРЬОХКАНАЛЬНИЙ БІОСЕНСОРНИЙ АНАЛІЗАТОР САХАРИДІВ

*С. В. Дзядевич, О. П. Солдаткін, О. О. Солдаткін, В. М. Пешкова, О. Д. Василенко,
В. Г. Мельник, О. О. Міхаль, Л. М. Семеничева, М. П. Рубанчук*

Анотація. Розглянуто проблеми реалізації високочутливих і точних кондуктометричних біосенсорних систем. Наведено склад, структурні схеми, функції програмного забезпечення та зовнішній вигляд мультисенсорного аналізатора сахаридів. Попередні експериментальні дослідження свідчать, що розроблена система дозволяє визначати роздільно концентрації цукрози, глюкози, лактози та мальтози з необхідною для промисловості чутливістю і може бути основою для створення сучасного аналітичного обладнання для одночасного оперативного визначення концентрації декількох сахаридів в харчовій промисловості.

Ключові слова: Біосенсор, аналізатор, вимірювальна система, сахариди

ЧЕТЫРЕХКАНАЛЬНЫЙ БИОСЕНСОРНЫЙ АНАЛИЗАТОР САХАРИДОВ

*С. В. Дзядевич, А. П. Солдаткин, А. А. Солдаткин, В. Н. Пешкова, А. Д. Василенко,
В. Г. Мельник, А. А. Михаль, Л. Н. Семенычева, М. П. Рубанчук*

Аннотация. Рассмотрены проблемы реализации высокочувствительных и точных кондуктометрических биосенсорных систем. Приведены состав, структурные схемы, функции программного обеспечения и внешний вид мультисенсорного анализатора сахаридов. Предварительные экспериментальные исследования свидетельствуют, что разработанная система позволяет определять отдельно концентрации сахарозы, глюкозы, лактозы и мальтозы с необходимой для промышленности чувствительностью и может служить основой для создания современного аналитического оборудования для одновременного оперативного определения концентрации нескольких сахаридов в пищевой промышленности.

Ключевые слова: Биосенсор, анализатор, измерительная система, сахариды

Introduction

Permanent control of saccharides concentration is vital in various branches of food industry and farming production. In biotechnology, saccharides monitoring is necessary for fundamental comprehension of processes of cultivation and fermentation, their optimization and regulation.

Determination of saccharose concentration is essential at all stages of sugar production — from its monitoring in white-beet roots during growing and storage and throughout the whole technological cycle of complete processing to the final product [1]. Lactose is intensively used in production of baby foods (along with saccharose), human milk substitutes, medicinal substances, antibiotics and food additives [2]. At present, maltose assumes ever greater importance in food production. Syrup containing maltose as a basic component is featured by high thermo-stability, low hydro-scopics also being less allergenic and viscous, it has sweet taste and do not crystallize at storage [3]. Maltose is used, in particular, in baby foods production as a saccharose constituent since its allergenic effect is essentially lower than that of the saccharose.

In sugar production technology, boiling water should be strictly controlled regarding the presence of invert (glucose and fructose) which causes pipeline corrosion and boiler failure and, as a result, defect and accidental additional cost.

Currently, saccharides concentration is regularly measured by analytical methods. Most traditional methods (liquid- and gas chromatography, chemical and optical methods) need expensive and complicated equipment and highly skilled personnel for its operation and maintenance, samples should be pretreated in a rather complex way [4, 5]. For

instance, the refractometry is used for saccharose analysis in beet pulp; this method is experienced labour- and time-consuming because of the requirement of samples pretreatment with harmful reagents (e.g., lead acetate) for over than 40 min.

Nowadays, the application of conductometric biosensors is a promising approach in development of apparatus for determination of saccharide concentration. Conductometric methods are sufficiently simple, easy-to-use and precise in terms of application for both research and commercial purposes. Conductometric transducers are advantageous as compared with electrochemical transducers of other types by following characteristics:

- absence of technologically complex and large-sized reference electrode;
- application of low-amplitude alternative current (which allows to avoid Faraday effect on electrodes);
- light insensitivity (in contrast to ion-selective field-effect transistors);
- a potential of miniaturization and high-rate integration assuming usage of inexpensive thin-film technology;
- low costs at mass production [6].

The four-channel biosensor analyzer of saccharides, described in this article, is suggested for determination of glucose, saccharose, lactose and maltose in aqueous solutions.

Design of conductometric biosensor analyzer and principles of operation

Measurement of tested analytes concentration by conductometric biosensors (CBS) is carried out in a buffer solution with ion conductivity. CBS consists of a selective biochemical transducer in the form

of a thin membrane deposited on planar electrodes placed on a thin plate. CBS is immersed in the buffer solution. The tested substrate being added in buffer solution, penetrates the selective membrane and the chemical reaction takes place resulting in change of ion concentrations. Consequent change in specific electric conductivity is proportional to the tested substrate concentration.

The system of planar electrodes transforms the changes of solution conductivity into a CBS output informational parameter — changes of active conductivity. However, along with this useful component, there are non-informative components in the CBS output signal: considerable background temperature-dependent (2 %/ °C) active conductivity of buffer solution and reactive conductivity connected with the processes at electrode/electrolyte interface.

To suppress non-informative components and ensure required measurement stability, a differential sensor is used which consists of two conductometric transducers (CT) included in a compensation-bridge circuit of a secondary transducer (ST). Considering difference in electric properties of CT and membranes to be negligible, the circuit can be taken as balanced. Both CT are geometrically identical, each CT consists of a pair of thin-film interdigital electrodes on an insulating support. Addition of the tested solution into buffer solution causes changes in specific conductivity of the active membrane while that of passive membrane remains the same. It causes the bridge circuit disbalance and the constituent of ST output voltage occurs which is proportional to the tested solution concentration.

Though the above-stated principles of conductometric biosensor systems are well-known, simple and metrologically reliable apparatuses are as yet far from realization. As the authors established, the main cause is that an effect of non-informative reactive component of differential CBS impedance on the transformation function of bridge circuit is more complicated than it has been assumed. Thus, as shown in [7, 8], the bridge sensitivity (i.e. the ratio of output signal increment $\Delta \dot{I}$ to active conductivity change ΔG) at fixed applied voltage \dot{U}_r strongly depends on the ratio between active and reactive components of the CT impedance (phase angle tangent $tg\phi$). This dependence is described by the expression:

$$\Delta \dot{I} = \dot{U}_r \Delta G \frac{1}{1 - tg^2\phi - j2tg\phi}.$$

On the other hand, the dependencies of CT equivalent circuit parameters on electrode circuit geometry, electrodes material, frequency of bridge applied voltage, concentration of buffer solution have been shown. The tangent of the phase angle can range from several tenths to one. At increase of frequency till 20 — 30 kHz, the tangent value drops (that is characteristic for the series equivalent circuit) while at higher frequencies, either stabilization, slight decrease or increase of this parameter is revealed. The frequency characteristics of the phase angle tangents for 6 pairs (firm lines and dashed lines, respectively) of planar conductometric transducers with $20 \times 20 \mu\text{m}$ inter-digital topology of gold electrodes are presented at Fig. 1. The data obtained testify the complication of the equivalent circuit and failure to improve characteristics via increasing frequency.

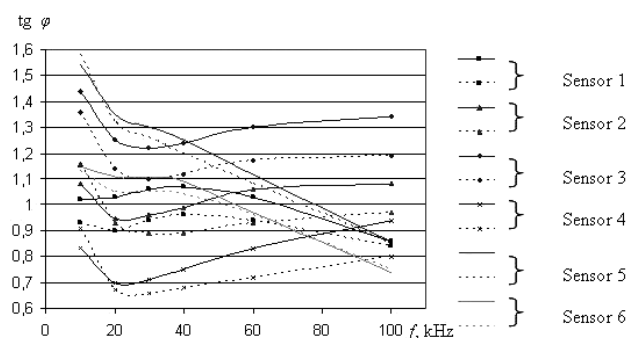


Fig. 1. Frequency characteristics of phase angle tangent

An influence of non-informative parameters of measuring transducers is especially challenging at development of multi-channel (multi-sensor) systems since these effects are to be taken into account and corrections have to be done for each channel separately. In the course of the research, causes and characteristics of the reported dependencies were studied; novel methods and means of transformation of differential CBS impedance parameters were suggested to ensure required stability of the transformation coefficient of measuring circuit as regards to the effect of non-informative parameters of the circuit elements [9, 10].

Basically, new measuring methods suggested distinguishing of the compensation (equilibration) of the voltage drop on the capacitive (non-informative) component of CT impedance which allows the normalization of test voltage on the active (informative) component at working frequencies of 20 — 30 kHz for CT of any kind. As a result are attained:

- the considerable increase in measuring channel sensitivity;
- decrease of its variation range;
- stability of transformation coefficient are attained.

Further sensitivity increase and stabilization can be obtained by complete equilibration of the bridge circuit and use of its output signal module as an informative parameter. Main transformation methods and functional schemes of some ST with compensation-bridge circuits have been reported in [9, 10].

Below the hardware and software packages are considered as a basis for realization of four-channel biosensor analyzer of saccharides composition in food production and allied industries.

At Fig. 2 the analyzer composition and interaction of its modules and units are shown. The sensor block consists of a stand with fixed block of holders (BH) containing four conductometric biosensors (CBS) with membranes, each of which is selective to either glucose, saccharose, lactose or maltose. CBS are immersed into a vessel filled with buffer solution; the sample solution is added in order to be measured. A magnetic stirrer (MS) ensures solution homogeneity throughout the measurement procedure. An electronic measuring block consists of two modules:

- the module of secondary transducers (MST);
- the basic measurement-control module (BMC) [11].

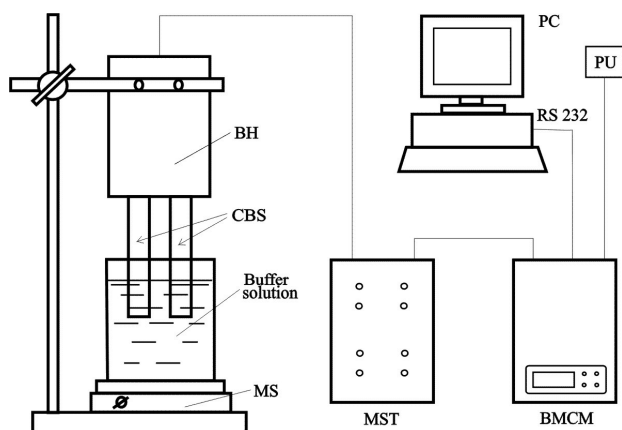


Fig. 2. Scheme of measuring conductometric system

Both of them are supplied with power unit. A personal computer (PC) with specific software support is also an integral part of the measuring block. It is noteworthy that BMC is a unified block which allows realization of wide range of measuring devices at low costs of elaboration [12].

A structural diagram of the measuring channel is presented at Fig. 3. MST module consists of four secondary transducers ST1 — ST4; each has a compensation-bridge circuit [9]. Output impedances (Z) of each CT pair are connected into the loops of certain ST. The sensors are supplied with sinusoidal potential, frequency of 20 — 30 kHz and amplitude of 10 mV, generated by the generator G . The output potential of each ST is proportional to CT impedance difference of the particular CBS. Output potentials of ST are connected in turn into BMC module input by means of an electronic switch $K1$. There are two synchronous detectors CD1 and CD2 intended for separation of ST output signal into two components, synchronous and meander, relative to G potential. These components in turn, via electronic switch $K2$, enter the input of the integrating analogue-digital converter (ADC), and then are connected, as the digital code, into the microcontroller (MC) for subsequent processing. MC is regulated with the software at lower level which guarantees the data exchange with ADC and PC, and control over G and switches $K1$ - $K2$ operation. BMC is provided with keyboard (KB) and indication block (IB) for autonomous (without PC) work of the analyzer.

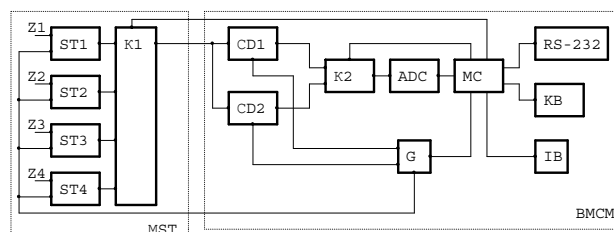


Fig. 3. Structural circuit of measuring channel of conductometric system

The operational algorithm consists of two stages: preliminary balancing of bridge circuit and determination of results of biochemical reaction.

At the first stage, CBS is placed into buffer solution without tested substrate. By means of regulation elements, the bridge circuits of ST1 — ST4 are in turn balanced with respect to two components (in-phase and meander) of the output potential. The results of output signals measurement from ST1 — ST4 are processed and displayed at the indicator (I) and are used as a balanced parameter.

At the second stage, the solution under test, containing saccharides of certain concentration, is added into the buffer solution. The biochemical reactions in selective membranes result in generation

of the unbalance potentials on ST outputs. Their in-phase components proportional to the concentration of particular saccharide are transformed into digital codes which enter PC via interface port RS-232C; they are displayed on digital indicator in an autonomous mode.

The personal computer with software of higher level (SHL) performs automatic control of the measuring complex, and complete processing, accumulation and plotting of the measurement results. The software consists of two modules. The basic one (BSHL) is a unified module which could be used for multi-channel measuring systems with rather wide range of regular functions. Another module takes into account the peculiarities of actual measuring complex intended for specific task.

SHL is featured in following functions:

- compensation of the voltage drop on a capacitive component of CT impedance and coarse balance of bridge circuit by in-phase components of a disbalance signal; accurate bridge balancing by meander components of a disbalance signal (for measurements with the equilibrium method);
- realization of multi-channel mode of measurement;
- calibration of measuring channels for correction of transfer functions and determination of saccharides concentration;
- regulation of the equivalent noise transmission band by the data averaging.

For realization of specific functions of a multi-channel biosensor analyzer, the BSHL is supplemented with:

- the software ensuring interface with a user of the analyzer;
- generation and transmission of the commands to equilibrium;
- BMCM and MST control;
- obtaining and specific processing of information.

Besides, the tracer programs are available for experimental investigation of apparatus and software of the conductometric complex.

Basic software is a set of various functional programs started by the operator via a system of multi-level menus. BSHL is a Windows applications with the menu and pictograms; it gives to users the wide scope of facilities for processing electric informative characteristics (U, I, R, etc.) obtained by transducers of various kinds as well as for computation of the parameters to be determined (solution concentration, specific conductivity, temperature, humidity,

mass, pressure, etc.) with the fourth power polynomial or specific formula.

BSHL functions are similar to those of other measuring systems:

- tuning for required number of channels (1 to 32);
- data exchange with the measuring block via interface RS-232C;
- summarizing measured and computed values of the parameters and other information (date, time, experiment number, notes) in the Excel tables with regard to the time of tabulation;
- saving information in a file in the text format convenient for other applets (Excel, Word, etc.);
- realization of different modes of measurement (single, continuous, cyclic).

BSHL allows performing the routine procedures of processing measurement information:

- accounting of the initial parameters;
- comparison with threshold values;
- calibration by external factors;
- determination of sum (difference) of the values obtained on various channels;
- plotting the results of measurement and calculation.

It provides the output of an arbitrary combination of measured or computed values to one or two axes, scaling of indicated values (by the user or automatic), viewing the data on horizontal and vertical axes with the possibility of selecting and scaling of a part of the graph.

The view of the main window of the developed BSHL on the PC display is presented at Fig. 4.

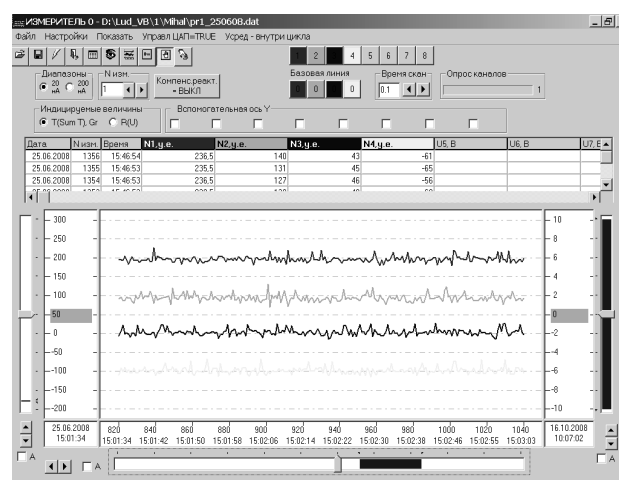


Fig. 4. View of main window of basic program

Results

The system was tested regarding determination of the saccharides such as saccharose, lactose, maltose, glucose. The basic enzymatic reactions are presented at Fig. 5.

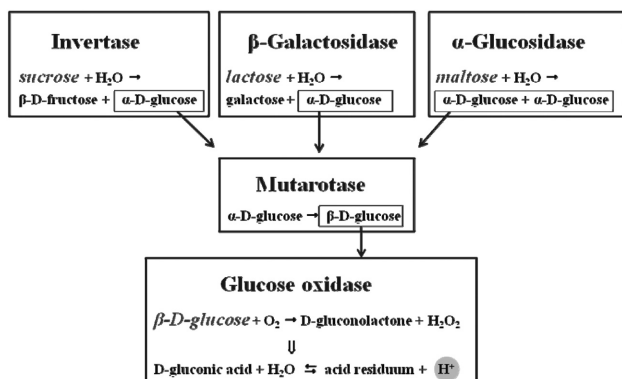


Fig. 5. Basic enzymatic reaction of conductometric analyzer of saccharides

Three enzymes are required for measurement of saccharose, lactose and maltose, whereas only glucose oxidase is necessary for glucose determination. The enzymes invertase, β -galactosidase and α -glucosidase decompose their substrates: saccharose, lactose and maltose to α -D-glucose. The latter is decomposed upon mutarotase action to β -D-glucose, then by glucose oxidase — to hydrogen peroxidase and D-gluconolactone which is spontaneously hydrolyzed to gluconic acid with subsequent dissociation into acid residue and proton generation. Therefore, the solution conductivity changes which can be registered by conductometric transducer.

Calibration curves obtained by the developed conductometric saccharides analyzer (Fig. 6) could be used for efficient concurrent measurement of concentrations of four saccharides, i.e. saccharose, lactose, maltose, and glucose.

The general view of the analyzer is presented at Fig. 7.

Conclusions

As the result of the experimental results discussion we could state the following:

1. The conductometric biosensor system using novel methods and measuring means is an example of convenient advanced analytical equipment for concurrent efficient determination of concentration of several saccharides in raw materials and

semi-processed goods, in final production and in technological media.

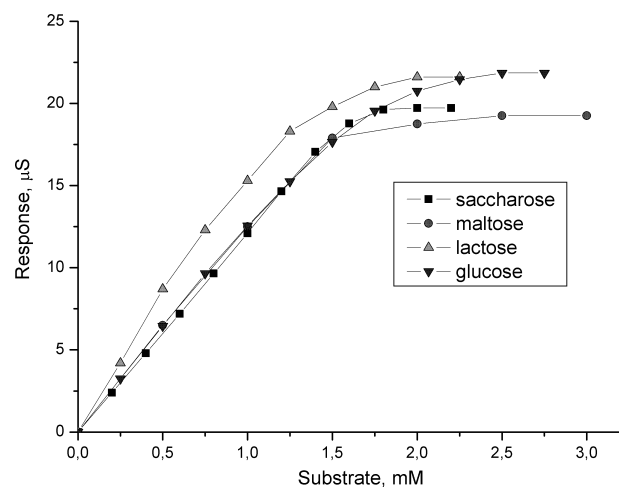


Fig. 6. Calibration curves of responses dependence for glucose, saccharose, maltose and lactose sensors on concentrations of glucose, saccharose, maltose and lactose, respectively

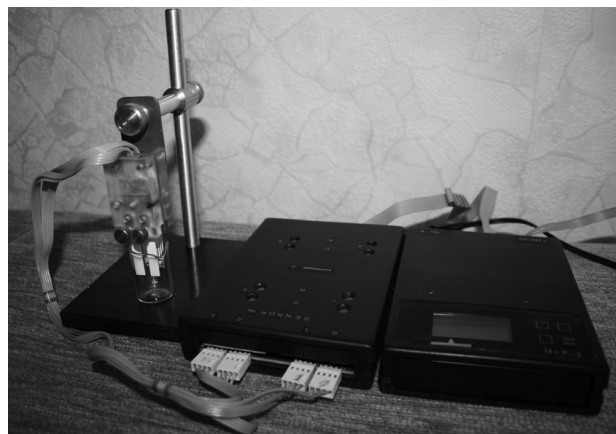


Fig. 7. General view of conductometric analyzer of saccharides

2. The preliminary experimental research presented testifies that the system ensures separate determination of concentration of saccharose, lactose, maltose and glucose with commercially available sensitivity.

3. The soft hardware applied provides high technical and economic parameters of the developed analyzer and could be used for solution of various tasks.

The work has been financially supported by National Academy of Sciences of Ukraine in the frame of complex scientific-technical program "Sensor systems for medical-ecological and industrial-technological needs".

References

1. H. Schiweck. Zusammensetzung von Zuckerbrennmelassen // Zuckerindustrie. — 1994. — 119, № 4. — P. 272 — 282.
2. V. M. Pyeshkova, O. Y. Sayapina, O. O. Soldatkin, O. L. Kukla, S. V. Dzyadevych. Enzyme conductometric biosensor for determination of lactose // Biotechnology. — 2008. — 1, No 4. — P. 76-84.
3. E. A. Obukhovskiy. Production of maltose treacle. — M.: Pischepromizdat, 1959.
4. E. L. Styskin, L. B. Itsyson, E. V. Braude E. B. Practical high-pressure liquid chromatography. — M.: Nauka, 1986. — 284 p.
5. K. Wilson, J. Walker. Methods of practical biochemistry. — M.: Mir, 1978. — 272 pc.
6. S. V. Dzyadevych. Conductometric enzyme biosensors: theory, technology and application // Biopolymers and Cell. — 2005. — 21, No 2. — P. 91 — 106.
7. V. G. Melnik, A. D. Vasilenko, M. P. Medvedenko, A. A. Mikhal, A. A. Soldatkin. Investigation of informative parameters of differential conductometric biosensors // Technical electrodynamics. Problems of modern electrotechnics. — 2006. — Part. 3. — P. 119 — 124.
8. V. G. Melnik. Investigation of sensitivity of bridge measurements circuit with differential conductometric transducer / Works of Institute of electrodynamics of National Academy of Sciences. K.: Institute of electrodynamics. — 2009. — volume 22.
9. V. G. Melnik, M. P. Rubanchuk, A. A. Mikhal. Measuring circuits for conductometric sensors with differential two-electrodes transducers // Technical electrodynamics. — 2008. — No 2. — P. 58 — 64.
10. A. D. Vasilenko, V. G. Melnik, A. I. Novik, M. P. Rubanchuk. Stabilization of sensitivity of differential conductometric biosensor transducers // Technical electrodynamics. — 2009. — No 3. — in press
11. A. D. Vasilenko, V. G. Melnik, A. A. Mikhal, M. P. Medvedenko, N. F. Starodub. Biosensor complexes based on impedimetric measuring systems. / Investigations in the field of sensor systems and technologies. — K.: IMBG, 2006. — P. 287 — 297.
12. V. G. Melnik, A. D. Vasilenko. Impedimetric measuring transducers for biosensor systems // Electronic components and systems. — 2008. — No 11. — P. 27 — 29.

МАТЕРІАЛИ ДЛЯ СЕНСОРІВ

SENSOR MATERIALS

UDC 544.023.57; 544.032.65; 535.41; 539.411

THIN FILMS OF TRET-BUTYL CALIXARENE AS SENSITIVE MATERIALS FOR ORGANIC COMPOUND DETECTORS

*A. L. Kukla, A. A. Vakhula, I. V. Kruglenko,
V. Yu. Khorouzhenko, I. A. Samoylova*

V.E. Lashkaryov Institute of Semiconductor Physics, NAS of Ukraine
03028, Kiev-28, pr. Nauki, 41, tel./fax 380 (044) 265-18-27, kukla@isp.kiev.ua

THIN FILM OF TRET-BUTYL CALIXARENES AS SENSITIVE MATERIALS FOR GAS SENSORS TO THE ORGANIC CHEMICAL COMPOUNDS

A. L. Kukla, A. A. Vakhula, I. V. Kruglenko, V. Yu. Khorouzhenko, I. A. Samoylova

Abstract. Adsorption properties of thin nanostructured films of tret-butylcalix[n]arenes ($n=3, 4, 5, 6, 8$) with thickness of about 200 nm to vapors of different organic solvents are investigated. Two methods were used for adsorption measurements — mass-sensitive quartz microbalance and interference colorimetry. Gas sensitive, selective and regenerative parameters of the used calixarene films as sensitive materials for chemical sensors were investigated. It is shown that the calix[5]arene films are most sensitive for detection of chlorine organic compounds. The comparative analysis of responses of quartz microbalance and optical sensor elements for each of the explored sensitive films have been carried out.

Keywords: QCM sensors, RGB-colorimetry, calix[n]arenes

ТОНКІ ПЛІВКИ ТРЕТ-БУТИЛ КАЛІКСАРЕНІВ ЯК ЧУТЛИВІ МАТЕРІАЛИ ДЛЯ СЕНСОРІВ ДО ОРГАНІЧНИХ СПОЛУК

О. Л. Кукла, О. А. Вахула, І. В. Кругленко, В. Ю. Хоруженко, І. О. Самойлова

Анотація. Досліджені адсорбційні характеристики тонких наноструктурованих плівок трет-бутилкалікс[n]аренів ($n=3, 4, 5, 6, 8$) товщиною близько 200 нм до парів різноманітних органічних речовин. Вимірювання адсорбції каліксаренових шарів проведено двома способами — за допомогою мас-чутливого кварцового мікробалансу та шляхом інтерференційних колориметричних вимірювань. Визначено газочутливі, селективні та регенеративні параметри досліджених плівок як чутливих матеріалів для хімічних сенсорів. Показано, що для детектування хлорвмісних сполук найбільш чутливими є шари на основі каліксарену C[5]A. Проведено порівняльний аналіз відгуків кварцових кристалічних та оптичних сенсорних елементів для кожної із досліджених чутливих плівок.

Ключові слова: QCM сенсор, RGB-колориметрія, калікс[n]арени

ТОНКИЕ ПЛЕНКИ ТРЕТ-БУТИЛ КАЛИКСАРЕНОВ КАК ЧУВСТВИТЕЛЬНЫЕ МАТЕРИАЛЫ ДЛЯ СЕНСОРОВ К ОРГАНИЧЕСКИМ ВЕЩЕСТВАМ

А. Л. Кукла, А. А. Вахула, И. В. Кругленко, В. Ю. Хоруженко, И. А. Самойлова

Аннотация. Исследованы адсорбционные характеристики тонких наноструктурированных пленок трет-бутилкаликс[*n*]аренов (*n*=3, 4, 5, 6, 8) толщиной около 200 нм к парам различных органических веществ. Измерения адсорбции каликсареновых слоев проводились двумя методами — с помощью масс-чувствительного кварцевого микробаланса и путем интерференционных колориметрических измерений. Определены газочувствительные, селективные и регенеративные параметры исследуемых пленок как чувствительных материалов для химических сенсоров. Показано, что для детектирования хлорсодержащих соединений наиболее чувствительными являются слои на основе каликсарена C[5]A. Проведен сравнительный анализ откликов кварцевых кристаллических и оптических сенсорных элементов для каждой из исследованных чувствительных пленок.

Ключевые слова: QCM сенсор, RGB-колориметрия, каликс[*n*]арены

Introduction

Chemical sensors are the rapidly evolving fields of the modern sensor science. Majority of investigations in this area is concentrated towards diminishing the sensor overall dimensions, achieving higher sensitivity and lower reaction times, and also search for new highly selective materials for various analytes detection. Chemical sensors are widely applied in medical diagnostics [1] and biomedical analysis [2, 3], in environmental monitoring (continuous and long-term monitoring of detrimental compounds) [4, 5], in food industry [6-8] and pharmacology [9-11], cosmetics production etc.

The necessity of characterization and identification of multicomponent mixtures has lead to development of the multisensor arrays. The question of sensitive layers selectivity to specific gaseous mixtures is essential for creation of intelligent systems for taste and odor discrimination based on such sensors.

Taking into account the ability of organic materials to form various types of molecular interactions and their variety, the organic sensitive layers are most attractive as to their use in the new generation of sensor arrays. Ability of volatile compounds to be adsorbed into molecular capsules of different forms and sizes provides the increased selectivity, good affinity and high sensitivity of such layers toward analytes. These properties are well pronounced in the volumetrically porous organic materials consisting of the complex multiatom molecules (macrocycles, calixarenes, polymers) which are able to bind various organic substances and gases due to the presence of molecular cavities.

Use of the molecular organic crystals opens wide possibilities for formation of sensitive architectures with predefined chemical functionality. Characteristic examples of this approach are given by the use of various cavitands, first of all calixarenes [12-14], which are very promising materials considering the possibility of optimization of their structure to match the analyte molecules' one [15-20]. These peculiarities of the molecular structure (presence of the nanocavities) and also the ability of molecular recognition of the organic compounds allow to utilize the calixarenes for creation of the gas sensors sensitive layers [21].

The aim of the present work is investigation of the sensitivity and selectivity of sensitive layers formed with thin films of tret-butylcalixarenes in chemical and gas sensors for detection of various organic substances, and also conduction of the comparative analysis of responses of the quartz crystal and optical sensor elements as related to correlation between the adsorbed molecular mass and corresponding change in optical parameters for each of the sensitive films under consideration.

Materials and methods

In this work thin films of C[3]A, C[4]A, C[5]A, C[6]A, C[8]A tret-butylcalixarenes were used as sensitive layers. Materials in powder form were synthesized at the Institute of Organic Chemistry of NASU and kindly provided by prof. V.I. Kalchenko. The films were obtained by thermal evaporation in vacuum (with the VUP-5M setup, residual pressure of 5×10^{-4} Pa) and deposition onto the metal electrodes of piezoelectric transducers [22], or onto

the polished silicon substrate 20x20 mm in size for optical transducers [23], in both cases at room temperature (297 ± 2 °K). The average deposition rate was about $10 \text{ nm} \cdot \text{min}^{-1}$. The films thickness was monitored during deposition by means of quartz thickness measuring device; the final thickness obtained for all cases was about 200 nm.

The following groups of organic compounds were used as analytes: chlorinated compounds (chloroform, dichlorethane), aromatic compounds (toluene, xylene), ketones (acetone), ethers (butylacetate) and alcohols (ethyl, isopropyl and butyl alcohol).

Experimental setup and measurement principles

In this work for direct experimental evaluation of organic compounds vapor adsorption onto the calixarene coatings, the 5-channel multisensor system based on AT-cut quartz resonators (with resonance frequency of 10 MHz) was used [22]. Upon adsorption of the analyte molecules on sensitive layer the working frequency of quartz resonator decreases. Basic equation describing the relation between the change in resonance frequency of AT-cut quartz crystal and the mass adsorbed on the crystal surface is according to [24, 25]

$$\Delta f = -\frac{2f_0^2}{A\sqrt{\rho_q\mu_q}} \Delta m \quad (1)$$

where Δf is the change in crystal oscillation frequency in Hz, f_0 is the piezoquartz frequency in MHz, Δm is the mass adsorbed on the sensitive film, g , A is the electrode surface area in cm^2 , $\rho_q = 2.648 \text{ g} \cdot \text{cm}^{-3}$ (the quartz density), $\mu_q = 2.947 \times 10^{11} \text{ g} \cdot \text{cm}^{-1} \cdot \text{s}^{-2}$ (the AT-cut quartz shear modulus).

For additional investigation of vapor adsorption onto the calixarene layers we used the optoelectronic interference multisensors with digital response registration in form of change in the color components (red, green and blue) of the interference-colored calixarene layers upon the adsorption of analyte molecules [23]. The sensor system included the white light source, device for image capturing (web camera) and the flow-type cell with the sensor array [26]. It was shown earlier, that the calixarene films can be used as sensitive layers in colorimetric gas sensor for detection of alcohol molecules of several types [27], chlororganic and aromatic compounds [28]. Interference coloration of the thin layer of sensitive coating deposited on reflective substrate

changes upon interaction with gas molecules due to change in refraction index and thickness of the film. Usually a change of the color vector length in the R, G, B values space is used as response of such colorimetric sensor [26]. However, as numerous experiments have shown, the calculation of angular coordinates of the color vector in above mentioned space provides more accurate representation of the colorimetric image of the film; this is achieved due to compensation of instability caused by fluctuations of the light source intensity and by noise in the data transmission channel [29]. Thus, we will define the response of interference colorimetric sensor upon the influence of analyte vapor as deviation of angular position of the color vector from its previous state [28]:

$$\Delta S = \sqrt{\left[\frac{R_1 - R_0}{L_1 - L_0}\right]^2 + \left[\frac{G_1 - G_0}{L_1 - L_0}\right]^2 + \left[\frac{B_1 - B_0}{L_1 - L_0}\right]^2} \quad (2)$$

where R, G, B are the measured values of the color vector components, $L = \sqrt{R^2 + G^2 + B^2}$ is the absolute length of the color vector in R, G, B space and indices 0 and 1 define the initial and subsequent states of the film (before and after its exposure to analyte vapor) respectively.

Methods of measurement

The colorimetric RGB-measurement method

The analyzed organic compound vapors with different concentrations were prepared by diluting the initial saturated vapors with dry air to the defined amount of dilution. Then the mixture was transported through the sampling cell with volume of 2 ml, where the sensor array with calixarene layers was installed. Table 1 shows concentration ranges for all used analytes as well as concentration change step value. Let us note that the maximum concentration listed in the table corresponds to 50 % dilution and the minimum concentration corresponds to 95 % dilution. The step at which the analyte concentration was increased corresponded to the 5 % change in analyte amount. The concentration value was calculated according to the following formula:

$$C = \frac{P_s}{P_{atm}} \frac{V_s}{V} 10^6 \quad (3)$$

where C is the analyte concentration in ppm, P_s is the analyte saturated vapor pressure, P_{atm} is the nor-

mal atmospheric pressure (766 mm Hg), V_s is the volume of a saturated vapor sample, V is the volume at which the dilution was performed (a 20 ml syringe).

Table 1

Minimum and maximum concentration values for the investigated analytes vapor supplied to the sensor cell, and the step of concentration change during the concentration dependencies measurement.

Analyte	Saturated vapor pressure at 23 °C, mm Hg	Minimum concentration, ppm	Maximum concentration, ppm	Concentration change step, ppm
Acetone	202	13185	131850	13185
Butanol	5	290	2900	290
Butylacetate	18	1174	11740	1174
Chloroform	177	11553	115530	11553
Dichlorethane	75	4895	48950	4895
Ethanol	50.5	3296	32960	3296
Isopropanol	39	2545	25450	2545
Toluene	25.5	1664	16640	1664
Xylene	6	392	3920	392

Registration of the colored image of investigated sample was performed at room temperature, first for the initial state of the sample, then every second during ten seconds after the exposure to analyte vapors and then at the point 2 minutes after purging the sample with dry air. In all cases the coloration state after 10 seconds from the start of analyte vapor supply was taken as the response signal for further processing.

The quartz microbalance (QM) method

The necessary conditions for gas mixtures analysis is the consistency of their composition and concentration during the entire period of experiment. For each of the investigated samples, the concentration was calculated according to the values listed in Table 1; the sample then was injected into the 110 ml cell through the inlet. The analyte vapor filling the cell contacted the sensor array. With the help of multisensor system the quartz elements response kinetics was simultaneously recorded for all calixarene layers, sequentially for each analyte at the given concentration. Response was registered during 10 minutes, however in all cases the maximum response value was taken as informative parameter, that is, the maximum deviation of the resonator oscillation frequency from its initial value. The temperature during the measurement was maintained at 20 °C by means of thermostat [22]. To ensure the

equal measurement conditions and eliminate the influence of previous experiments after each measurement the cell was cleaned by blowing with carrier-gas (argon), which always lead to restoration of the sensors working characteristics.

Results and discussion

Using both the above described measurement methods, the responses for five types of calixarene films to the vapor of nine organic analytes in wide range of concentrations were obtained.

Fig.1 shows the calculated from formula (1) mass of adsorbed molecules for each of the investigated analytes depending on its concentration for QM-sensors based on respective calixarene layers.

Fig.2 shows the concentration dependencies for responses of optical RGB-sensors based on the same sensitive layers, calculated from formula (2). Let us note that the concentrations scale for each analyte for all presented curves is identical and corresponds to the data in Table 1.

As it could be seen from the presented curves, the responses of all investigated QM-sensors (which are proportional to the adsorbed molecules mass) show monotonous growth upon the increase of analyte concentration, and the mass increase rate varies depending on the analyte type. At the same time behavior of concentration dependencies for majority of RGB-sensors responses is somewhat different: with concentration increase the responses change insignificantly, and only after some threshold concentration the response value starts to increase quite rapidly. Such response behavior is typical for C[3]A, C[6]A and C[8]A films. Only the C[5]A calixarene demonstrates responses close to linear.

For more intuitive juxtaposition of QM and RGB-sensors sensitivity and selectivity Fig.3 shows normalized responses to investigated analytes at fixed concentration equal to $P_{\#}/2$.

Reasoning from the present data, we may outline the following characteristic features of calixarene layers as sensitive materials that were equivalently evidenced in both types of sensors.

First, all films appeared to be least sensitive to alcohol, especially in RGB-measurements. Second, the largest responses were observed for chlorinated analytes (chloroform, dichlorethane). Most sensitive in respect to all considered analytes are the C[5]A and C[6]A films, and the least sensitive is C[4]A.

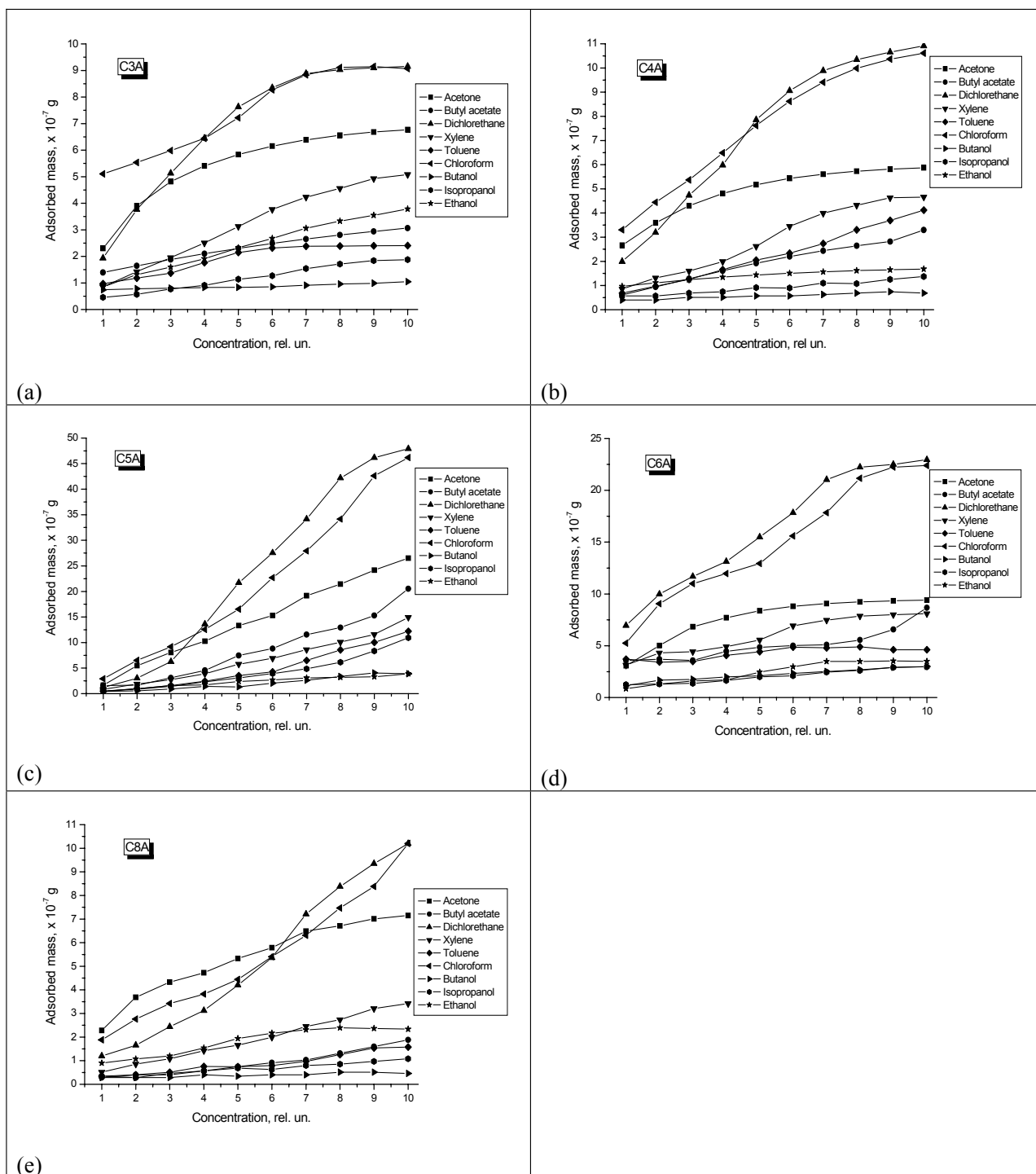


Fig. 1. Concentration dependencies for the mass adsorbed on calixarene layers of specified types for the entire set of investigated analytes: (a) C[3]A, (b) C[4]A, (c) C[5]A, (d) C[6]A, (e) C[8]A; concentration range for each of the given analytes are listed in Table 1.

To specific differences in responses of QM and RGB-sensors we may attribute the following: among the QM-sensors maximum absolute sensitivity to the majority of used analytes is observed for sensors with the C[5]A sensitive layer (see Fig.3,a). Less sensitive are the sensors with C[6]A layer (approximately by factor of two) and the least sensi-

tive are sensors with C[3]A, C[4]A, C[8]A layers (by factor of 4-5). At the same time RGB-sensors with different calixarene layers differ from each other not as much by sensitivity but more by dynamics of the sensitivity change depending on concentration. However, the sensors with C[5]A sensitive layer also stand out here demonstrating nearly linear dynam-

ic range of responses in considered concentrations range; on the contrary, sensors based on the C[4]A

film demonstrate weak reaction to all analytes at any concentrations.

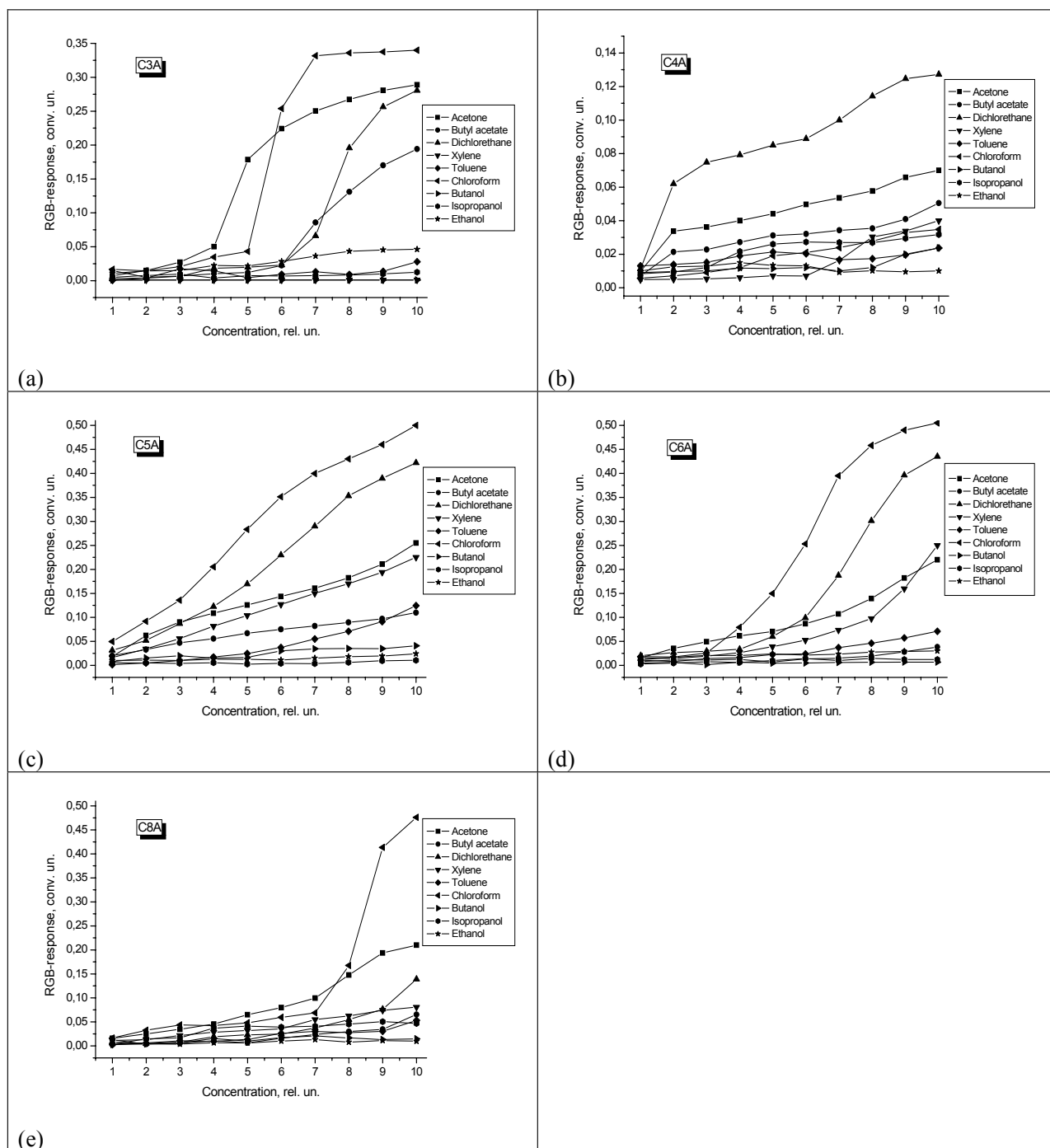


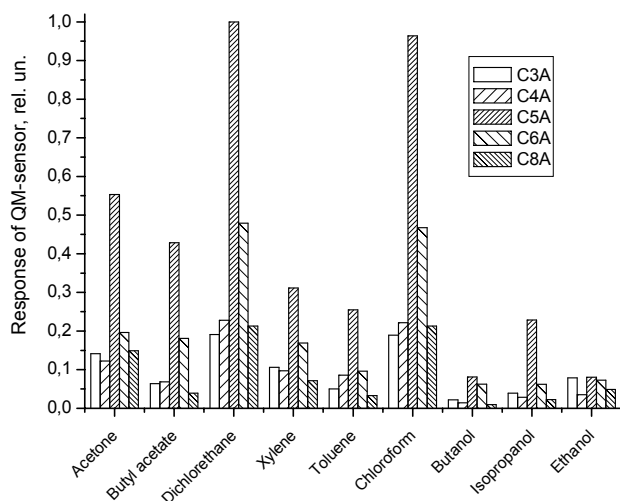
Fig. 2. Concentration dependencies for responses of the RGB-sensors with sensitive layers formed with calixarenes of five types to the vapor of specified analytes: (a) C[3]A, (b) C[4]A, (c) C[5]A, (d) C[6]A, (e) C[8]A; concentration range of the analytes are listed in Table 1.

When analyzing the obtained responses, one has to keep in mind that variation of concentration in experiments was achieved by dilution of saturated vapor, and since the saturated vapor pressure for considered analytes significantly varies (see Ta-

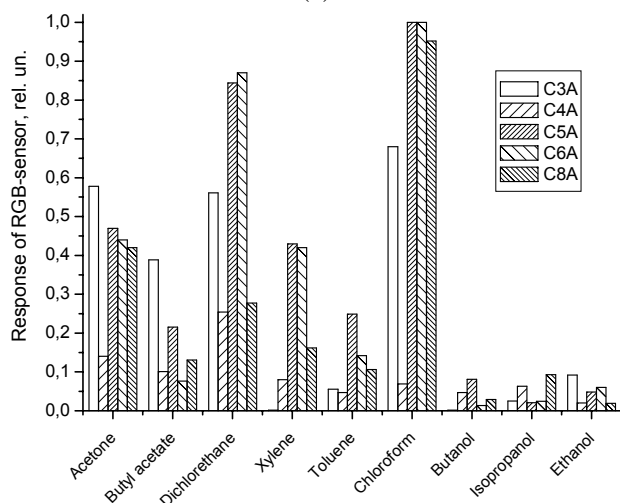
ble 1), the concentration scale is actually different for different analytes.

However, from the diagrams in Fig.3, one may notice that the magnitude of response to various analytes is not proportional to their concentration

and even not correlate with it. E.g. responses to the acetone vapor ($P_s = 202$ mm Hg) are equal to responses to butyl acetate (18 mm Hg) and xylene (6 mm Hg) and approximately 2 times lower than responses to dichlorethane (75 mm Hg) and chloroform (177 mm Hg).



(a)



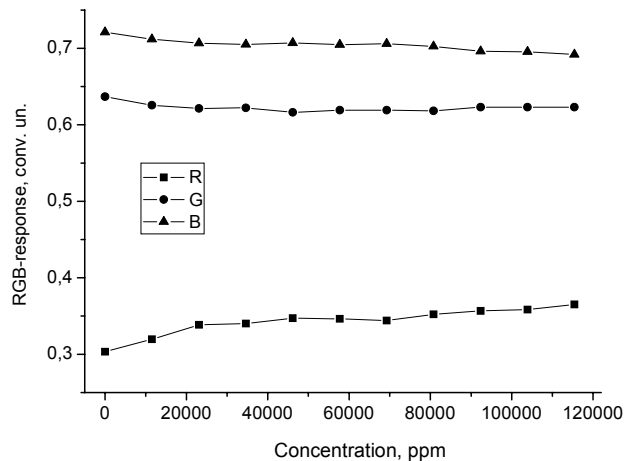
(b)

Fig. 3. Relative responses of QM-sensors (a) and RGB-sensors (b) with sensitive layers of C[3]A, C[4]A, C[5]A, C[6]A, C[8]A to the vapors of all investigated analytes at fixed concentration of $P_s/2$.

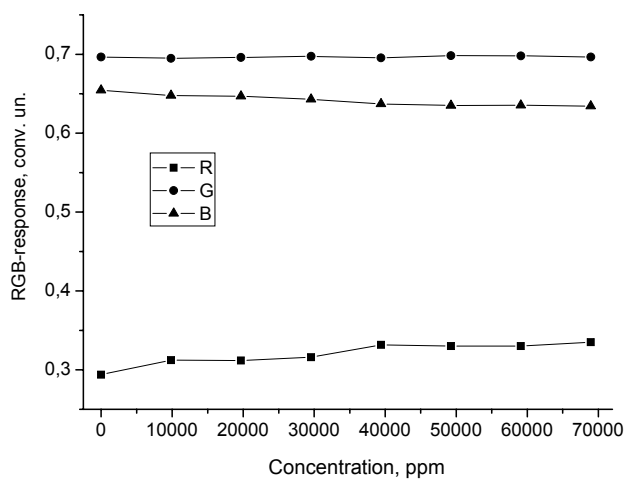
Obviously, the individual selective properties of the “analyte — sensitive layer” system play more important role than the analyte concentration.

Regenerative properties of calixarene sensitive layers upon the influence of organic compounds vapor were also investigated. Fig.4 shows (by the example of sensor with C[5]A layer) the RGB-sensor regeneration curves (that is, the return to initial baseline after exposure to the analyte vapor at various concentrations and subsequent purging with

dry air). The results indicate high reproducibility of responses in a wide range of concentrations (300 through 100000 ppm, depending on analyte). Similar data were also obtained for sensors with sensitive layers of other types.



(a)



(b)

Fig. 4. Regeneration curves for RGB-sensor with the C[5]A sensitive layer, characterizing the return of the film color to its initial state after the exposure to acetone (a) and chloroform (b) vapor in various concentrations and subsequent purging with dry air.

It has to be mentioned that in both types of measurement that was conducted at room temperature after purging and regeneration of sensor element the informative parameter magnitude (the film color or quartz resonator frequency) practically always returned to its initial value, which indicates the absence of strong chemical bonding of molecules within the calixarene films, that is the interaction is characterized by rather weak (coordination, van der Waals) bounds.

As could be seen from the responses of QM and RGB-sensors (see Fig.3), the different calixarene

layers has overlapping but at the same time quantitatively different sensitivity to investigated analytes. This fact could be put to the base of development of the multielement multiparametric sensor for organic substances based on the sensitive films of various calixarenes, when the output signals from each separate sensor element are being registered and form the multidimensional response, which is then to be processed with the help of statistical pattern recognition techniques.

Each analyte or mixture forms its own unique chemical image, which can be mathematically represented, transformed and compared to other images. Fig.5 shows the result of processing the obtained 5-dimensional response vectors from the array of five QM-sensors and five RGB-sensors respectively, by means of principal component analysis [30]. This method allows do reduce the dimensionality of the initial data to two dimensions and visualize it with convenient graphical representation on the principal coordinates plane. Each point on the plane corresponds to one of the analytes at specific concentration and the series of one-kind points corresponding to different concentrations forms certain chemical image of the given analyte occupying a certain region. Absence of overlapping regions would indicate the high selectivity of the sensor array.

As could be seen, in our case reliable discrimination is possible for chlororganic compound and acetone for both sensor arrays, other analytes are more difficult to discriminate, especially at small concentrations. The better selectivity results are demonstrated by the QM-sensors array, probably due to wider range of sensitivity to various analytes.

Comparative analysis of QM and RGB-sensor responses

If one compare the diagrams of the sensor responses for QM and RGB-sensors to the entire set of used analytes (see Fig.3,a,b), one could notice a certain similarity at least in general tendency of change that's why we may suppose that there exists a correlation between the magnitudes of these responses. The reason for this assumption is that the both sensor types used the same calixarene films as sensitive layers, of the same thickness and obtained with identical technology. Besides, the measurement conditions for quartz and optical sensors were also chosen to be identical. The physical and

chemical processes taking place upon adsorption of the analyte vapor onto the sensitive layer are also identical.

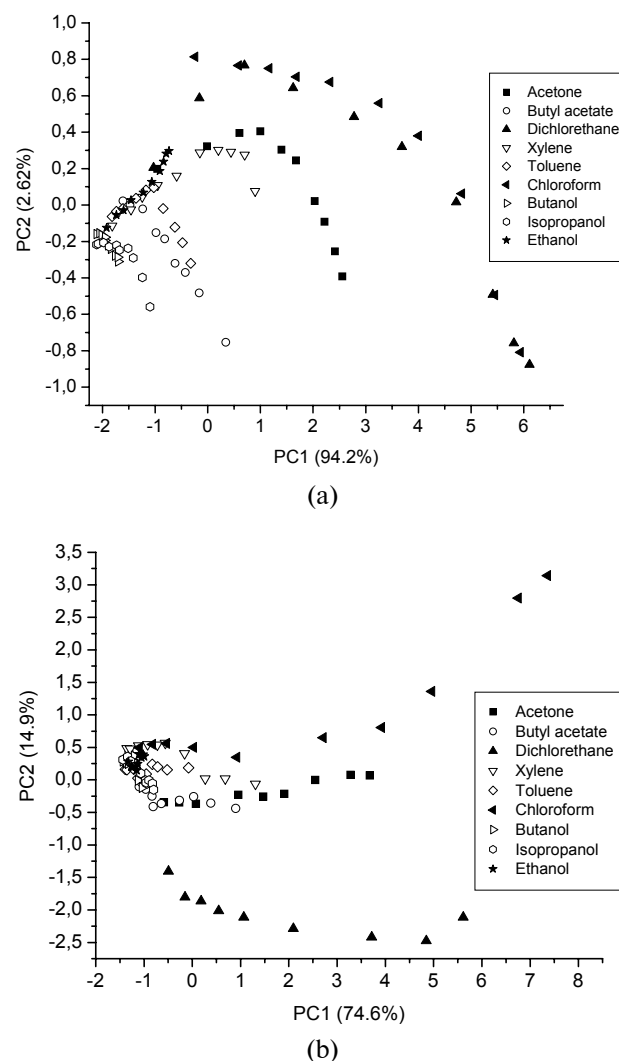


Fig. 5. Disposition of the investigated analytes images on the principal coordinates plane for the five QM sensors array (a) and five RGB-sensors array (b); as the source statistic for calculation all available response values shown in Fig.1 and 2 were used.

Thus, it would be interesting to compare the responses of two types of sensors to find out the grade of similarity in responses caused by identical processes, that is to find out if there exists correlation between the adsorbed molecular mass and corresponding change in optical parameters for each of the investigated sensitive films.

Using all the available response values for QM and RGB-sensors obtained in the experiments, the two-dimensional response diagrams were built for all investigated calixarene films used as sensitive layers for respective sensors (Fig.6). As can be seen, the registered distribution statistics shows general ten-

gency of simultaneous increase on both axes, that is the positive correlation between the QM and RGB-responses. Table 2 lists the calculated correlation coefficients for each type of calixarene film over the

various data sets, namely (a) by the whole totality of collected responses, (b) separately by each fixed concentration for all analytes and (c) separately by each analyte for all its concentrations.

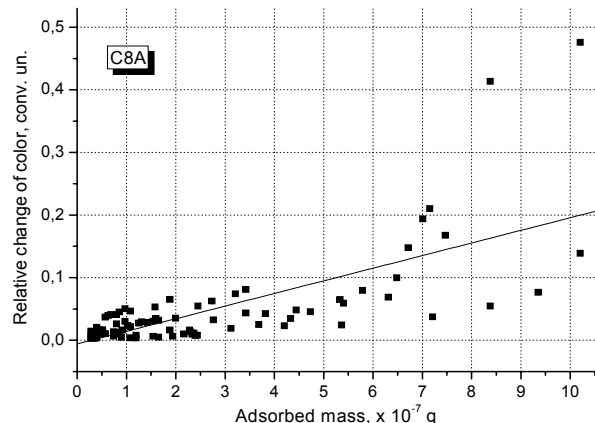
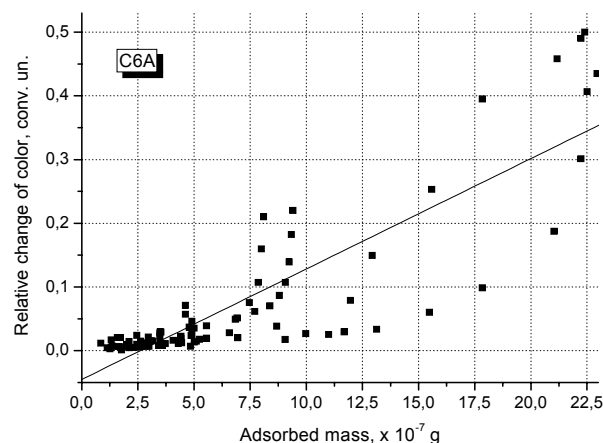
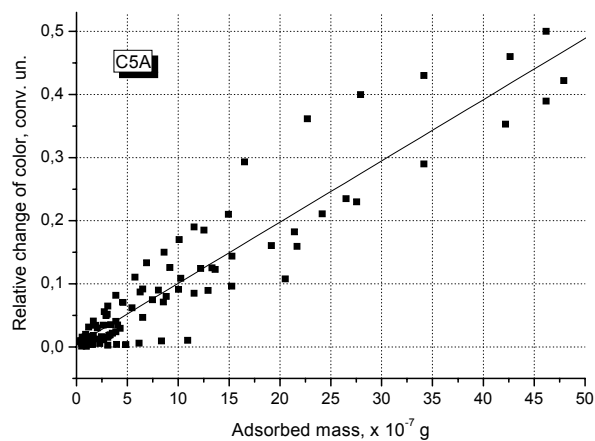
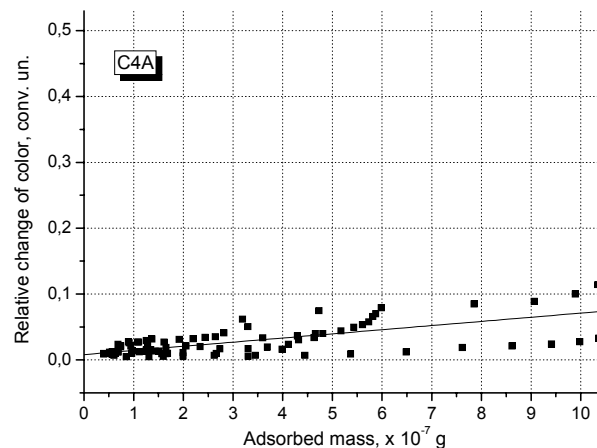
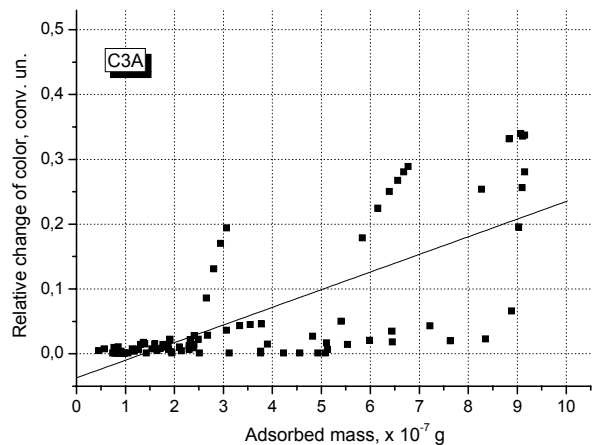


Fig. 6. Correlation diagrams for QM and RGB-sensor responses for five types of the investigated sensitive calixarene films; straight lines show the least squares linear approximation of the obtained data.

For further analysis let us denote the following. Used calixarenes, being the volumetrically porous organic materials, are composed of cyclic

macromolecules having a cup-like shape and the nanocavities between them. The volatile analyte molecules easily penetrate to the bulk of the film.

Basing on the concept that this leads either to the film material the density increase due to the increasing number of particles per unit of volume, when the analyte molecules are being bound within the film, or the organic film swells as a result of adjacent film fragments being pushed aside by the embedding analyte molecules [26–28], we could assume that in the first case such interaction leads

to increase of the refraction index of the film and in the second case to increase of the film thickness. This model is confirmed by the papers [31, 32], where it is shown that the contact of calixarene films with saturated vapor of benzene, toluene and chloroform may lead to the increase of film thickness by 10–20 % and/or increase of its refraction index by 0.01–0.1.

Table 2

Correlation coefficients for QM and RGB-sensor responses calculated for each type of calixarene film over the following data sets: whole totality of the obtained responses, by every fixed concentration for all analytes, and by every analyte for all its concentrations.

Calixarene	C[3]A	C[4]A	C[5]A	C[6]A	C[8]A	Calculation method
Correlation coefficient $r(S_{\text{RGB}}, S_{\text{QM}})$	0.726	0.637	0.935	0.862	0.709	Over entire data set
	0.773	0.374	0.910	0.823	0.681	Averaging by concentrations
	0.616	0.497	0.924	0.778	0.821	Averaging by analytes

Now we need to relate the magnitude of RGB-sensor response calculated from (2) to a change of optical parameters of the thin film — thickness d , refraction index n and their product nd . Simulation of the response for three-layer thin film system with Fresnel equations with varying optical parameters of the film [33] in vicinity of the used calixarene films parameters $n = 1.5$ and $d = 200$ nm shows that with the increase of parameters by the above mentioned relatively small deviations of thickness and refraction index the colorimetric response magnitude increases monotonically with the change of nd product. This means that we can unambiguously relate the RGB-sensor response to the change in the film optical parameters.

Returning to the two-dimensional response diagrams for QM and RGB-sensors (see Fig.6), we may state the positive correlation between the changes in optical parameters and adsorbed mass in general for all considered calixarene films. However, from the Table 2, it follows that the correlation strength significantly differs for different films: it is profoundly maximal for C[5]A layers independently of calculation method, a little lower for C[6]A, intermediate correlation is observed for C[3]A and C[8]A layers, and the minimum correlation in all cases is characteristic for C[4]A layers.

We may suppose that the presence of strong correlation between QM and RGB-responses, that is the synchronous change in adsorbed mass and the nd parameter of the film, indicates that the whole bulk of the film is involved into adsorption process, being uniformly filled with the analyte molecules. This effect is most pronounced for the C[5]A films.

If the correlation is weak, it is logical to assume that molecules mostly accumulate on the surface of the film and do not penetrate into the bulk. This effect, as we can see, is mostly characteristic for the C[4]A films. Considering the C[3]A, C[6]A and C[8]A films, we may assume that both adsorption types may take place.

Conclusion

Obtained results allow to predict which of the investigated sensitive materials may be promising for use in the sensory systems for specific applications. It is shown that the most sensitive type of calixarene layers for all considered analytes appear to be the C[5]A and C[6]A films, and the least sensitive is C[4]A. At this, for classification of the chlorinated chemical compounds most sensitive and promising are the layers based on the C[5]A calixarene.

It is shown that with the increase of concentration of the analytes the mass of adsorbed molecules for all investigated calixarene films gradually aggregates on the films however for different films at a different rate. At the same time optical parameters of the C[3]A, C[4]A, C[6]A and C[8]A films change insignificantly and only start to rapidly increase after the exceeding of a certain concentration threshold, which varies depending on both calixarene and analyte types.

For the C[5]A layers optical parameters change quite synchronously with the growth of adsorbed mass. The positive correlation between the change of these parameters is strongest for the C[5]A layers (0.93) and weakest for the C[4]A layers (0.63).

References

1. A. K. Pavlou, A. P. F. Turner. Sniffing out the Truth: Clinical Diagnosis Using the Electronic Nose. // *Clin. Chem. Lab. Med.*, 2000, V. 38, p. 99–112.
2. M. Holmberg, F. Gustafsson, E. G. Hornsten, F. Winquist, L. E. Nilsson, L. Ljung, I. Lundstrom. Feature extraction from sensor data on bacterial growth // *Biotechnol. Tech.* 1998, V. 12, p. 319–324.
3. L. Vergnais, F. Masson, M. C. Montel, J. L. Berdaguy, R. Talon, J. Agric. Evaluation of solid-phase microextraction for analysis of volatile metabolites produced by staphylococci // *Food Chem.* 1998, V. 46, p. 228–234.
4. S. Singh, E. L. Hines, J. W. Gardner, Fuzzy neural computing of coffee and tainted water data on electronic nose // *Sens. Actuators*, 1996, B30, p. 185–190.
5. P. Hübner et al. Quantitation of genetically modified organism in food // *Nat. biotechnology*, 1999, V. 17, p. 1137–1138.
6. A. Stephan, M. Bücking, H. Steinhart. Novel analytical tools for food flavours // *Food Res. Int.* 2000, 33(3), p. 199–209.
7. C. D. Natale, M. Zude-Sasse, A. Macagnano, R. Paolesse, B. Herold, A. D'Amico. Outer product analysis of electronic nose and visible spectra: application to the measurement of peach fruit characteristics // *Anal. Chim. Acta*, 2002, V. 459, p. 107–117.
8. M. Minunni et al. Biosensor as a new analytical tool for detection of genetically modified organisms (GMOs) // *J. Anal. Chem.*, 2001, V. 369, p. 589–593.
9. J. Giese, Emerging Food Quality Assessment Techniques // *Food Technol.* 2000, V. 54, p. 96–100.
10. R. D. Braatz. Advanced control of crystallization processes // *Annual Reviews in Control* 2002, 26, p. 2687–2699.
11. V. Anand, M. Kataria, V. Kukkar, V. Saharan and P. K. Choudhury. The latest trends in the taste assessment of pharmaceuticals // *Drug Discovery Today* 2007, V. 12, N. 5/6, p. 257–265.
12. A. Ikeda, S. Shinkai. Novel Cavity design Using Calix[n]arene skeletons: toward molecular recognition and metal binding // *Chem. Rev.*, 1997, V. 97, p. 1713–1734.
13. S. Roesler, R. Lucklum, R. Borngraeber, J. Hartmann, P. Hauptmann. Sensor system for the detection of organic pollutants in water by thickness shear mode resonators // *Sens. Actuators*, B48, 1998, p. 415.
14. J. W. Grate, G. C. Frye. Acoustic wave sensors, in: Balthes H., Goepel W., Hesse J. // *Sensors Update*, Chap. 2, 1996, Vol. 2, p. 37–83.
15. G. Harsanyi. Polymer films in sensor applications: a review of present uses and future possibilities // *Sensor Review*, 2000, V. 20, p. 98–106.
16. M. M. Conn, J. Rebek. Self-assembling capsules // *Chem. Rev.*, 1997, V. 97, p. 1647–1668.
17. R. Caciuffo, G. Amoretti, C. Carlile, C. Ferrero, S. Geremia, B. Paci, M. Prager, F. Ugozzoli. Molecular dynamics and tunnelling in supramolecular complexes // *Physica*, 1997, B234–236, p. 115–120.
18. R. Paolesse, C. Di Natale, V. Dall'Orto, A. Macagnano, A. Angelaccio, N. Motta, M. Sgarlata, J. Hurst, I. Rezzano, M. Mascini, A. D'Amico. Porphyrin thin films coated quartz crystal microbalances prepared by electropolymerization technique // *Thin Solid Films*, 1999, V. 354, p. 245–250.
19. G. Harsanyi, M. Reczey, R. Dobay, I. Lepsenyi, Z. Illyfalvi-Vitez, J. Van den Steen, A. Vervaeet, W. Reinert, J. Urbancik, A. Guljajev, Cs. Visy, Gy. Inzelt, I. Barsony. Combining inorganic and organic gas sensors elements: a new approach for multi-component sensing // *Sensor Review*, 1999, V. 19, p. 128–135.
20. C. Wang, F. Chen, X. He, S. Kang, C. You, Yu. Liu. Cyclodextrin derivative-coated quartz crystal microbalances for alcohol sensing and application as methanol sensors // *The Analyst*, 2001, V. 126, N10, p. 1716–1721.
21. I. A. Koshets, Z. I. Kazantseva, Yu. M. Shirshov, S. A. Cherenok, V. I. Kalchenko. Calixarene films as sensitive coatings for QCM-based gas sensors, *Sensors and Actuators*, 2005, B106, p. 177–181.
22. I. V. Kruglenko, B. A. Snopok, Y. M. Shirshov, E. F. Venger. Digital aroma technology for chemical sensing: temporal chemical images of complex mixtures // *Semiconductor Physics, Quantum Electronics & Optoelectronics*, 2000, V. 3, N4, p. 529–541.
23. R. V. Khristosenko, V. Yu. Khorouzhenko, E. V. Kostyukevich, I. A. Samoylova, A. S. Samoylov, Yu. M. Shirshov. Changes in R, G, B components for interferentially colored films of calixarens as response for adsorption of volatile organic compositions // *Article of inter-universities scientific conference PHOTOELECTRONICS*, Odesa, Mechnikov National University, N14, 2005, p. 26–29.
24. G. Sauerbrey. Use of quartz vibrator from weight thin film on a microbalance // *Z. Phys.*, 1959, V. 155, p. 206.
25. C. D. Stockbridge. Effects of Gas Pressure on Quartz Crystal Microbalances // *Vacuum Microbalance Techniques*, 1966, V. 5, p. 193.
26. R. V. Khristosenko, V. Yu. Khorouzhenko, E. V. Kostyukevich, I. A. Samoylova, A. S. Samoylov, Yu. M. Shirshov. Analysis of thin films color change as basis for creation of interference gas sensors // *Optoelectronics and semiconductor engineering*, Kyiv, Naukova dumka, 2005, V. 40, p. 172–178.
27. Yu. M. Shirshov, V. Y. Khorouzhenko, E. V. Kostyukevich, R. V. Khristosenko, etc. Analysis of some alcohol molecules based on the change of RGB components of interferentially colored calixarene films // *Sensors and Actuators*, 2007, B122, p. 427–436.
28. A. A. Vahula, V. Yu. Khorouzhenko, A. L. Kukla, I. A. Samoylova. Utilization of calixarene thin films

- as sensitive layers for interference gas sensor // *Optoelectronics and semiconductor engineering*, Kyiv, Naukova dumka, 2007, V. 42, p. 89-95.
29. Colorimetric detector for analysis of components of gas and liquid mixtures / V. Yu. Khorouzhenko, A. A. Vahula, E. V. Kostyukevich, A. L. Kukla, I. A. Samoylova, R. V. Khristosenko // Ukrainian patent N 84899. publ. 10. 12. 2008, Rel. N23.
30. P. C. Jurs, G. A. Bakken and H. E. McClelland. Computational Methods for the Analysis of Chemical Sensor Array Data from Volatile Analytes // *Chemical Review*, 2000, V. 100, p. 2649–2678.
31. Yu. M. Shirshov, S. A. Zynio, E. P. Matsas, G. V. Beke-
tov, A. V. Prokhorovich and E. F. Venger. Optical pa-
rameters of thin calixarene films and their response to
benzene, toluene and chloroform adsorption // *Supramolecular Science*, 1997, Vol. 4, No. 3-4, p. 491-494.
32. Yu. Shirshov, G. Beke-
tov, O. Rengevich, R. Lamar-
tine, A. Coleman, C. Bureau. Influence of solvent
molecules adsorption on thin calixarene films thick-
ness and refractive index measured by surface plas-
mon resonance // *Functional Materials*, 1999, V. 6,
No. 3, p. 589-593.
33. A. A. Vahula, A. L. Kukla, V. Yu. Khorouzhenko,
I. A. Samoylova. Optimization of thin films opti-
cal parameters for colorimetric analysis of gaseous
medium // *Optoelectronics and semiconductor
engineering*, Kyiv, Naukova dumka, 2008, V. 43,
p. 58-66.

PACS: 75.20.CK, 81.40.EF
UDC 535.37:537.311.33

IMPACT OF PRE-IRRADIATION ON THE MAGNETIC SUSCEPTIBILITY OF Cz-Si THERMALLY TREATED AT 700-1000 °C

*V. M. Tsmots¹, P. G. Litovchenko², Yu. V. Pavlovskyy^{1,2}, O. P. Litovchenko²,
I. S. Pankiv^{1,2}, M. M. Luchkevych^{1,2}*

¹ Solid-State Microelectronics Laboratory of NASU and MONU
at the Ivan Franko Drohobych State Pedagogical University,
36 Franko Str., Drohobych, 82100, tsmots@drohobych.net
² Institute of Nuclear Research of NASU, 47 Nauky avenue, Kyiv

IMPACT OF PRE-IRRADIATION ON THE MAGNETIC SUSCEPTIBILITY OF Cz-Si THERMALLY TREATED AT 700-1000 °C

*V. M. Tsmots, P. G. Litovchenko, Yu. V. Pavlovskyy, O. P. Litovchenko,
I. S. Pankiv, M. M. Luchkevych*

Abstract. Dependence of paramagnetic component of silicon magnetic susceptibility on pre-irradiation by fast neutrons (fn) after subsequent thermal treatment of samples at 700-1000 °C has been studied. It has been shown based on the measurements of magnetic susceptibility that the value of the paramagnetic component arising after the said thermal treatment of silicon is influenced by up to 10^{18} fn/cm² pre-irradiation. With the increase of the irradiation rate this impact decreases significantly. Probable mechanisms of defect creation explaining the discovered peculiarity are discussed.

Keywords: silicon, oxygen, magnetic susceptibility, irradiation, thermal treatment

ВПЛИВ ПОПЕРЕДНЬОГО ОПРОМІНЕННЯ НА МАГНІТНУ СПРИЙНЯТЛИВІСТЬ Cz-Si, ТЕРМООБРОБЛЕНОГО ПРИ 700-1000 °C

*В. М. Цмоць, П. Г. Литовченко, Ю. В. Павловський, О. П. Литовченко,
І. С. Паньків, М. М. Лучкевич*

Анотація. Досліджено залежності парамагнітної складової магнітної сприйнятливості (МС) кремнію від дози попереднього опромінення швидкими нейтронами (fn), після послідувочої термообробки зразків при 700-1000°C. На основі результатів вимірювання магнітної сприйнятливості показано, що на величину парамагнітної складової, яка виникає після зазначених термообробок кремнію, суттєво впливає попереднє опромінення дозами до величини порядку 10^{18} fn/cm². При подальшому збільшенні дози опромінення цей вплив значно послаблюється. Розглянуто імовірні механізми дефектоутворення, які пояснюють виявлені особливості.

Ключові слова: кремній, кисень, магнітна сприйнятливості, опромінення, термообробка

ВЛИЯНИЕ ПРЕДВАРИТЕЛЬНОГО ОБЛУЧЕНИЯ НА МАГНИТНУЮ ВОСПРИИМЧИВОСТЬ Cz-Si, ТЕРМООБРАБОТАННОГО ПРИ 700-1000 °C

В. М. Цмоць, П. Г. Литовченко, Ю. В. Павловский, О. П. Литовченко, И. С. Панькив, М. М. Лучкевич

Аннотация. Исследовано зависимости парамагнитной составляющей магнитной восприимчивости кремния от дозы предварительного облучения быстрыми нейтронами (бн), после последующей термообработки образцов при 700-1000°C. На основании результатов измерения магнитной восприимчивости показано, что на величину парамагнитной составляющей, которая появляется после указанных термообработок кремния, существенно влияет предварительное облучение дозами до величины порядка 10^{18} бн/см². При дальнейшем увеличении дозы облучения это влияние значительно ослабевает. Рассмотрено вероятные механизмы дефектообразования, которые объясняют выявленные особенности.

Ключевые слова: кремний, кислород, магнитная восприимчивость, облучение, термообработка

Introduction

Silicon remains the most convenient and best developed semiconductor to be used in physical sensors and planar structures. The major technological impurity in Cz-Si is oxygen, which exists in oversaturated state in the crystals. During thermal treatment of silicon samples the oxygen precipitation in the nucleus centers takes place. Newly-created precipitates could serve as the impurity and point defects sinks. In this case they act as getters and clear the crystal of impurities (e.g. doping metallic atoms).

During the irradiation of silicon by neutrons disordering areas and point defects are generated in it, which could be the centers of precipitate generation. Pre-irradiation by neutrons allows not only to decrease the temperature and duration of thermal treatment, but also to control the precipitate concentration and to change their properties. The pre-irradiation of silicon is also known to accelerate the oxygen precipitation at subsequent thermal treatments [1]. Therefore, the study of irradiation and thermal treatment effect on oxygen precipitation is topical for a wide range of tasks, both scientific and practical ones.

We had established a correlation between the oxygen precipitation process and change of magnetic susceptibility [2]. The effect of pre-irradiation by various fast neutron doses on the thermal formation of defects in silicon and respectively on the change of its magnetic properties is discussed.

Experimental results and discussion

For the experiment the Cz-Si monocrystals grown in the $\langle 100 \rangle$ direction with dissolved oxygen concentration of $8 \cdot 10^{17}$ cm⁻³, specific resistance ~ 10 Ohm·cm were used. Si samples were irradiated by fast neutrons on a VVR-M reactor at the temperature under 70 °C by fluencies of 10^{15} , $5 \cdot 10^{16}$, 10^{18} and $2 \cdot 10^{19}$ fn/cm².

Samples were produced from the same 5 mm thick silicon plate, cut perpendicularly to the ingot growth axis.

Before measurements the sample surface was mechanically and chemically treated. Subsequently the crystals were rinsed in distilled water.

The samples were annealed in tube heater in the air, the annealing temperature control accuracy being ± 2 °C.

Fig. 1 shows the magnetic susceptibility vs. magnetic field intensity ($\chi(H)$) of the samples thermally treated at 700-1000 °C and pre-irradiated by different doses of fast neutrons. A shift of $\chi(H)$ dependences towards the decrease of diamagnetism is evident as compared with the original sample ($\chi_{Si} = -11.6 \cdot 10^{-8}$ cm³/g), which is attributed to the appearance of the MS paramagnetic component, and in the samples with maximum shift (annealed at 850 and 900°C) non-linearity of $\chi(H)$ dependences is observed. The effect is enhanced with the increase of the sample pre-irradiation dose (Fig. 1, b-d).

Fig. 2 (curves 2-5) shows the magnetic susceptibility in 4 kOe field (when MS approaches saturation) vs. the annealing temperature. Obviously these dependences a similar to those obtained on the non-irradiated samples (Fig. 2, curve 1).

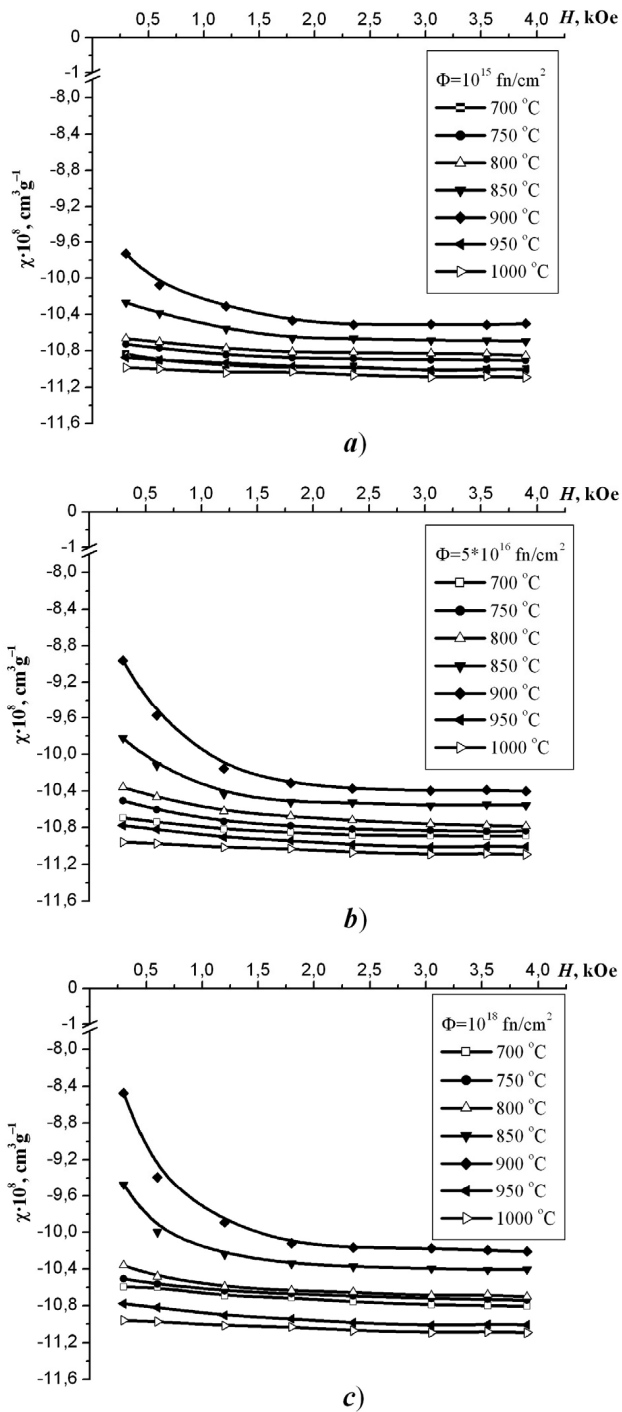


Fig. 1. Magnetic susceptibility vs. magnetic field intensity of the annealed silicon samples pre-irradiated by different fast neutron doses: a) $\Phi = 10^{15}$ fn/cm²; b) $\Phi = 5 \cdot 10^{16}$ fn/cm²; c) $\Phi = 10^{18}$ fn/cm²; d) $\Phi = 2 \cdot 10^{19}$ fn/cm²

Comparing them we can see that the paramagnetic component of the magnetic susceptibility of the samples irradiated by fast neutrons increases with the increase of the radiation dose, especially in the 850-900 °C range. It leads to the conclusion that the pre-irradiation by fast neutrons causes the acceleration of thermal defect generation.

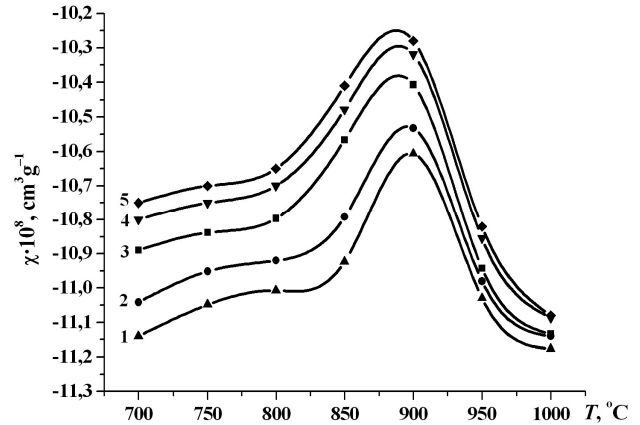


Fig. 2. Magnetic susceptibility (in 4 kOe field) vs. sample annealing temperature with pre-irradiation by different fast neutron doses: 1 — no irradiation; 2 — $\Phi = 10^{15}$ fn/cm²; 3 — $\Phi = 5 \cdot 10^{16}$ fn/cm²; 4 — $\Phi = 10^{18}$ fn/cm²; 5 — $\Phi = 2 \cdot 10^{19}$ fn/cm²

In papers [3, 4], the measurements of IR-absorption of neutron-irradiated silicon show that the ratio of defect concentrations of vacancy and interstitial types is defined by the neutron flow. Thus, with the flow of up to 10^{16} fn/cm² the vacancy type defects prevail, while with the flow over $5 \cdot 10^{16}$ fn/cm² interstitial type defects begin to actively form.

It is known [5], that with the excessive concentration of thermal point defects in silicon the process of oxygen precipitation significantly changes. The data on the role of inherent interstitial silicon atoms in this process are contradictory. It has been established that with the excessive concentration of inherent interstitial atoms formed in the process of silicon ingot growth preventing their condensation into A-defects the precipitate nucleus concentration increases.

Meanwhile, the oversaturation of silicon lattice with inherent interstitial atoms under the condition of silicon oxidation [6], caused deceleration of oxygen precipitation attributed to the destruction of precipitate nuclei by these defects.

The role of vacancies accelerating precipitation of the excessive oxygen is in the opinion of [5] authors the opposite — stabilization of nuclei by forming complexes similar by their structure to donors in silicon [7].

Since the main components of radiation defects in the silicon irradiated by high-energy particles are the vacancies, the acceleration of oxygen precipitation observed in crystals irradiated by fast neutrons could be attributed to the participation of these defects and their complexes in formation and stabilization of precipitation nuclei.

Besides, due to increase of probability of oxygen atoms being built into precipitate through creating bonds with vacancies [6], the surface energy on the silicon-precipitate matrix boundary could decrease. Decrease of the precipitate surface energy by several per cent may cause a several times increase of the precipitation rate.

Thus, deceleration of the increase of MS paramagnetic component in irradiated silicon with the increase of neutron radiation flow exceeding 10^{18} fn/cm² (observed at Fig. 3) could be explained by the inherent interstitial atoms participation in the oxygen precipitation process.

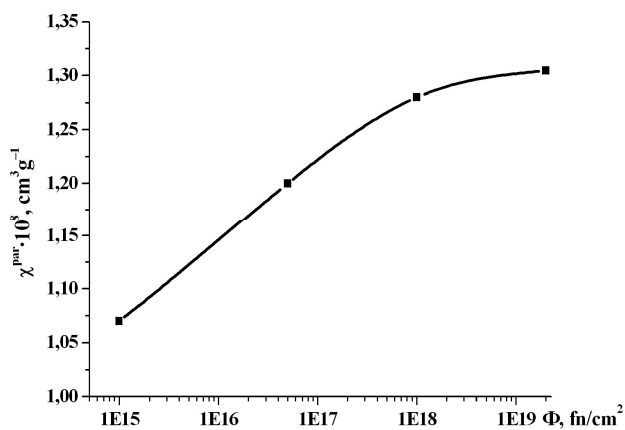


Fig. 3. Dependence of the paramagnetic component of samples after thermal treatment at 900°C on the pre-irradiation dose

If this effect does have place, with an increase of the neutron radiation flow from 10^{16} cm⁻² to $2 \cdot 10^{19}$ cm⁻² together whose vacancy type defects, which concentration is growing and which accelerate oxygen precipitation in silicon the contribution of interstitial type defects decelerating the precipitation becomes significant.

Superimposition of these two processes will lead to the fact that the value of the paramagnetic component correlating (as established in [2]) with the excessive oxygen precipitation rate will change little with the increase of the irradiation flow, which has been proved experimentally.

Conclusions

As the result of the experimental data discussion, it was shown:

1. The pre-irradiation of silicon samples with fast neutrons leads to acceleration of paramagnetic

center generation in the process of thermal treatment in the 700-1000 °C temperature range.

2. The effect is significant at the irradiation doses of the order 10^{18} fn/cm².

3. Further increase of the pre-irradiation dose does not lead to drastic changes of the magnetic susceptibility paramagnetic component with subsequent thermal treatment.

4. This is attributed to the fact that together with vacancy type defects accelerating the oxygen precipitation in silicon and respectively, as had been established previously in [2], the increase of paramagnetic component, the contribution of interstitial type defects decelerating the precipitation becomes significant.

References

1. Варніна В. І., Гроза А. А., Литовченко П. Г., Старчик М. І., Шматко Г. Г., Марченко Л. С., Семенюк А. К., Литовченко О. П., Вплив радіаційних дефектів на преципітацію кисню в кремнії при термообробці // УФЖ. — 2001. — Т. 46, №2. — С. 205-210.
2. Литовченко П. Г., Литовченко О. П., Старчик М. І., Павловський Ю. В., Гроза А. А., Шматко Г. Г., Цмоць В. М., Петренко В. В., Кореляція між процесами преципітації кисню і поведінкою магнітної сприйнятливості в опроміненому нейтронами кремнії // НУ “Києво-Могилянська академія”. Фіз. — мат. науки. — 2004. — Т. 23. — С. 63-66.
3. Гроза А. А., Хиврич В. И., Околокраевое поглощение в кремнии облучённом нейтронами и 1, 5 МэВ электронами // ФТП. — 1979. — Т. 13, №5, — С. 870-874.
4. Литовченко П. Г., Гроза А. А., Варенцов М. Д., Хиврич В. И., Томчук Л. В., Николаева Л. Г., Заславский Ю. И., Старчик М. И., Шматко Г. Г. Особенности действия быстрых и тепловых нейтронов, электронов на оптические, электрические и структурные свойства кремния // Вопр. ат. науки и техн. Сер.: Физ. радиац. поврежд. — 1986. — №3. — С. 75-77.
5. De Kock A. J. R., Wijgert W. M., The Influence of Thermal Point Defects on the Precipitation of Oxygen in Dislocation Free Silicon Crystals // Appl. Phys. Lett. — 1981. — V. 38, №11. — P. 888-900.
6. Graven R. A. Semiconductor Silicon, //ed. H. R. Huff, R. J. Kriepner, J. Tamishi., The Electrochemical Society Inc. — 1985. — №4. — P. 254-258.
7. Mikkelsen J. C. Oxygen, Carbon, Hydrogen, and Nitrogen in Crystalline silicon // J. of Metals. — 1985. — V. 37. — P. 51-54.

СЕНСОРИ ТА ІНФОРМАЦІЙНІ СИСТЕМИ

SENSORS AND INFORMATION SYSTEMS

PACS 07.07.Mp

SENSOR SYSTEM FOR AUTOMATIC PAPER THICKNESS DETECTION BASED ON UNIVERSAL SENSORS AND TRANSDUCERS INTERFACE

S. Yu. Yurish

Technical University of Catalonia (UPC-Barcelona), CDEI,
C/Llorens Artigas, 4-6, planta 0, Edifici U, Campus Sud, 08028, Barcelona, Spain
Tel: + 34 696067716, fax: +34 93 4011989, e-mail: syurish@sensorsportal.com

SENSOR SYSTEM FOR AUTOMATIC PAPER THICKNESS DETECTION BASED ON UNIVERSAL SENSORS AND TRANSDUCERS INTERFACE

S. Yu. Yurish

Abstract: A low cost, automatic, transmissive paper thickness sensor system with increased reliability and a short detection time (~ 15 ms) is described in the paper. The sensor system is based on a cheap light-to-frequency converter and universal sensors and transducers interfacing IC. The designed automotive paper thickness sensor system has a wide dynamic range of 5 000 000 : 1, immunity against high noises, high resolution and minimum component interface. Due to low price, minimum possible conditioning and interfacing hardware such sensor system can be used not only in photo- but also in office laser and ink printers.

Keywords: Paper thickness optical sensor, Light-to-frequency converter, Universal sensors and transducers interface

СЕНСОРНАЯ СИСТЕМА ДЛЯ АВТОМАТИЧЕСКОГО ОПРЕДЕЛЕНИЯ ТОЛЩИНЫ БУМАГИ НА БАЗЕ УНИВЕРСАЛЬНОГО СЕНСОРНОГО ИНТЕРФЕЙСА

С. Ю. Юриш

Аннотация: в статье описана недорогая автоматическая сенсорная система повышенной надежности и быстродействия (~ 15 мс) для определения толщины бумаги. Сенсорная система содержит недорогой преобразователь освещенности в частоту и интегральную микросхему универсального сенсорного интерфейса. Разработанная сенсорная система имеет широкий динамический диапазон 5 000 000 : 1, высокую помехоустойчивость и разрешающую способность, а также минимальные аппаратные затраты. Благодаря невысокой цене и минимальному числу электронных компонентов, такая сенсорная система может использоваться не только в фотопринтерах, но и в офисных лазерных и струйных принтерах.

Ключевые слова: оптический датчик толщины бумаги, преобразователь освещенность-частота, универсальный сенсорный интерфейс

СЕНСОРНА СИСТЕМА ДЛЯ АВТОМАТИЧНОГО ВИЗНАЧЕННЯ ТОВЩИНИ ПАПЕРУ НА БАЗІ УНІВЕРСАЛЬНОГО СЕНСОРНОГО ІНТЕРФЕЙСУ

С. Ю. Юриш

Анотація: у статті описана недорога автоматична сенсорна система підвищеної надійності та швидкодії (~ 15 мс) для визначення товщини паперу. Сенсорна система містить недорогий перетворювач освітленості в частоту й інтегральну мікросхему універсального сенсорного інтерфейсу. Розроблена сенсорна система має широкий динамічний діапазон 5 000 000 : 1, високу завадостійкість і роздільчу здатність, а також мінімальні апаратурні витрати. Завдяки невисокій ціні й мінімальному числу електронних компонентів, така сенсорна система може використовуватися не тільки у фотопринтерах, але й в офісних лазерних і струминних принтерах.

Ключові слова: оптичний сенсор товщини паперу, перетворювач освітленість-частота, універсальний сенсорний інтерфейс

1. Introduction

Modern photo printers have automatic paper-type optical sensors that detect a type and thickness of paper. These sensors are able to recognize plain paper, coated paper, glossy/photo paper and transparencies in the in-tray. Whether using plain paper or specialty papers such as photo papers or transparencies, the paper type will be detected and the printer will automatically make the appropriate driver settings to produce a high quality print. This detection is not always a perfect process — the sensor nearly always reads “plain paper” when it shouldn’t. For instance, it will misread paper that is marked, scratched, or wrinkled; paper that has letterhead or markings at the top; and paper that is dark (or that contains metallic filaments). Photo printers will print in lower quality (or “draft mode”) for plain paper, because they cannot handle the resolution and ink quantity that is needed for a real photo-quality image. In addition, reflective configuration type sensors give an opportunity to recognize only photo paper, plain paper or transparencies but not its real thickness; and the sensing process adds up to 5 s to the print process.

In order to eliminate the mentioned problems a new, low cost, automatic, transmissive configuration paper thickness sensor system with an increased reliability and short detection time was design.

2. Sensor System Design

The proposed sensor system consists of visible light source (red light emitting diode (LED)), low-cost light-to-frequency converter (LFC) TSL237 (TAOS, Inc., USA) [1], and universal sensors and transducers interface (USTI) IC [2].

The LED is an ideal monochromatic light source for such application because of its high energy efficiency, small size, low operating voltage and cost [3].

A traditional automatic paper-type reflective sensor configuration is shown in Fig. 1 (a); but in order to be able detect a paper’s thickness and count the number of paper sheets in in-tray it is expediently to use a proposed transmissive type sensor with a configuration shown in Fig.1 (b). The automatic paper-type sensor works by the following way. An LED shines onto the surface of the paper. The transmissive through the paper light is captured and recognized. This gives the printer information about the paper thickness and characteristics for the particular paper. This information is compared to a reference table of paper types that the printer has stored internally. Then, based on the information, the printer determines color mapping, half-toning, and number of print passes to produce the best output for the paper being used.

Nevertheless analog photodiodes or light-to-voltage converters can be used as a sensing element in such sensor systems, an output informative parameter as frequency on light-to-frequency converter’s output has many advantages in comparison with analog output of sensing elements, namely: high noise immunity, power of signal and reference accuracy; wide dynamic range; multiparametricity; simple interfacing, integration and coding [4].

In the traditional solution, the current from a photodiode is very small (μA), making it susceptible to picking up noise, particularly if the transimpedance amplifier is separated from the photodiode by a considerable distance. In some applications, it is necessary to add shielding around the photodiode

to keep electromagnetic interference and radio frequency interference from interfering with the signal. However, additional shielding is not needed with a light-to-frequency converter as long as adequate power supply is provided [5].

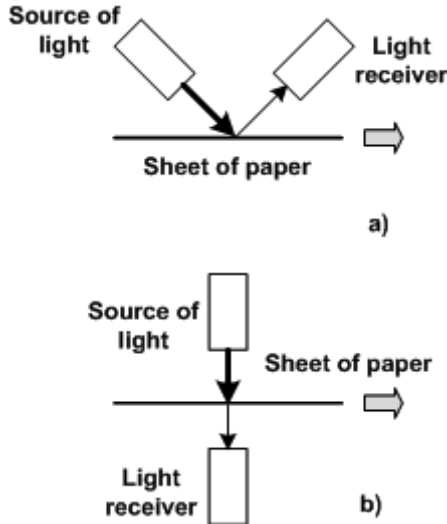


Fig. 1. Automatic paper-type sensor configurations: (a) tradition reflective type sensor; (b) proposed transmissive type sensor.

The TSL237 light-to-frequency converter combines a silicon photodiode and a current-to-frequency converter on a single monolithic CMOS integrated circuit. Output is a square wave (50 % duty cycle) with frequency directly proportional to light intensity (irradiance) on the photodiode. The digital output allows direct interface to a microcontroller or other logic circuitry. The device has been temperature compensated for the ultraviolet-to-visible light range of 320 nm to 700 nm and responds over the light range of 320 nm to 1050 nm [1]. The frequency at the output pin (OUT) is given by:

$$f_o = f_d + (R_e) \cdot (E_e), \quad (1)$$

where f_o is the output frequency; f_d is the output frequency for dark condition ($E_e = 0$); R_e is the device responsivity for a given wavelength of light given in kHz/($\mu\text{W}/\text{cm}^2$); E_e is the incident irradiance in $\mu\text{W}/\text{cm}^2$.

The dark frequency f_d is a constant error term in the output frequency calculation resulting from leakage currents, and is independent of light intensity. The TSL237 die is trimmed to minimize the magnitude of this dark frequency component so that it can be neglected in the transfer function calculation. In many applications, measurement of the actual dark frequency may be impractical due to

measurement times ranging from several seconds to several minutes, and the fact that some devices may never transition (zero dark frequency).

The output of the device can be changed in a wide frequency range from 0.1 Hz to 2 Hz (dark frequency typical range) and from 0.5 to 1 MHz (maximum output frequency) and is designed to drive a CMOS logic input over short distances. Due to a wide dynamic range of ~120 dB this device is well suited for this paper thickness sensor system application.

The choice of interface and measurement technique depends on the desired resolution and data-acquisition rate. Maximum resolution, conversion speed and accuracy will be obtained by using the USTI especially designed for such kind of sensors applications. The IC can measure frequency in a wide range from 0.05 Hz to 9 MHz without prescaling; with constant programmable relative error (from 1 to 0.0005 %) in the whole frequency range, scalable resolution and non-redundant conversion time [2]. The USTI is based on the patented modified method of the dependent count [6]. It allows a high-resolution direct interface to these types of light sensors and its digital output also allows a simple interface to popular sensors serial buses as SPI, I²C and RS-232. The designed sensor system is shown in Fig.2 and its main components — in Fig. 3.

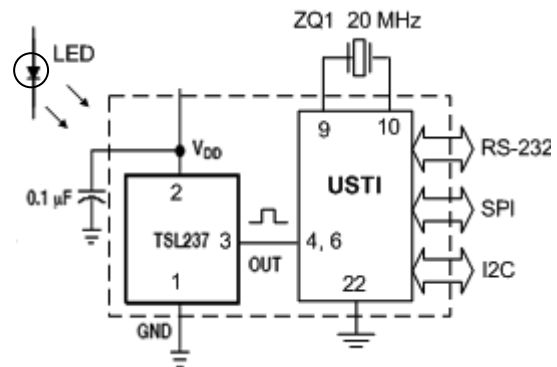


Fig. 2. Automatic paper thickness sensor system circuit diagram.

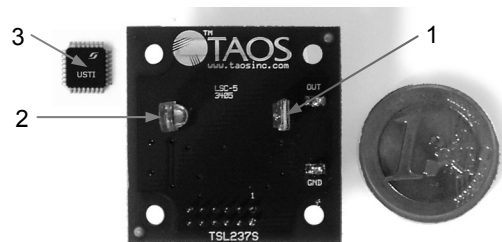


Fig. 3. Main sensor system components: light sensor TSL237 (1); LED (2); USTI (3).

Power-supply lines of TSL237 must be decoupled by a 0.01 μF to 0.1 μF capacitor with short leads placed close to the TSL237 (Fig. 2). A low-noise power supply is required to minimize jitter on output pulse.

Taking into account that the USTI has two identical channels, another light sensor TSL237 can be connected to the second measuring channel (for example, in the reflective type configuration working with the same LED) or color sensor with frequency output, for example, TCS230. Such advanced mul-

tisensors system configuration lets improve significantly reliability for paper-type recognition and make possible to control a paper quality at paper manufacturing processes and real-time measurement of paper sheet content at paper sorting and recycling.

The commands and appropriate comments for the USTI working with the RS232 interface (slave mode) in two-channel configuration for paper type and thickness determination are shown in Figure 4.

```

>A03          ; Set the relative error for the 1st channel  $\delta = 0.1 \%$ 
>M00          ; Choose the frequency measuring mode in the 1st channel
>S            ; Start measurement
>R            ; Read result in Hz
100000.0254

>A03          ; Set the relative error for the 2nd channel  $\delta = 0.1 \%$ 
>MOE         ; Choose the frequency measuring mode in the 2nd channel
>S            ; Start measurement
>R            ; Read result in Hz
70128.966

```

Fig. 4. Commands for USTI working with the RS232 interface (slave mode) in two-channel configuration.

It is also expediently to use the additional command “C” between “S” and “R” commands to check the measurement status. It returns “r” if the result is ready and “b” if the measurement is in a progress. It is especially important at measurements in low frequency range.

The detection time should be calculated according to the following equation:

$$T_{\text{detection}} = t_{\text{conv}} + t_{\text{comm}} + t_{\text{calc}}, \quad (2)$$

where t_{conv} is the frequency-to-digital conversion time; t_{comm} is the communication time; t_{calc} is the calculation time.

The conversion time for the USTI can be calculated according to the following equation:

$$\begin{cases} t_{\text{conv}} = \frac{1}{f_x} & \text{if } \frac{N_\delta}{f_0} < T_x \\ t_{\text{conv}} = \frac{N_\delta}{f_0} + (0 \div T_x) & \text{if } \frac{N_\delta}{f_0} \geq T_x, \end{cases} \quad (3)$$

where $N_\Delta = I/\Delta$ is the number proportional to the required programmable relative error Δ ; $T_x = I/f_x$ is the period of converted frequency; $f_0 = 600$ kHz is the internal reference frequency for USTI.

The communication time for a slave communication mode (RS232 interface) can be calculated according to the following equation:

$$t_{\text{comm}} = 10 \cdot n \cdot t_{\text{bit}}, \quad (4)$$

where $t_{\text{bit}} = 1/300, 1/600, 1/1200, 1/2400, 1/4800, 1/9600, 1/14400, 1/19200, 1/28800$ or $1/38400$ is the time for one bit transmitting; n is the number of bytes ($n=13 \div 24$ for ASCII format). As usually, at the right chosen of baud rate (maximum possible for a certain application) the $t_{\text{comm}} \leq t_{\text{conv}}$. For example, the communication time at 38400 baud rate will be $t_{\text{comm}} = (0.0034 \div 0.00625)$ s.

The communication time for SPI interface should be calculated as:

$$t_{\text{comm}} = 8 \cdot n \cdot \frac{1}{f_{\text{SCLK}}}, \quad (5)$$

where f_{SCLK} is the serial clock frequency, which should be chosen for the USTI in the range from 100 to 500 kHz; $n=12 \div 13$ is the number of bytes. The number n is dependent on measurement result format: BCD ($n=13$) or binary ($n=12$).

The communication standard mode speed for I²C interfaces can be determined according to the following equation:

$$t_{\text{comm}} = 8 \cdot n \cdot \frac{1}{f_{\text{SCL}}}, \quad (6)$$

where f_{SCL} is the serial clock frequency, which should be equals to 100 kHz for the USTI; $n=12 \div 13$ is the number of bytes for measurement result: BCD ($n=13$) or binary ($n=12$).

The calculation time depends on operands and is as usually $t_{calc} \leq 4.5$ ms.

As it visible from (3) the conversion time is mainly determined by the programmable relative error Δ . The dependence of conversion time on relative error is shown in Figure 5.

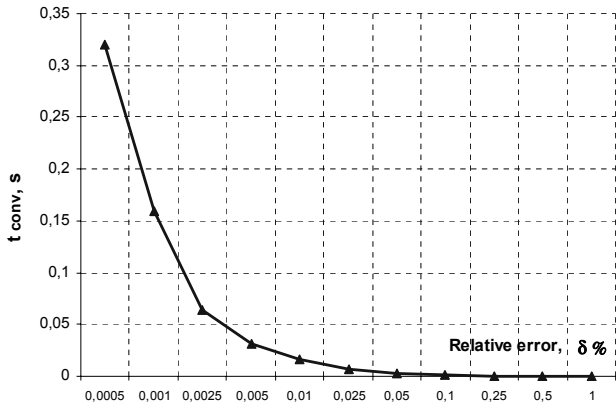


Fig. 5. Dependence of conversion time t_{conv} on relative error Δ .

The USTI is also suitable for working with multiparametric optical sensors in which the output frequency is proportional to the light intensity (luminance) and duty-cycle at the same sensor's output is proportional to the spectral distribution (chrominance), for example, described in [7]. The colour information is obtained using the wavelength dependence of the absorption coefficient in the silicon in the optical part of the spectrum, so no filters are required [8]. At the use of such optical sensors, one mentioned multiparametric reflective type sensors can be connected to the 1st USTI's channel and other light sensor of transmissive type (for example) can be connected to the 2nd USTI's channel.

The similar sensor systems can be designed also based on any frequency output light or infrared sensors such as TSL230, TSL235, TSL238, TSL245 (TAOS, Inc., USA), S9705 (Hamamatsu Corp., Japan) and MLX75304 (Melexis, Belgium) [9]. These low-cost sensors have become attractive for such application, combining with the high-performance frequency-to-digital conversion based on the USTI to achieve the required accuracy and reduced conversion time at a lower overall system cost.

3. Experimental Results

The measurement set up that was used in experimental investigations is based on the light-to-frequency evaluation module from TAOS, Inc. [10]. A

motherboard with an appropriate device-specific daughterboard, which were used in experiments is shown in Fig. 6. The mother board was connected via USB port to a host PC running the Windows compatible host software application, which was used mainly for the ambient light subtraction in order to get rid of the effect of ambient light, and strobe LED control during all measurements. According to the algorithm, each time the sensor is measured, and extra measurement is made with the LED off. The value "Ambient" is then subtracted from the actual frequency measurement. The calculation used is as follows:

$$Reading = (Signal + Ambient) - Ambient, \quad (7)$$

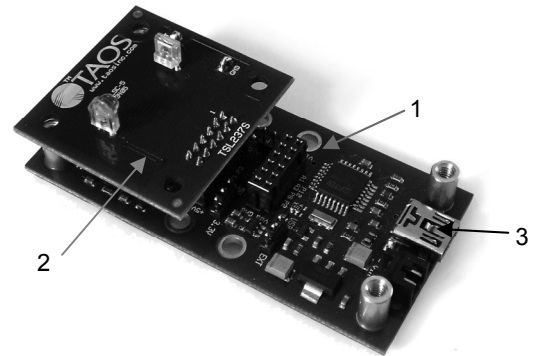


Fig. 6. Evaluation module's motherboard (1) with TSL237 daughterboard (2) and USB connector (3).

The sensor's output was directly interfaced to the first USTI's channel working in a frequency measurement mode with programmable constant relative error 0.1 % in the whole frequency range. Taking into account the sensor's error, this frequency-to-digital conversion error can be neglected at sensor system accuracy evaluation. The USTI was connected via RS-232 to the same host PC running the Terminal V1.9b software. The measurement set up for automatic paper thickness sensor system investigation is shown in Figure 7.

During experiments 8 paper patterns with different thickness from 0.086 to 0.217 mm including standard office types of paper 70 and 80 g/mm² were investigate. The oscillograms at sensors output correspond to paper sheets with maximal and minimal thickness are shown in Fig. 8. The dependence of sensor output on paper thickness is shown in Fig. 9.

A reference table of paper types can be stored in the USTI's or printer's memory.

In addition to the paper thickness the developed sensor can detect the number of paper sheets

of the same thickness, for example, office paper with 0.095 mm thickness (Fig. 10). The maximum counted number of sheets is $N=24$ for 0.086 mm thickness and $N=20$ for 0.095 mm thickness at the distance between LED and LFC in 15 mm. This number can be increased by decreasing the distance between light source and sensing element. In spite of the fact that at $N > 8$ the dependence of frequency on number of sheets is not so well expressed, the USTI is capable to distinguish such changes due to a high resolution and low absolute error (± 2 Hz at $f_x=2000$ Hz) at relative error 0.1 %.

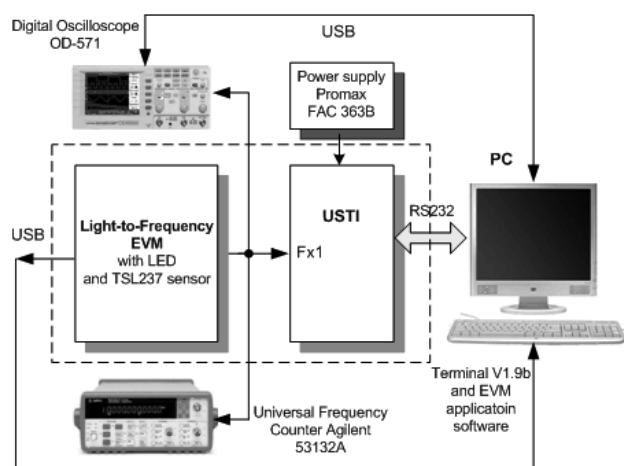


Fig. 7. Measurement set-up for automatic paper thickness sensor system investigation.

The detection time in both experiments together with communication time does not exceed 15 ms at 0.1 % error for frequency-to-digital conversion.

The designed sensor can be also used for detection of paper sheets sticking in order to eliminate two leaves feeding at the same time.

In order to validate a high accuracy for frequency-to-digital conversion in a wide frequency range the frequency measurements for maximum possible sensor output frequency $f_{x\max} \approx 520$ kHz (paper absent status) and the minimum possible sensor output frequency $f_{x\min} \approx 0.27$ Hz (low dark frequency $f_o = f_D$) for the light sensor were taken every second by the USTI and high precision calibrated counter (Agilent 53132A) until totaling 60 measurements. The measuring results are shown in Figure 11 (a, b). The measurements errors were evaluated from histograms and appropriate statistical characteristics. In both cases it does not exceed the programmable relative error $\Delta \leq 0.1$ %, therefore it can be neglected in comparison with the light sensor's error. Statistical characteristics are added in Table 1.

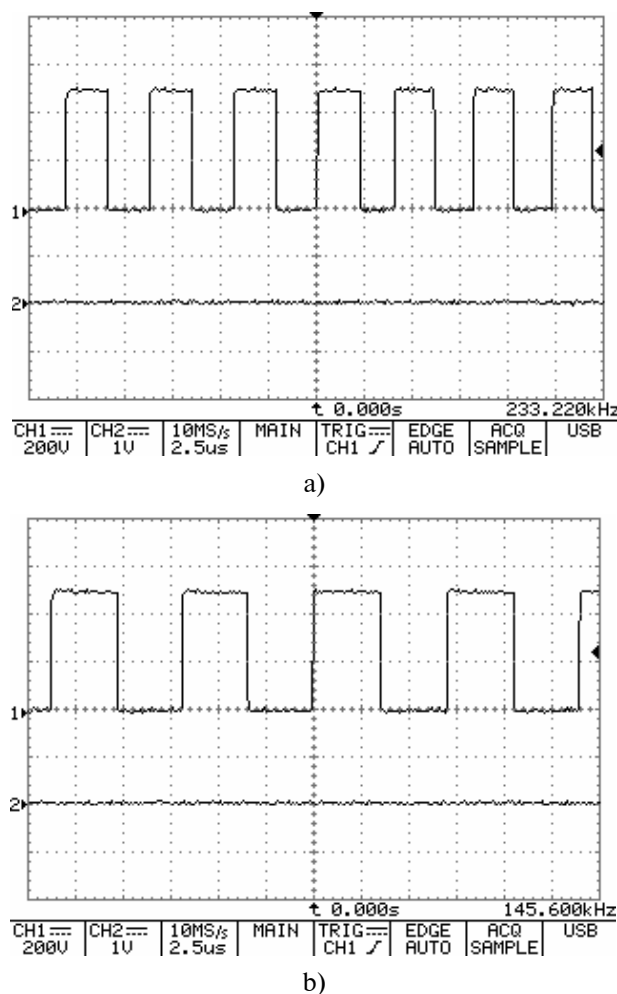


Fig. 8. Sensor output signals at 0.086 mm (a) and 0.217 mm (b) paper sheet thickness.

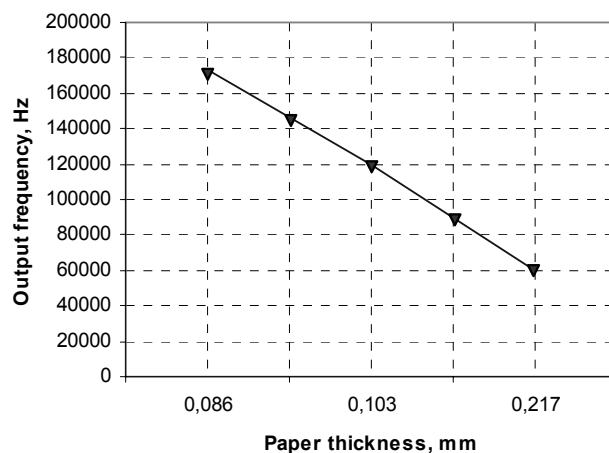
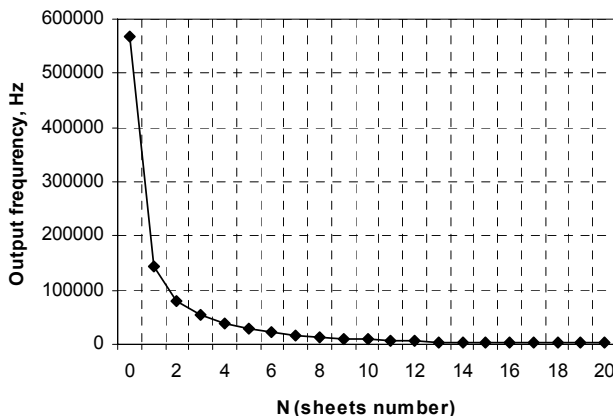


Fig. 9. Sensor output vs. paper thickness.

The χ^2 -test for goodness of fit was applied to investigate the significance of differences between observed data in histograms and the theoretical frequency distribution for data from a normal population. At five equidistant classes ($k=5$) and

a probability $P = 97 \%$, according to the χ^2 -test, $S < \chi^2_{max}$, where $S = 6.1584$ and 1.1586 is the sum of deviations between the data set and the assumed distribution for minimum and maximum fre-

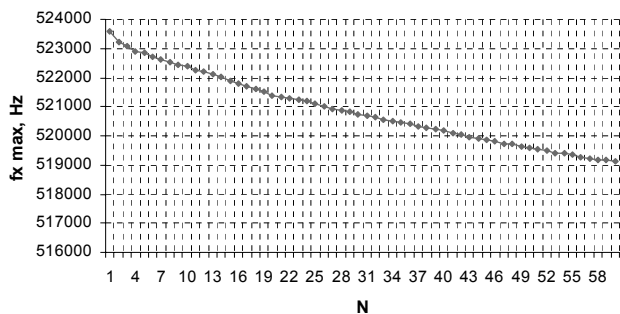
quency measurement accordingly; $\chi^2_{max} = 7.0$ is the maximal possible argument of the χ^2 distribution. Hence, the hypothesis of Gaussian (normal) distribution can be accepted in both cases.



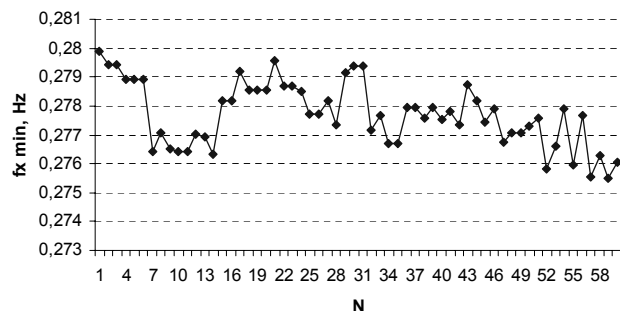
Data Table:

N	1	2	3	4	5	6	7	8	9	10
f_y, Hz	143000	81100	55500	39400	29500	22400	17350	12600	10350	8300
N	11	12	13	14	15	16	17	18	19	20
f_y, Hz	6900	5800	4600	3980	3400	2850	2510	2150	2000	1900

Fig. 10. Sensor output vs. sheets number (at 0.095 mm thickness).

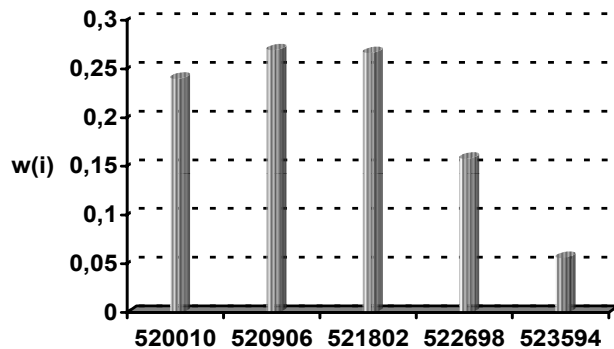


a)



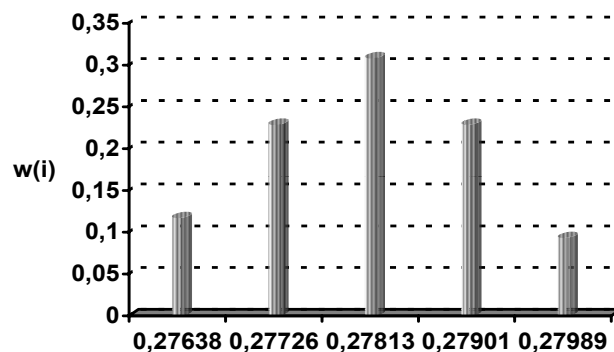
b)

Fig. 11. Measurement results for $f_{x\ max} \approx 520$ kHz and $f_{x\ min} \approx 0.27$ Hz.



fx max, Hz

a)



fx min, Hz

b)

Fig. 12. Distribution functions $w[i]$ changes.

Table 1

Statistical characteristics

Parameter	$f_{x_{max}}$	$f_{x_{min}}$
Number of measurements, N	60	60
Minimum f_x (min), Hz	519114.393	0.2755
Maximum f_x (max), Hz	523594.121	0.2799
Sampling Range, f_x (max) – f_x (min), Hz	4479.7277	0.0044
Median	0	0
Arithmetic Mean, Hz	520887.935	0.2777
Variance	1497556.04	1.2E-0006
Standard Deviation	1223.7467	0.0011
Coefficient of Variation	425.6501	251.5468
Confidence interval for arithmetic mean at $P=97\%$	$520545.093 \leq f_x \leq 521230.777$	$0.2774 \leq f_x \leq 0.278$
Relative error, %	0.07	0.1

Table 2

 χ^2 -test results: for $f_{x_{max}}$ (a) and $f_{x_{min}}$ (b)

Classes	Observed incidence $b[i]$	Distribution function changes $w[i]$	Expected incidence $c[i]$	Deviation $A[i]$
1. 520010.33931	18	0.236644	14.20	1.018
2. 520906.28486	15	0.269337	16.16	0.083
3. 521802.2304	12	0.266525	15.99	0.996
4. 522698.17595	9	0.157958	9.48	0.024
5. 523594.12149	6	0.056031	3.36	2.070

a)

Classes	Observed incidence $b[i]$	Distribution function changes $w[i]$	Expected incidence $c[i]$	Deviation $A[i]$
1. 0.27638	7	0.116967	7.02	0
2. 0.27726	14	0.22875	13.72	0.006
3. 0.27813	17	0.308403	18.50	0.122
4. 0.27901	14	0.228827	13.73	0.005
5. 0.27989	8	0.093383	5.60	1.025

b)

Due to low cost and minimum hardware the designed paper thickness sensor system can be used in high quality modern photo- as well as in office budget laser or ink jet printers. A short detection time (~ 15 ms) do not introduce an additional significant time to the print process in comparison with traditional automotive paper thickness sensor system.

4. Conclusions

The designed automotive paper thickness sensor system has a wide dynamic range of 5 000 000 : 1, immunity against high noises, high resolution and minimum component interface. Due to low price, minimum possible conditioning and interfacing hardware such sensor can be used not only in photo- but also in office laser and ink printers. In turn,

low-cost light- and color-to-frequency converters have become attractive for different applications, combining with high-performance frequency-to-digital conversion based on the USTI to achieve the required accuracy, true digital output according to three popular serial sensors buses at a lower overall system cost.

Further research aims towards a fully integrated light-, color-to-frequency converters and USTI in CMOS technology as well as creation multisensor systems for different applications on its basis.

Acknowledgment

These research and development were funded in the frame of EC Marie Curie Excellence Chairs (EXC) project MEXT-CT-2005-023991 'Smart Sensor Systems Design' (SMARTSES).

References

1. TSL237 High sensitivity light-to-frequency converter, TAOS 052G, USA, 2007.
2. S. Y. Yurish, Smart universal sensor and transducer interface, in: Proceedings of SENSOR+TEST Conference 2007, vol.1, Nurnberg, Germany, 22-24 May 2007, pp. 307-312.
3. Hai Yang, Xue Wei, Xianghui Liang, Mingwei Su, Xiaohua Lu, A SoC and LED based reconfigurable subminiature spectrometer for hand-held measurement applications, Measurement 41 (2008), pp. 44-54.
4. S. Y. Yurish, Sensors and transducers: frequency output versus voltage output, Sensors & Transducers, vol. 49, 11 (2004), pp. 302-305.
5. Ray King, LFT technology simplifies light sensing, Control Engineering, 6/1/2007.
6. S. Y. Yurish, Novel modified method of the dependent count for high precision and fast measurements of frequency-time parameters of electric signals, in: Proceedings of 2008 IEEE International Instrumentation & Measurement Technology Conference (I2MTC), Victoria, Vancouver Island, British Columbia, Canada, 12-15 May 2008, pp. 876-881.
7. G. de Graaf, F.R. Riedijk, R.F. Wolffenbuttel, Colour-sensor system with a frequency output and an ISS or I2C bus interface, Sensors and Actuators A61 (1997), pp.441-445.
8. G. de Graaf, R.F. Wolffenbuttel, Light-to-frequency converter using integrated mode photodiodes, in: Proceedings of IMTC'96; Brussels, Belgium, 4-6 June 1996, pp.1072-1075.
9. List of optical sensors manufacturers at Sensors Web Portal: <http://www.sensorsportal.com>
10. Light-to-frequency EVM. User's guide, TAOS, Inc., USA.

UDC 53.082:612.017.1

CORRELATIVE PROCESSING OF INFORMATION IN BIOSENSORS BY SURFACE PLASMON RESONANCE

I. Voitovych, I. Yavorsky

V. Glushkov Institute of Cybernetics of the National Academy of Sciences of Ukraine, 40, Academician
Glushkov av., 03680, Kyiv, Ukraine. Telephone: 38-044 5260128, Facsimile: 38-044 5263348,
e-mail: d220@public.icyb.kiev.ua

CORRELATIVE PROCESSING OF INFORMATION IN BIOSENSORS BY SURFACE PLASMON RESONANCE

I. Voitovych, I. Yavorsky

Abstract. The paper considers the possibility of using the anti-noise correlation technique of signal processing in biosensors based on surface plasmon resonance (SPR sensors). Application of the said technique is rationalized to define the coordinate shift of resonance parameter which indicates analyte available in the sample under investigation. The example of analytic calculation of correlation signal is presented for Gauss distribution of information luminous flux intensity. It is shown that the correlation technique being dependant on the specific purpose and the cost of a sensor can provide angular resolution $\Delta\theta_{\min} \sim 0,01^{\circ} - 0,0003^{\circ}$.

Keywords: surface plasmon resonance, SPR sensor, correlation technique, resolution capacity

КОРЕЛЯЦІЙНА ОБРОБКА ІНФОРМАЦІЇ В БІОСЕНСОРАХ НА ОСНОВІ ПОВЕРХНЕВОГО ПЛАЗМОННОГО РЕЗОНАНСУ

І. Д. Войтович, І. О. Яворський

Анотація. Розглянута можливість використання антишумового кореляційного методу обробки сигналів в біосенсорах на основі поверхневого плазмонного резонансу (ППР-сенсорах). Обґрунтоване застосування вказаного методу для визначення координатного зсуву резонансної характеристики, який є показником наявності аналіту в досліджуваній пробі. Наведено приклад аналітичного розрахунку кореляційного сигналу для гаусівського розподілу інтенсивності інформаційного світлового потоку. Показано, що кореляційний метод, в залежності від конкретного призначення і вартості сенсора, може забезпечити кутову роздільну здатність $\Delta\theta_{\min} \sim 0,01^{\circ} - 0,0003^{\circ}$.

Ключові слова: поверхневий плазмонний резонанс, ППР-сенсор, кореляційний метод, роздільна здатність

КОРЕЛЛЯЦИОННАЯ ОБРАБОТКА ИНФОРМАЦИИ В БИОСЕНСОРАХ НА ОСНОВЕ ПОВЕРХНОСТНОГО ПЛАЗМОННОГО РЕЗОНАНСА

И. Д. Войтович, И. А. Яворский

Аннотация. Рассмотрена возможность использования антишумового корреляционного метода обработки сигналов в биосенсорах на основе поверхностного плазмонного резонанса (ППР-сенсорах). Обосновано применение указанного метода для определения координатного сдвига резонансной характеристики, являющегося показателем присутствия аналита в исследуемой пробе. Приведен пример аналитического расчёта корреляционного сигнала для гауссовского распределения интенсивности информационного светового потока. Показано, что корреляционный метод, в зависимости от конкретного назначения и стоимости сенсора, может обеспечить угловое разрешение $\Delta\theta_{\min} \sim 0,01^{\circ} - 0,0003^{\circ}$.

Ключевые слова: поверхностный плазмонный резонанс, ППР-сенсор, корреляционный метод, разрешающая способность

Introduction

For the SPR sensor to be operated efficiently, it is essential to determine correctly the coordinates of the angular distribution intensity of the luminous flux reflected from the sensitive receiver chip. The resonance curve of the sensor corresponding to the above distribution is usually noise-affected and has no designated minimum. Therefore, it is rather difficult to define with sufficient precision its shift from a reference curve which characterizes the examined sample in quantitative terms, e.g. indicating the analyte available.

Parasitic optical reflections in an optoelectronic channel and that of receiving chip are the sources of the SPR sensor noise. In addition, the SPR sensors are affected by the factors related to the ultimate dimensions of the radiation source and photosensitive elements, production flaws and adjustment precision of the optical elements, monochromatic radiation etc. This results in the limitation of *physical* angular separate capacity of the sensor (if there is no or insufficient designated program algorithmic processing of the information signals) by the values of several tenth of a degree [1]. For instance, in the sensor described in [2], the precision of $\sim 0,01^{\circ}$ of the turning angle of a prism makes an angular separate capacity $\Delta\theta_{\min} \sim 0,3^{\circ}$. Sensor Spreeta by Texas Instruments, on the other hand, employing the luminodiode with the emitting area of $\sim 200\mu\text{m}$, wave length $\lambda \sim 830\text{nm}$ and monochromaticity $\Delta\lambda \sim 15\text{nm}$ and discreet photo detecting line of 128 pixels with basic distance between the radiation source and photodetector $\sim 5-7\text{cm}$ the *physical* angular separate capacity makes mere $\Delta\theta_{\min} \sim 2,3^{\circ}$ [1,3]. All this can be explained by an

ambiguity (fault) of the angular position of a resonance parameter as resulting from the instability factors described above in action.

Traditional approaches (design improvements, installation of diaphragms, coating of the optics, application of various absorbing coatings as well as band pass electric filters on the signal's way etc.) unfortunately allow only partial decrease of noises and interferences. The only radical solution in our view is to employ electronic devices of filtration and processing of information signals [1,4]. For this purpose it is feasible to apply correlation technique in the SPR sensor [5]. It uses integral properties of a data array defining the whole resonance parameter of the sensor.

Phenomena model

Let us consider the SPR sensor, in which the angular scanning of light on a receiving chip is made by means of a luminous flux with an angular distinction. Let the intensity distribution of a reflected luminous flux (resonance parameter) on the surface of a photo detector (photosensitive CCD range) corresponding to the clean (analyte-free) sample under examination looks as follows:

$$F(x) = I(x - \delta) + S(x), \quad (1)$$

where $I(x - \delta)$ — an information component of the distribution, x — coordinate along the CCD range, δ — ambiguity (fault) of the information component position due to instability factors (δ can be preceded with different signs), $S(x)$ — noise component. Expression (1) will designate a etalon signal.

Light intensity distribution which corresponds to the sample with analyte also contains information and noise components and looks as follows:

$$\tilde{F}(x) = \tilde{I}(x - \delta) + \tilde{S}(x). \quad (2)$$

Expression (2) will define the operating signal.

It is worth mentioning that functions (1) and (2) are not identical as the resonance parameters for the clean samples and the sample with an analyte can be shifted against each other by the x axis by the value ξ which is an amount of analyte available in the sample. Such functions are defined in the range $-\frac{L}{2} \leq x \leq +\frac{L}{2}$, where L — value of photosensitive area of the CCD range on which resonance parameters are registered. Such amount is defined by the expected range of the shifts of the resonance angles of the SPR θ_0 and e.g. with $\theta_0 = 64,5 \pm 3^\circ$ it makes $\sim 1\text{cm}$. General look of the functions $F(x)$, $\tilde{F}(x)$, $I(x - \delta)$, $\tilde{I}(x - \delta)$, which provides their qualitative characteristic is shown on fig. 1.

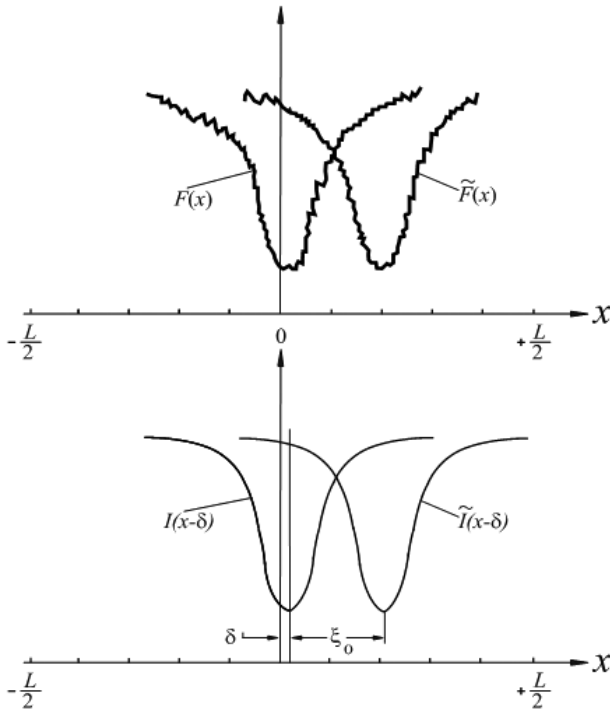


Fig. 1. The overall qualitative appearance of the function of the reflected light intensity distribution for the net sample $F(x)$ and the sample with analyte $\tilde{F}(x)$ along with their data components $I(x - \delta)$ i $\tilde{I}(x - \delta)$.

The correlation technique is to ensure finding of the value of the coordinate shift $\xi = \xi_0$, which occurs between the reference and operation signals with the analyte available in a sample under inves-

tigation. To this end firstly for the reference signal $F(x)$ we develop its autocorrelation function $\psi(\xi)$ as follows:

$$\begin{aligned} \psi(\xi) &= \int_{-\frac{L}{2} + \xi}^{+\frac{L}{2}} F(x)F(x - \xi)dx = \quad (3) \\ &= \int_{-\frac{L}{2} + \xi}^{+\frac{L}{2}} I(x - \delta)I(x - \delta - \xi)dx + \\ &\quad + \int_{-\frac{L}{2} + \xi}^{+\frac{L}{2}} I(x - \delta - \xi)S(x)dx + \\ &\quad + \int_{-\frac{L}{2} + \xi}^{+\frac{L}{2}} I(x - \delta)S(x - \xi)dx + \int_{-\frac{L}{2} + \xi}^{+\frac{L}{2}} S(x)S(x - \xi)dx. \end{aligned}$$

For the 1st integral in (3) having replaced the variable the following can be constructed:

$$\begin{aligned} &\int_{-\frac{L}{2} + \xi}^{+\frac{L}{2}} I(x - \delta)I(x - \delta - \xi)dx = \\ &= \int_{-\frac{L}{2} + \xi - \delta}^{+\frac{L}{2} - \delta} I(z)I(z - \xi)dz = \int_{-\frac{L}{2} + \xi}^{+\frac{L}{2}} I(z)I(z - \xi)dz + \\ &\quad + (\Delta\psi)_\delta, \quad (4) \end{aligned}$$

where

$$\begin{aligned} (\Delta\psi)_\delta &= \delta \cdot \left[I\left(-\frac{L}{2} + \xi - \frac{\delta}{2}\right) \cdot I\left(-\frac{L}{2} - \frac{\delta}{2}\right) - \right. \\ &\quad \left. - I\left(\frac{L}{2} - \xi - \frac{\delta}{2}\right) \cdot I\left(\frac{L}{2} - \frac{\delta}{2}\right) \right]. \end{aligned}$$

With $\left|\frac{\delta}{2}\right| \ll \left|\frac{L}{2}\right|$ the value

$$(\Delta\psi)_\delta \approx (1 \div 2)\delta \cdot I\left(\frac{L}{2}\right) \cdot \left[I\left(-\frac{L}{2}\right) - I\left(\frac{L}{2}\right) \right]. \text{Removal}$$

of the δ effect can be done provided

$$\begin{aligned} &\int_{-\frac{L}{2} + \xi}^{+\frac{L}{2}} I(x - \delta)I(x - \delta - \xi)dx \approx \\ &\approx \int_{-\frac{L}{2} + \xi}^{+\frac{L}{2}} I(z)I(z - \xi)dz = \int_{-\frac{L}{2} + \xi}^{+\frac{L}{2}} I(x)I(x - \xi)dx, \quad (5) \end{aligned}$$

when $(\Delta\psi)_\delta \approx 0$. This requires in its turn $I\left(-\frac{L}{2}\right) = I\left(\frac{L}{2}\right)$, i.e. on the limits of integration the information component is to have similar values. It results in that the value of the said integral (from mathematical standpoint the area limited with sub-integral function and x-axis) will not depend on the shift of the information component along the axis and the impact of the coordinate ambiguity δ will be gone.

Three last integrals in expression (3) with the precision up to the value of the 2nd infinitesimal order $(\Delta\psi)_s$ equal to “0”, as wideband statistical noises $S(x)$ i $S(x-\xi)$ do not correlate with the functions $I(x-\delta)$ i $I(x-\delta-\xi)$ and between each other. This conclusion is true for the integration of functions oscillating rapidly (noises correlate with the similar oscillations) [6].

Filtration properties of the correlation technique but ensure removal of the instabilities and noises. After the filtration expression (3) with the precision up to $\Delta\psi_\Sigma = (\Delta\psi)_\delta + (\Delta\psi)_s \approx 0$ will look as follows:

$$\psi(\xi) = \int_{-\frac{L}{2}+\xi}^{+\frac{L}{2}} I(x)I(x-\xi)dx \pm \Delta\psi_\Sigma. \quad (6)$$

Theoretically, while the correlation technique is applied the effect of the coordination shift and noises can be reduced to zero so as the annex connected therewith $\Delta\psi_\Sigma = 0$. However separate capacity will be then defined not by the destabilization factors depicted above but by the threshold of the response of a registering device and digit capacity of its AD converter.

Next step is to calculate the specific value $\psi(\xi_0)$ of the mutual correlation function for $F(x)$ and $\tilde{F}(x)$:

$$\psi(\xi_0) = \int_{-\frac{L}{2}}^{+\frac{L}{2}} F(x)\tilde{F}(x)dx. \quad (7)$$

Accounting for the mentioned above filtration, one has:

$$\psi(\xi_0) \approx \int_{-\frac{L}{2}}^{+\frac{L}{2}} I(x)\tilde{I}(x)dx. \quad (8)$$

It is clear, that in practice it is necessary to apply numeric techniques of finding autocorrelation and mutual correlation functions as the distributions $F(x)$ and $\tilde{F}(x)$ are assigned experimentally.

For numeric calculations the popular rule applies, that is, for instance, the integral value in (7) can be obtained by adding the discrete values of coupled products of signals $F(x) \cdot \tilde{F}(x)$, multiplied by intervals Δx , such as

$$\psi(\xi_0) = \sum_{j=0}^N F\left(-\frac{L}{2} + j\Delta x\right) \cdot \tilde{F}\left(-\frac{L}{2} + j\Delta x\right) \cdot \Delta x. \quad (9)$$

To provide the higher precision level of the calculations, the interval lengths Δx are not to be extended ($\Delta x \sim 10 \cdot 10^{-4} \text{ cm}$), and number $N = \frac{L}{\Delta x}$ is to be substantial ($N \sim 1000$). The total calculation duration for the correlation function inside the microcomputer (inclusive of the time needed for converting signals into the digital format) is $\leq 1s$, which is an acceptable value.

Fig. 2 presents the configuration of the device intended for processing of SPR signals with the correlation method. This configuration differs from the layouts traditionally employed for similar purposes only by its software algorithm [7].

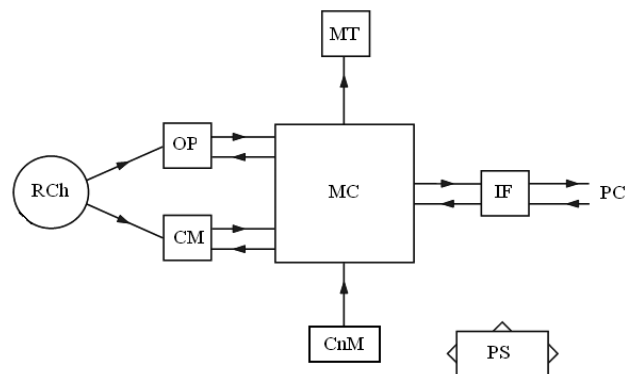


Fig. 2. The configuration scheme of the device for the correlation data processing: RCh — receiver chip, OP—optical receiver, MC — microcomputer, MT — monitor, CnM — control module, CM — communication module, IF - interface, PS — power supply module.

At first, the optical receiver *OP* registers and stores, inside the microcomputer *MC*, the light intensity distribution value $F(x)$ obtained from the “etalon” sample located at the receiver chip *RCh*. Next, the corresponding ‘etalon’ *auto-correlation* function $\psi(\xi)$ is being calculated (including the numerical integration) and is stored inside *MC*. After that, the light intensity distribution from the analyte $\tilde{F}(x)$ is registered and stored (this distribution comprises the data on shift ξ_0). Further on, $F(x)$ and $\tilde{F}(x)$ are used to calculate in the *MC* the concrete value of the *inter-correlation* function $\psi(\xi_0)$, which is also being registered. Given

the latter value, with the “etalon” correlation $\psi(\xi)$ stored inside the *MC*, the corresponding value ξ_0 is obtained. The outcomes are shown at the monitor *MT* and could be transmitted further, via the interface *IF*, on to the external personal computer *PC* for further data processing and accumulation. The change in the conditions of the analysis (the change of an individual under examination, relocation and replacements of receiver chips, etc.) is performed via communication module *CnM*. The control of the device is performed by control module *CM*, and power supply is provided by module *PS*.

Below is the analytical calculation of an *auto-correlation* function $\psi(\xi)$ for an instance approximated to the real conditions (Fig.1), when

$$I(x-\delta) = I_0(1 - e^{-\alpha(x-\delta)^2}) + const, \\ S(x) = \sum_{i=1}^n a_i \sin(\omega_i x + \phi_i), \quad (10)$$

where a_i , ω_i , ϕ_i is the amplitude, circular frequency and the phase of the corresponding noise components (such as sinusoidal). Number n of the such components can be rather extended, as the noise is multi-band. Primarily, for the reasons of convenience, the expression for $I(x-\delta)$ is to be simplified by taking out the constant component $I_0 + const$, hence, the intensity distribution of the reflected light becomes similar to the gauss format:

$$I(x-\delta) = -I_0 e^{-\alpha(x-\delta)^2}. \quad (11)$$

Then, for the first integral in (3) the following is true:

$$J_1 = \int_{\frac{L}{2}+\xi}^{\frac{L}{2}} I(x-\delta) I(x-\delta-\xi) dx = \\ = I_0^2 e^{-\frac{\alpha}{2}\xi^2} \int_{\frac{L}{2}+\xi}^{\frac{L}{2}} e^{-\frac{\alpha}{2}(2x-2\delta-\xi)^2} dx. \quad (12)$$

The second integral in (3) becomes

$$J_2 = \sum_{i=1}^n \int_{\frac{L}{2}+\xi}^{\frac{L}{2}} I(x-\xi) \cdot a_i \sin(\omega_i x + \phi_i) dx. \quad (13)$$

Next, in compliance with integration rules for accelerated oscillating functions [6]

$$J_2 \approx \sum_{i=1}^n \frac{I_0 a_i}{\omega_i} \left\{ e^{-\alpha\left(\frac{L}{2}-\xi\right)^2} \cos\left(\omega_i \frac{L}{2} + \phi_i\right) - \right.$$

$$\left. - e^{-\alpha\left(\frac{L}{2}\right)^2} \cos\left[\omega_i \left(-\frac{L}{2} + \xi\right) + \phi_i\right] \right\}. \quad (14)$$

It is obvious that with the high values of the circular frequencies ω_i , integral $J_2 \approx 0$, i.e. the noise is being filtered. The 3rd integral in (3) is approximated to 0 in the similar manner.

The next step is to show that the 4th interval in (3) is also close to 0. The expression for this is:

$$J_4 = \int_{\frac{L}{2}+\xi}^{\frac{L}{2}} \sum_{i=1}^n a_i \sin(\omega_i x + \phi_i) \times \\ \times \sum_{i=1}^n a_i \sin[\omega_i(x-\xi) + \phi_i] dx. \quad (15)$$

The sub-integral total values in (15) can be replaced with their mean values:

$$J_4 \approx n^2 \overline{a^2} \overline{\sin(\omega x + \phi)} \cdot \overline{\sin[\omega(x-\xi) + \phi]} \cdot (L-\xi). \quad (16)$$

As $\overline{\sin(\omega x + \phi)} = 0$, then $J_4 \approx 0$.

As was intended by substantiation (4) – (5), integration (12) leads to eliminating of the impact from coordination shift δ , as irrelevant to the latter shift, the sub-integral exponent at the integration margins is characterized by practically identical values. As the result, *autocorrelation* function $\psi(\xi) \approx J_1$, and corresponding standardized function $\bar{\psi}(\xi)$ becomes:

$$\bar{\psi}(\xi) = \frac{\psi(\xi)}{I_0^2} \approx \sqrt{\frac{\pi}{2\alpha}} e^{-\frac{\alpha}{2}\xi^2} \Phi(t), \quad (17)$$

where $\Phi(t)$ is credibility integral, $t = \sqrt{\alpha}(L-\xi)$ [6].

To determine ξ_0 , the value of *inter-correlative* function $\psi(\xi_0)$ (such as from (8)) is to be introduced in equation (17), which is next resolved relative to ξ . This can be done with numerical methods only, as ξ is not a direct component of (17). An essentially similar operation is performed inside our microcomputer *MC* by means of comparing the values of *auto-correlation* and *inter-correlation* functions.

Fig.3 shows standardized gauss light intensity distribution $\bar{I}(x)$ and corresponding *auto-correlation* function $\bar{\psi}(\xi)$, both calculated analytically. As the value of the correlation function is related to shift ξ between the signals generating it, this enables to determine the above shift in each particular instance. For instance, with the change of correlation function $\Delta\bar{\psi}_{\min} = 0,001 \cdot \bar{\psi}_{\max} \approx 1,5 \cdot 10^{-4} cm$, that can equal the total value of the inconsistency

and noise $\Delta\bar{\Psi}_\Sigma$, the minimum shift (linear distributive capacity) is $\xi_{\min} \approx 35 \cdot 10^{-4} \text{ cm}$. In an inexpensive portable SPR sensor, with the standard distance between the radiation source point and the optical receiver line of $\sim 10 - 15 \text{ cm}$, this would correspond to angular distributive capacity $\Delta\theta_{\min} \sim 0,01^\circ$.

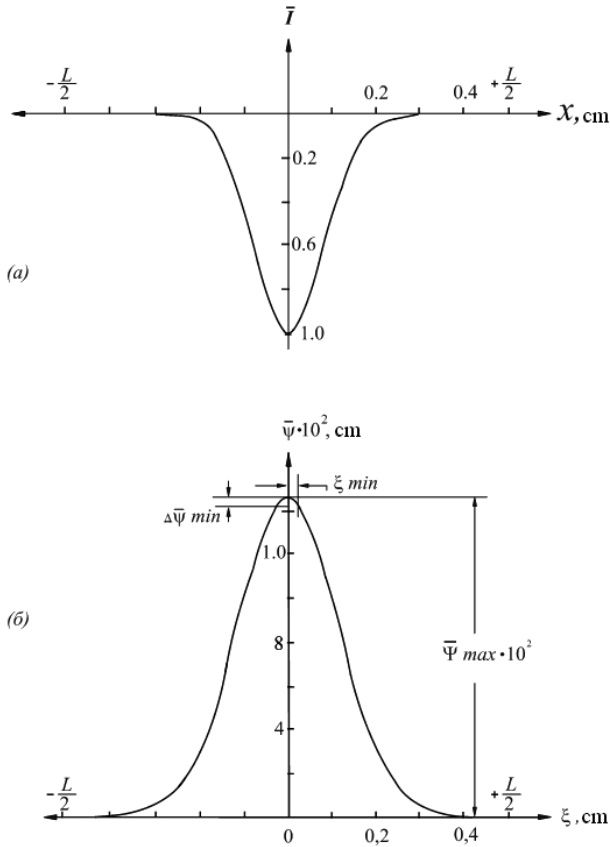


Fig. 3. Standardized gauss distribution of the reflected light intensity distribution $\bar{T}(x) = -e^{-75x^2}$ (a) and its autocorrelation function $\bar{\Psi}(\xi)$ (b).

Linear distributive capacity ξ_{\min} (the corresponding angular distributive capacity is $\Delta\theta_{\min}$) is an important parameter in the correlation method. As was observed earlier, ideally, in case of complete elimination of the impact from the inconsistencies and the noise, it is determined by the minimum shift in the correlation signal $\Delta\bar{\Psi}_{\min}$, that can be whatsoever registered. For the suggested instance of a gauss distribution the linear distributive capacity is described with the expression:

$$\xi_{\min} = \frac{|\Delta\bar{\Psi}_{\min}|}{\left| \frac{\partial\bar{\Psi}}{\partial\xi} \right|_{\xi=\xi_{\min}}} \approx \left[\frac{2}{\pi\alpha} (\Delta\bar{\Psi}_{\min})^2 \right]^{1/4}. \quad (18)$$

It is clear that the distributive capacity can be increased (ξ_{\min} can be decreased) by increasing

the sensitivity of registering devices (by decreasing $\Delta\bar{\Psi}_{\min}$) and by increasing the ratio of the correlation function $\left| \frac{\partial\bar{\Psi}}{\partial\xi} \right|_{\xi=\xi_{\min}}$. For the same gauss distribution with $\Delta\bar{\Psi}_{\min} = 1 \cdot 10^{-6}$ $\bar{\Psi}_{\max} = 1,5 \cdot 10^{-7} \text{ cm}$ one can obtain $\xi_{\min} = 1 \cdot 10^{-4} \text{ cm}$ and correspondingly $\Delta\theta_{\min} = 0,0003^\circ$. For this, the sensor should have an ADC with the order level of $N = 20$ (it is determined with the expression $\frac{\bar{\Psi}_{\max}}{\Delta\bar{\Psi}_{\min}} = 2^N$).

In existing sensors, depending on their configuration, application and cost, the distributive capacity can vary within a wide range — from several 0.1 [2] up to several 10^{-4} degrees [8]. Increase in distributive capacity is typically achieved by multiple measurements of data signals (in order to average the results and increase the “signal-noise“ ratio), by selecting adequate registering devices and software applications, and also by performance configuration of the optic electronic channel. In this connection, findings [9] of achieving angular distributive capacity $\Delta\theta_{\min} \sim 0,0001^\circ$ (0,1 milli degree) is of particular interest, although no particular methods, their complexity or cost are being specified.

The achieved range of the angular distributive capacity $\Delta\theta_{\min} \sim 0,01^\circ - 0,0003^\circ$ is the evidence of the vast application potential of the correlation method. For instance, value $\Delta\theta_{\min} \sim 0,01^\circ$ is applicable for inexpensive portable SPR sensors intended to operate in field conditions. In SPR refractometers this value corresponds to the difference of the examined substance refraction parameter $\Delta n \sim 0,1 \cdot 10^{-5}$ [10], which is higher than the relative values of the renowned sensor *BIACORE 2000* (its sensitivity is $\Delta n \sim 1 \cdot 10^{-5}$). The similar order of the calculation value (not *physical* property) of the *calculated* distributive capacity ($\sim 0,03^\circ$) is achieved in the mentioned above sensor Spreeta [3], yet this sensor is rather a lab device and the data are processes with the external computer and complex software application. As for the value $\Delta\theta_{\min} \sim 0,0003^\circ$, there is a particular need in SPR sensors characterized by such distributive capacity, as, to achieve this, the existing limitations are to be surpassed in terms of specifications for registering and processing of the data (sensitivity, numerical order ADC, etc.) and the incurred costs. Increased distributive capacity also demands optimization of formatting methods, in particular, registration and processing procedures for the sensor data signals, as well as introduction of

the complementary methods, such as optical phaseometry techniques, etc. [9, 11].

It is worth mentioning, that though eliminating the impact from coordinate ambiguity δ noise filtering are important properties of the correlation method, these are not its only advantages. Both the “etalon” and the “operational” signals of the SPR sensor can have insignificant minimum values. Hence, if identifying the shift ξ_0 between these signals with direct methods (such as with the signal minimums), it is difficult to select a reference point. Even in case of complete noise elimination it would be difficult to achieve the needed precision of the measurements. As was mentioned above, the correlation method employs the vast data base to determine the shift value (thousands of gauge results from the signal, including registries from its side beams). For instance, according to (9) each value of the *inter-correlation* function $\psi(\xi_0)$ accumulates inside it the data from $2N \sim 2000$ values of the “etalon” and “operational” signals. That is why applying the correlation method means high levels of the data averaging and hence high precision of measurements, there is no longer need to determine the measurement reference points.

There is also a possibility of instances when the “etalon” and the “operational” signals are shifted between themselves to the extent that they are not overlaid at any point. Then the relevant value of the *inter-correlation* function equals 0. This in turn means that the correlation method cannot determine shift ξ_0 . Yet, in this particular case, there is no need to apply the former method and one can refer to the above-mentioned simpler approaches. For this, the software can be furnished, for example, by sub-programs to determine the shift with the points of changing the polarity of the derivatives at signal minimums or by the method of “moments” [3].

Conclusions

1. It was shown that with the help of the correlation method in SPR sensors there can be eliminated the coordinate ambiguity of the resonance parameter related to the finite dimensions of the light source, optically sensitive elements, faults in the configuration, the precision limits of adjustment and the monochromatic property of the radiation, as well as the noise, also there could be achieved the angular distributive capacity $\Delta\theta_{\min} \sim 0,01^0 - 0,0003^0$.

2. The further increase of the distributive capacity is related to the updating of the existing formatting methods, methods of registering and processing of the information signals and their back-up with alternative approaches.

References

1. Бююн В. П., Войтович І. Д. та ін. Сенсорний пристрій // Пат. України №78998. МПК G01 N21/55. Заявл. 27. 12. 2004, опубл. 10. 05. 2007. — Бюл. №6.
2. Ширшов Ю. М., Венгер Є. Ф. та ін. Спосіб детектування та визначення концентрації біомолекул та молекулярних комплексів та пристрій для його здійснення // Пат. України №46018. МПК G01 N21/55. Заявл. 22. 10. 1997, опубл. 15.05.2002. — Бюл №5.
3. Suzuki M., Ozawa F., Sugimoto W., Aso S. Miniaturization of SPR Immunosensors // *Analytical Sciences*. — 2001. — V. 17. — P. 1265-1267; www.ti.com/spreeta; www.aigproducts.com/surface-plasmon-resonance/spr-curve-analysis.htm.
4. Войтович І. Д., Корсунський В. М., Косогор А. Н., Стародуб Н. Ф., Яворський І. А. Перспективи створення портативних біосенсорів на основі поверхнового плазмонного резонанса // *Сенсорна електроніка і мікросистемні технології*. — 2005. — №. 3. — С. 56 — 65.
5. Голдман С. Теорія інформації. — М.:И. Л., 1957. — С. 325 — 331.
6. Зельдович Я. Б., Мышкис А. Д. Елементи прикладної математики. — М.:Наука, 1972. — С. 79 — 82, 510.
7. Войтович І. Д., Корсунський В. М. Інтелектуальні сенсори. — Київ: ІК НАНУ, 2007. — С. 5 — 67.
8. Ширшов Ю. М., Самойлов А. В. и др. Анализ и численное моделирование ППР-спектрометров с механической развёрткой по углу: алгоритм определения угловой позиции минимума // *Рестрація, зберігання і обробка даних*. — 2004. — Т. 6. — №3. — С. 3-18.
9. Handbook of Surface Plasmon Resonance (Edit. by R. V. M. Schasfoort and Anna J. Tudos, Netherlands). — 2008. — P. 22 — 23, 59.
10. Stemmler I., Brecht A., Gauglitz G. Compact surface plasmon resonance-transducers with spectral readout for biosensing applications // *Sensors and Actuators*. — V. 54. — 1999. — P. 98 -105.
11. Кабашин А. В., Никитин П. И. Интерферометр с использованием поверхностного плазмонного резонанса для сенсорных измерений // *Квантовая электроника*. — 1997. — Т. 24. — №7. — С. 671 — 672.

ВИМОГИ ДО ОФОРМЛЕННЯ СТАТЕЙ У ЖУРНАЛ ІНФОРМАЦІЯ ДЛЯ АВТОРІВ

Журнал “Сенсорна електроніка і мікросистемні технології” публікує статті, короткі повідомлення, листи до Редакції, а також коментарі, що містять результати фундаментальних і прикладних досліджень, за наступними напрямками:

1. Фізичні, хімічні та інші явища, на основі яких можуть бути створені сенсори
2. Проектування і математичне моделювання сенсорів
3. Сенсори фізичних величин
4. Оптичні, оптоелектронні і радіаційні сенсори
5. Акустoeлектронні сенсори
6. Хімічні сенсори
7. Біосенсори
8. Наносенсори (фізика, матеріали, технологія)
9. Матеріали для сенсорів
10. Технологія виробництва сенсорів
11. Сенсори та інформаційні системи
12. Мікросистемні та нано- технології (MST, LIGA-технологія, актюатори та ін.)
13. Деградація, метрологія і сертифікація сенсорів

Журнал публікує також замовлені огляди з актуальних питань, що відповідають його тематиці, поточну інформацію — хроніку, персоналії, платні рекламні повідомлення, оголошення щодо конференцій.

Матеріали, що надсилаються до Редакції, повинні бути написані з максимальною ясністю і чіткістю викладу тексту. У поданому рукописі повинна бути обґрунтована акту-

альність розв’язуваної задачі, сформульована мета дослідження, міститися оригінальна частина і висновки, що забезпечують розуміння суті отриманих результатів і їх новизну. Автори повинні уникати необґрунтованого введення нових термінів і вузькопрофільних жаргонних висловів.

Редакція журналу просить авторів при направленні статей до друку керуватися наступними правилами:

1. Рукописи повинні надсилатися у двох примірниках українською або російською і англійською мовами і супроводжуватися файлами тексту і малюнків на дискеті. Електронна копія може бути надіслана електронною поштою.

2. Прийнятні формати тексту: MultiEdit (txt), WordPerfect, MS Word (rtf, doc).

3. Прийнятні графічні формати для рисунків: EPS, TIFF, BMP, PCX, WMF, MS Word і MS Graf, JPEG. Рисунки створені за допомогою програмного забезпечення для математичних і статистичних обчислень, повинні бути перетворені до одного з цих форматів.

Рукописи надсилати за адресою:

**Лепіх Ярослав Ілліч, Зам. гол. Редактора,
Одеський національний університет імені
І. І. Мечникова, МННФТЦ (НДЛ-3),
вул. Дворянська, 2, Одеса, 65082, Україна.**

**Телефон / факс +38(048) 723-34-61,
тел. +38(048) 726-63-56.**

E-mail: semst-journal@onu.edu.ua,

semst-journal@ukr.net

http://www.semst.onu.edu.ua

Правила підготовки рукопису:

Рукописи повинні супроводжуватися офіційним листом, підписаним керівником установи, де була виконана робота. Це правило не стосується робіт представлених міжнародними групами авторів.

Авторське право переходить Видавцю.

Титульний аркуш:

1. **PACS** і Універсальний Десятковий Код Класифікації (**УДК**) (для авторів із країн СНД) — у верхньому лівому куті. Допускається декілька відділених комами кодів. Якщо ніякі коди класифікації не позначені,

код(и) буде(-уть) визначено Редакційною Колегією.

2. **Назва роботи** (по центру, прописними літерами, шрифт 14pt, жирно, укр., рос., англ. мовами).

3. **Прізвище (-а) автора(-ів)** (по центру, шрифт 12pt, укр., рос., англ. мовами).

4. **Назва установи**, повна адреса, телефони і факси, e-mail для кожного автора, нижче, через один інтервал, окремим рядком (по центру, шрифт 12pt).

Анотація: до 200 слів українською, англійсь-

кою і російською мовами. Перед текстом анотації потрібно вказати на тій же мові: назву роботи, прізвища і ініціали всіх авторів.

Для авторів з закордону, які не знають української або російської мови, достатньо анотації і прізвища англійською.

Ключові слова: їхня кількість не повинна перевищувати вісьми слів. В особливих випадках можна використовувати терміни з двома — чи трьома словами. Ці слова повинні бути розміщені під анотацією і написані тією самою мовою.

Текст повинен бути надрукований через 1,5 інтервали, на білому папері формату А4. Поля: зліва — 3см, справа — 1,5см, вверху і знизу — 2,5см. Шрифт 12pt. Підзаголовки, якщо вони є, повинні бути надруковані прописними літерами, жирно.

Рівняння повинні бути введені, використовуючи MS Equation Editor або MathType. Роботи з рукописними вставками не приймаються.

Таблиці повинні бути представлені на окремих аркушах у форматі відповідних текстових форматів (див. вище), чи у форматі тексту (з колонками, відділеними інтервалами, комами, крапкам з комою, чи знаками табулювання).

Список літератури повинен бути надрукований через 1,5 інтервали, з літературою, пронумерованою в порядку її появи в тексті.

Порядок оформлення літератури повинен відповідати вимогам ВАК України, наприклад

1. Берестовский В.Б., Лифшиц Е.М., Питаевский Л.П., Квантовая электродинамика. — М.: Наука, 1984. — 430 с.

2. Сергиенко А.М., Чернова Р.И., Сергиенко А.Я., Оптимизация цифровой сети //ФТТ. — 1992. — Т.7, №6. — С. 34-38.

3. Bramley R., Faber J.M., Nelson C.N. et al., Gas sensor research // Phys. Rev. — 1978. — №6. — P. 34-38.

4. Stirling A.N. and Watson D. Progress in

Low Temperature Physics. — North Holland, Amsterdam.: ed. by D.F. Brewer, 1986. — 248 p.

5. Громов К.Д., Ландсберг М.Э., Оптимальное назначение приоритетов //Труды международного конф. “Локальные вычислительные сети”(ЛОКСЕТЬ 88). — Том 1. — Рига:ИЭВТ АН Латвии. — 1988. — С.149-153.

6. Elliot M.P., Rumford V. and Smith A.A. The research of the optical sensors. — NY. 1976. — 37 p.(reprint./ТН 4302-CERN).

7. Шалимова А.Н., Гаків А.С. Дослідження оптичних сенсорів. — К: 1976. — 37 с. (Препр./АН України. Ін-т кібернетики; 76-76).

8. Васильев Н.В. Оптические сенсоры на плівках A_2B_6 : Дис. канд.фіз. — мат. наук, 05.05.04. — К.,1993. — 212 с.

Підписи до рисунків і таблиць повинні бути надруковані в рукописі з двома пробілами після списку літератури.

Виносок, якщо можливо, бажано уникати.

Рисунки будуть скановані для цифрового відтворення. Тому приймаються тільки високоякісні рисунки.

Написи і символи повинні бути надруковані усередині рисунку. Негативи, слайди, і діапозитиви не приймаються.

Кожен рисунок повинен бути надрукований на окремому аркуші і мати розмір, що не перевищує 160x200 мм. Для тексту на рисунках використовуйте шрифт 10pt. Одиниці виміру повинні бути позначені після коми (не в круглих дужках). Усі рисунки повинні бути пронумеровані в порядку їх появи в тексті, з частинами позначеними як (а), (б), і т.д. Розміщення номерів рисунків і напису усередині малюнків не дозволяються. Зі зворотньої сторони, напишіть олівцем назву, прізвище(а) автора(-ів), номер малюнка і позначте верх стрілкою.

Фотографії повинні бути оригінальними.

Кольоровий друк можливий, якщо його вартість сплачується авторами чи їх спонсорами.

INFORMATION FOR CONTRIBUTORS THE REQUIREMENTS ON PAPERS PREPARATION

“Sensor Electronics and Microsystems Technologies” publishes articles, brief messages, letters to Editors, comments containing results of fundamental and applied researches, on the following directions:

1. Physical, chemical and other phenomena, as the bases of sensors
2. Sensors design and mathematical modeling
3. Physical sensors
4. Optical and optoelectronic and radiation sensors
5. Acoustoelectronic sensors
6. Chemical sensors
7. Biosensors
8. Nanosensors (physics, materials, technology)
9. Sensor materials
10. Sensors production technologies
11. Sensors and information systems
12. Microsystems and nano- technologies (MST, LIGA-technologies, actuators)
13. Sensor's degradation, metrology and certification

The journal publishes the custom-made reviews on actual questions appropriate to the mentioned subjects, current information — chronicle, special papers devoted to known scientists, paid advertising messages, conferences announcements.

The materials sent to Editors, should be written with the maximal clearness. In the submitted man-

uscript the actuality of problem should be reflected, the purpose of the work should be formulated. It must contain an original part and conclusions providing understanding of essence of received results and their novelty. The authors should avoid unreasonable introduction of the new terms.

The Editors asks the authors to follow the next rules:

1. Manuscripts should be submitted in duplicate in Ukrainian, English, or Russian, a hard copy and supplemented with a text file and figures on a diskette. An electronic copy may be submitted by e-mail.
2. Acceptable text formats: MultiEdit (txt), WordPerfect, MS Word (rtf, doc).
3. Acceptable graphic formats for figures: EPS, TIFF, BMP, PCX, CDR, WMF, MS Word and MS Graf, JPEG. Figures created using software for mathematical and statistical calculations should be converted to one of these formats.

Manuscripts should be sent to:

Lepikh Yaroslav Illich, The Vice Editor, Odessa National I.I. Mechnikov University, ISEPTC (RL-3), str. Dvoryanskaya, 2, Odessa, 65082, Ukraine.

**Phone/fax +38(048) 723-34-61,
phone +38(048) 726-63-56.**

**E-mail: semst-journal@onu.edu.ua,
semst-journal@ukr.net
<http://www.semst.onu.edu.ua>**

The manuscript preparation rules:

The manuscripts should be supplemented with the Official letter signed by a chief manager of the institution where the work was performed. This requirement does not apply to papers submitted by international groups of authors.

Copyright transfer to the Publisher.

Title Page:

1. **PACS and Universal Decimal Classification code** (for authors from FSU). Several comma-separated codes are allowed. If no classification codes are indicated, the code(s) will be assigned by the Editorial Board.

2. **Title of the paper** (central, capital, bold, 14pt)

3. **Name (-s) of the author(s)** below, in one space (central, normal face, 12pt).

4. **Name of affiliated institution**, full address, telephone and fax numbers, e-mail addresses (if avail-

able) for each author below, in one space (central, normal face, 12pt).

Abstract: up to 200 words, must be presented in English, Ukrainian and Russian. Before the abstract text one should indicate in the same language: the paper title, surnames and initials of all authors.

Keywords: its amount must not exceed eight words. In the specific cases it is acceptable to use two- or three-word terms. These words must be placed under the abstract and written in the same language.

Text should be printed 1,5-spaced on white paper A4 format with a 12pt, margins: left — 3sm, right — 1,5, upper and lower — 2,5sm. Titles of the sections if it is present should be typed bold, capitals.

Equations should be entered using MS Equation Editor or MathType. Papers with handwritten equa-

tions are not accepted. Notations should be defined when the first appearing in the text.

Tables should be submitted on separate pages in the format of appropriate text formats (see above), or in the text format (with columns separated by interval, commas, or tabulation characters).

List of references should be 1,5-spaced, with references numbered in order of their appearance in the text.

The format for references is as follows:

1. Берестовский В.Б., Лифшиц Е.М., Питаевский Л.П., Квантовая электродинамика. — М.: Наука, 1984. — 430 с.

2. Сергиенко А.М., Чернова Р.И., Сергиенко А.Я., Оптимизация цифровой сети //ФТТ. — 1992. — Т.7, №6. — С. 34-38.

3. Bramley R., Faber J.M., Nelson C.N. et al., Gas sensor research // Phys. Rev. — 1978. — №6. — P. 34-38.

4. Stirling A.N. and Watson D. Progress in Low Temperature Physics. — North Holland, Amsterdam.: ed.by D.F. Brewer, 1986. — 248 p.

5. Громов К.Д., Ландсберг М.Э., Оптимальное назначение приоритетов //Труды междунар. конф. “Локальные вычислительные сети”(ЛОКСЕТЬ 88). — Том 1. — Рига:ИЭВТ АН Латвии. — 1988. — С.149-153.

6. Elliot M.P., Rumford V. and Smith A.A. The research of the optical sensors. — NY.: 1976. — 37 p. (reprint./ TH 4302-CERN).

7. Шалимова А.Н., Крюков А.С. Исследо-

вание оптических сенсоров. — К: 1976. — 37 с. (Препр. /АН Украины. Ин-т кибернетики; 76-76).

8. Васильев Н.В. Оптичні сенсори на A_2B_6 : Дис. канд.фіз. — мат. наук,05.05.04. — К.,1993. — 212 с.

Figures and tables captions should be printed in the manuscript double-spaced after the list of references.

Footnotes should be avoided if possible.

Pictures will be scanned for digital reproduction. Only high-quality pictures can be accepted. Inscriptions and symbols should be printed inside. Negatives, and slides are not accepted.

Each figure should be printed on a separate page of the manuscript and have a size not exceeding 160x200 mm. For text inside figures, use 10pt. Measurement units should be indicated after a comma (not in blankets). All figures are to be numbered in order of its appearance in the text, with sections denoted as (a), (b), etc. Placing the figure numbers and captions inside figures is not allowed. On the backside, write with a pencil the paper title, author(s) name(s) and figure number, and mark the topside with an arrow.

Photographs should be submitted as original prints.

Color printing is possible if its cost is covered by the authors or their sponsors.

For information about the rules and costs, contact with the Editorial Staff.

Підписано до друку 15.10.2009. Формат 60x84/8. Папір офсетний. Гарнітура «Newton». Друк офсетний.
Ум. друк. арк. 10,46. Тираж 100 прим. Зам. № 530.

Видавництво і друкарня «Астропринт»
65091, м. Одеса, вул. Разумовська, 21.
Тел.: (048) 37-07-95, 37-24-26, 33-07-17, 37-14-25.
www.astroprint.odessa.ua; www.fotoalbom-odessa.com
Свідоцтво суб'єкта видавничої справи ДК № 1373 від 28.05.2003 р.